Development of a Measurement Instrument Using Capacitance Sensors Techniques to Image and Measure the Skin Surface Hydration

Harjinthar Singh

London South Bank University

November 2010

Abstract

Studies have shown that capacitance sensors can be used for skin hydration imaging, surface analysis and skin micro relief measurements. In this report, development of a hardware measurement instrument and accompanying software that was made is discussed. Work then focussed on stratum corneum (SC) dynamic water concentration measurements using the capacitance sensor. To further validate the measurement results, the capacitance sensors SC surface hydration results are compared with the opto-thermal transient emission radiometry (OTTER) and trans-epidermal water loss (TEWL) results measured by using the condenser-chamber TEWL method.

To achieve the aim of this project, a hand-held probe, based on the FingerPrint Card area sensor development kit (FPC-SMD 5410, FPC-AMD 6410 and then on the FUJITSU MBF-200), has been developed and used in this research. The development kit contains an array area sensor chip, a processor board and a serial/USB connecting cable for connecting to a PC.

Dedicated JAVA, C++ and Mathworks MatLab programs have also been developed, which can capture the images, process the images, perform grayscale value calculation and display the images. A secondary program was developed in MatLab that allows extraction of data from raw image files created by the sensor. These data are then processed to show mathematical calculations and image profiling of the subject skin site. Additionally, the MBF-200 sensor is able to record live video files of the skin.

The precision of the resulting data is analysed and multiple experiments are conducted to test the viability and usage of the capacitance sensor in different areas of research such as skin hydration, occlusion, depilation and scar measurement. Further test were also conducted on a multitude of hydrated surfaces both live an non-live.

To my late father

Acknowledgement

To Dr. Perry Xiao who not only provided academic motivation but also friendship that I value very much. To Dr. Lorelai Ciortea who kept good company and advice on diverse topics during my studies.

To my wife Low Siew Kheng and my son Harman Singh who I miss very much during my final days of completing this dissertation.

Contents

CHAPTER 1: INTRODUCTION

The human skin is the largest organ and comprises more than 10% of the body mass. Its main functions, to act as a protective barrier between the body and the environment, to prevent fluid loss and to exclude environmental toxins, are fundamental to life.

Despite this, little is known of how the barrier works and how environmental and metabolic factors influence it. Although various techniques have been used such as electrical measurements, evaporimetry, infrared spectroscopy, photoacoustic spectroscopy, photothermal imaging, all of them have limitations that impede a good understanding of the skin (Frodin T, Helander P, Molin L, Skogh M, 1988).

Technologies that have helped to better understand how the barrier works; among others are the OTTER (opto-thermal transient emission radiometry) and (AquaFlux) a more accurate method of measuring trans-epidermal water loss.

The main aim of the investigation is to develop a novel prototype device employing the technique of capacitance sensors that is quick, cheap and small albeit not as sensitive as the AquaFlux or OTTER for measuring skin surface water and its benefits in a multitude of applications.

This research will then focus on testing the feasibility and accuracy of the device by developing software analysis tools to measure the instrumentation range; and conducting necessary skin experiments on test subjects.

This chapter presents a brief introduction to the structure and properties of human skin together with a short review of the methods used to measure skin hydration and TEWL using OTTER and AquaFlux. Finally a brief introduction of the chapters in this report is given.

1.1 Skin

The skin is the largest specialised organ in the body with area of about 1.5 m^2 to 2 m^2 of the surface area providing a protective barrier against water loss and poisoning by external chemicals, mechanical protection, temperature regulation and repair after trauma. It is the first line of defence against pollution, micro-organisms, radiation and physical trauma. It is also a sensory organ containing many nerve endings which enable us to sense heat, pressure, temperature, pain and touch (Swarbrick J, Boylan J.C, 1995). Skin varies in texture, structure and thickness and is made up of three main layers: namely the epidermis, the dermis and the subcutaneous layer (or hypodermis), as illustrated in Figure 1.1.

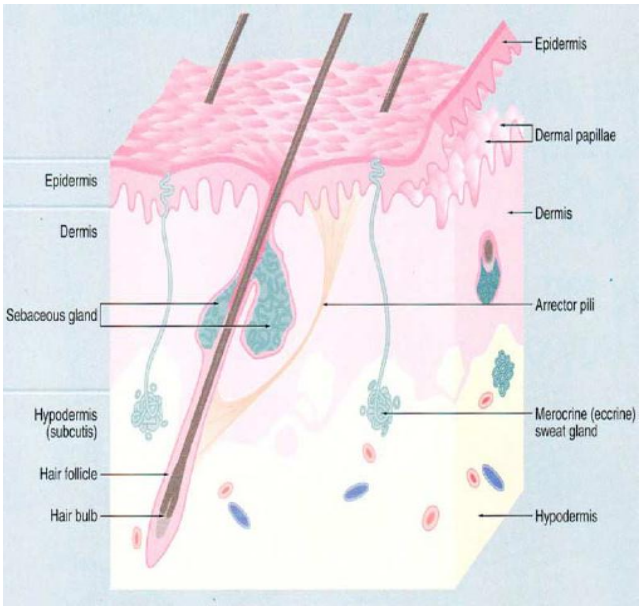

Figure 1.1: Structure of the skin (reproduced from [6]).

1.1.1 Epidermis

The epidermis is the uppermost epithelial layer of the skin. It usually measures less than 1mm in thickness and is thickest on the palms and soles and thinnest on the eyelids. It is thickest on the sole as it has nearly constant contact with the ground and supports the total weight of the body. Palms have a large role of having contact with materials that the human holds and touches with the hand.

The skin on the palm and soles also has friction ridges and they have a biological function to allow grasping and holding of objects. The epidermis can be subdivided into five layers: stratum basale, stratum spinosum, stratum granulosum, stratum lucidum and stratum corneum (SC), as shown in Fig.1.2.

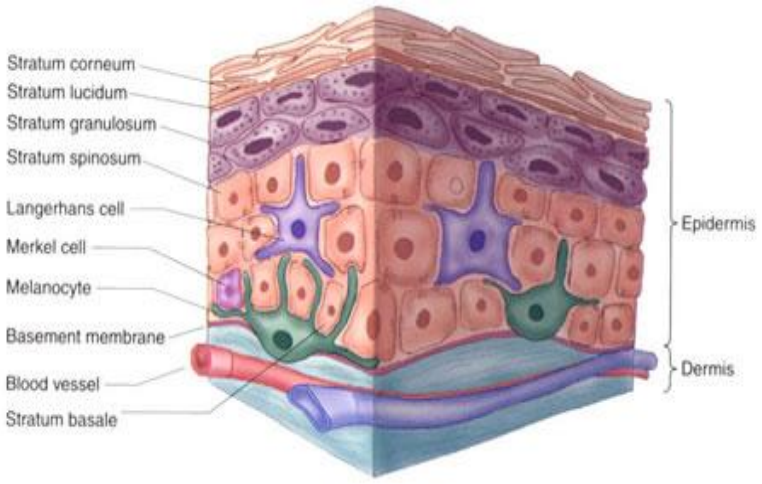

Figure 1.2: Epidermis structure (reproduced from [22]).

The stratum lucidum, a thin and clear layer is found only in the epidermis of the palm and soles.

Cell division occurs in the basal layer of the epidermis. The basal keratinocytes are one of the most actively dividing cells in the body. They produce new keratinocytes which move upwards pushing the older cells above towards the surface of the skin. In the next layer, the stratum spinosum, the cells begin to flatten and take on a polygonal shape.

As they enter the stratum granulosum, the cells form keratohyalin granule. As the cells continue to move up, these granules are converted into keratin by an enzyme. The nuclei then disappear and the cells die and become hard (the process is called keratinisation). When they arrive at the SC, the most superficial layer of the skin, they are fully keratinized and dead. SC cells are constantly exposed to and damaged by external factors and need to be shed and replaced by newer cells from below. It takes approximately 28 days for the new cells to reach the surface of the skin and to be

shed as scales (Plewing G, Jansen T, 1997). The SC is the last stage of the basal cells but not the least important stage, because it is the main protective barrier of the skin.

1.1.2 Stratum Corneum

The SC is a horny or cornified layer located on the outer surface of the skin and comprises 25 to 30 layers of dead cells with approximately 10-20μm thickness. It is made up of keratinized flat, roughly hexagonally shaped, partly overlapping cells embedded in a lipid matrix. Its main constituents are proteins (70% of the total dry weight), lipids (5-15%) and water (10-20%). The proteins are composed of α-keratin, β-keratin and cell envelope. The lipids consist of neutral lipids (75%), sphingolipids (18%), polar lipids (5%) and cholesterol sulphate (2%) (Lampe, M.A., Burligame A.L., 1983).

The structure of the SC itself can be explained in terms of the so-called "brick and mortar" model, in which horny keratinocytes (corneocytes) represent the bricks while the intercellular lipids and water-retaining natural moisturizing factors (NMF) act as the mortar (Fig.1.3) (Elias P.M.,1981).

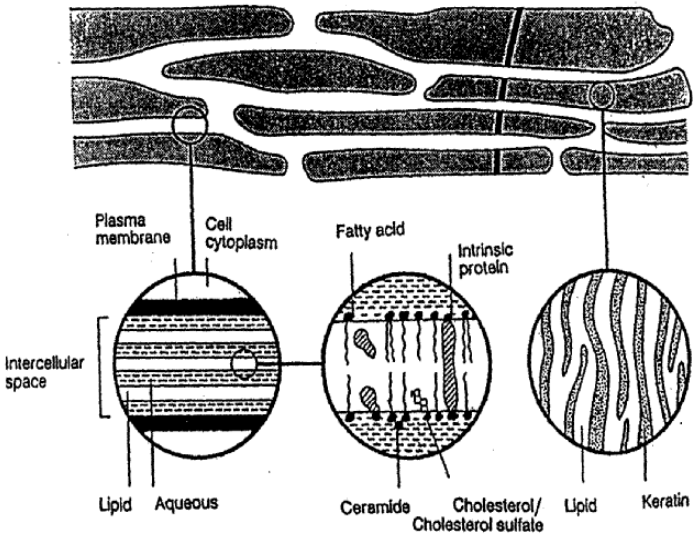

Figure 1.3: Schematic diagram of the brick and mortar model of the SC (reproduced from [40]).

Experimental work has shown the importance of the SC as the barrier between the living cells and the surrounding environment (Forslind B, Engstrom S, 1997). Thus, it prevents water loss from the inner layers of the skin to the ambient environment and it is a barrier against the entry of xenobiotics from the environment. Investigations have shown that the barrier property resides in the lipids covalently bound to the surface of the cornecytes.

The SC contains water, which is necessary to maintain its flexibility. Diseased skin is often associated with a dry and scaly appearance. Research demonstrates that the water-soluble materials or NMF are responsible for water uptake. The NMF are intracellular components (within corneocytes), composed of free amino acids and polypeptides, minerals, pyrrolidone carboxilic acid, sodium lactate, urea, carbohydrates and sodium citrate (Harding, C.R., Watkinson, A, 2000).

1.1.3 Dermis

The dermis is the second connective layer of the skin and acts as a supportive layer for the epidermis. It has the role of regulating temperature and providing nourishment to the epidermis. It is comprised of a matrix of connective tissue that contains collagen fibres interlaced with elastic fibres structure as illustrated in Fig. 1.4.

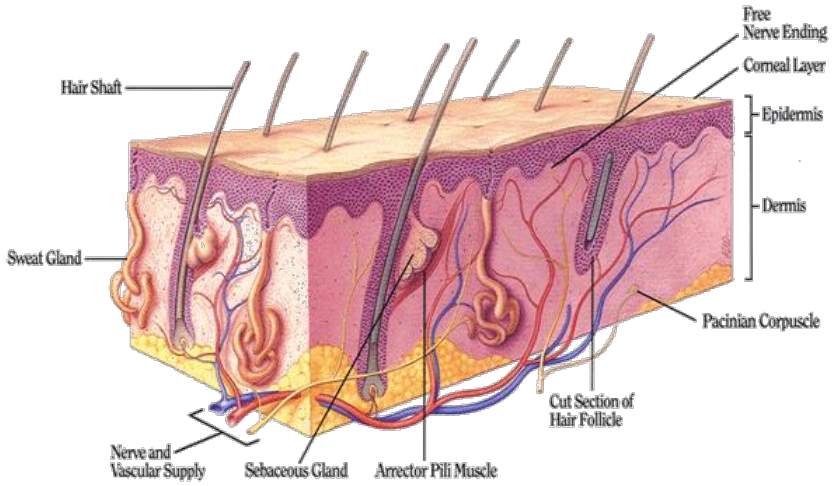

Figure 1.4: Structure of the dermis (reproduced from [40]).

The dermis is divided into two layers: papillary and reticular layer. The papillary dermis is the outermost part of the dermis in direct contact with the epidermis. It is irregular in shape with protrusions into the epidermis called papillae, containing the elastin and collagen fibers and also the lymphatic and blood vessels. In some of these papillae are found Meissner's Corpuscles, serving the sense of touch. In addition, there are connective tissue cells and inter-fibrillar gel in the papillary dermis. The reticular dermis is under the papillary dermis and is found to have fewer cells, relatively few blood vessels, dense collagen bundles and coarse elastin fibres and the Pacinian Corpuscles serving the sense of pressure such as poking the skin.

Basically, the components of the connective tissue are collagen, elastin, reticulin fibres and ground substance. Collagen is the most abundant protein in the body and forms the structural network of the skin. Collagen fibres are wavy structures that interlock with each other, providing firmness (tensile strength) and also allow the skin to be stretched without tearing.

Elastin fibres are similar to collagen but are more stretchable protein. They are loosely interwoven like a latticework and can be stretched and yet return to their original shape and length, providing elasticity and resilience to the skin. Together, collagen and elastin are the main proteins responsible for elasticity, tone and texture of the skin. These proteins give the skin its firmness, elasticity and strength. Reticulin fibres run in between and through the collagen and elastin fibres and help to support and keep these fibres in place. Ground substance is composed of complexes of proteins and sugars called mucopolysaccharides. They provide support for the connective tissue and have good water-binding abilities (Katz, M. and Poulsen, B.J., 1971).

The dermis also contains hair follicles, sebaceous glands, sweat glands, nerve endings, lymphatic vessels and blood vessels. The nerve endings provide sensory

perception for heat, pressure, pain and touch. They keep the body informed of changes in the environment and impending danger. Blood vessels provide the skin with nutrients and oxygen and remove waste products as carbon dioxide. They also play a vital part in temperature regulation and skin self-repair. Lymphatic vessels are important components of the body's immune system. They carry lymphocytes throughout the body and help defend the body against infection and other foreign invaders.

The depth of the dermis is about 3-5 mm in thick skin and is about 1-2mm in thin skin (Katz, M. and Poulsen, B.J., 1971).

1.1.4 The Hypodermis

Usually considered part of the skin, the hypodermis subcutaneous layer (see Fig.1.1) consists mainly of cells which produce and store fat, but it also contains blood vessels, sebaceous glands, sweat glands and arrector pili muscles for the hair. It acts as a shock absorber, protecting deeper structures, insulating against heat loss and also acting as an energy reserve. The layer thickness is variable from part to part, all over the body (Fuchs E., 2007).

1.2 Measurement Methods of Skin Hydration and TEWL using OTTER and AquaFlux

The two main techniques for skin measurement used in this project are Opto-Thermal Transient Emission Radiometry (OTTER) and the AquaFlux. In this chapter, these two techniques are discussed:

1.2.1 Opto-Thermal Transient Emission Radiometry Technique (OTTER)

Opto-thermal transient emission radiometry technique (Imhof, R.E., Birch, D.J.S,

1984) is a relatively new technique that can be used to study SC hydration (Bindra R M S, Imhof R E, 1994). Its main practical features of remote sensing, non-contact and non-invasive measurement makes it particularly attractive for *in-vivo* measurements. A schematic diagram of the technique is shown in Fig. 1.5 below.

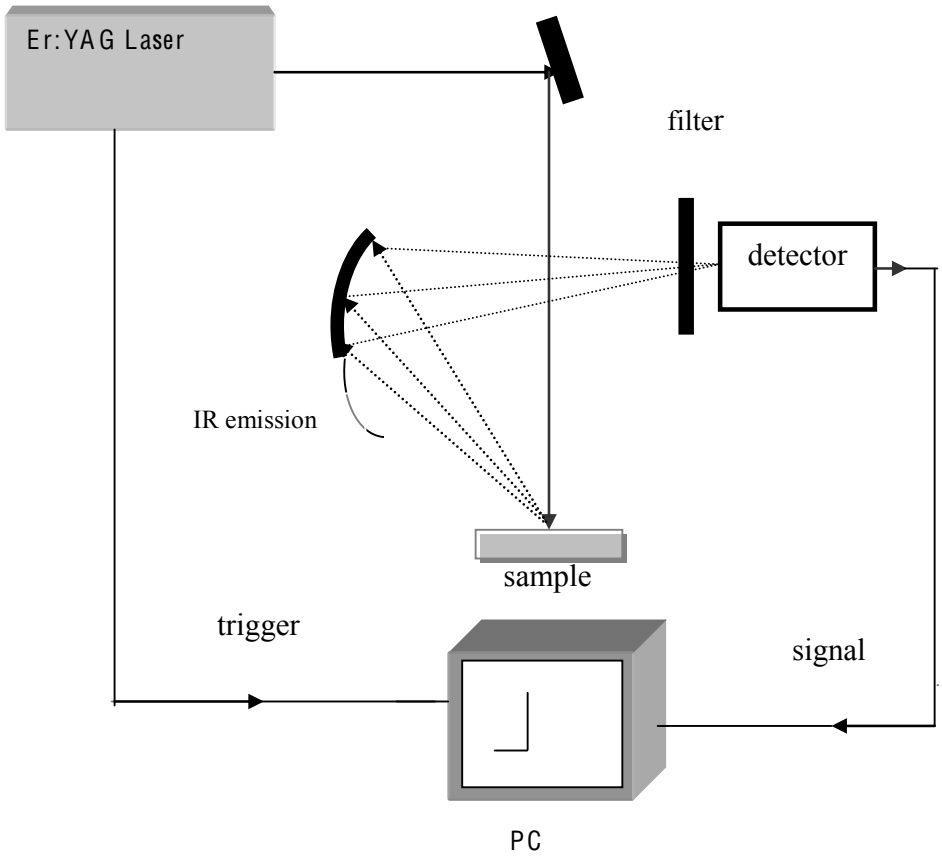

Figure 1.5: Schematic diagram of the Opto-Thermal Transient Emission Radiometry (OTTER).

An IR pulsed laser is used to heat a small volume of the sample, causing the temperature near the surface to jump to the order of a few °C and then decay back to ambient temperature. A high-speed detector senses the corresponding transient in thermal infrared emission. (Xiao P, Zheng X, Imhof R.E., Hirata K, McAuley W.J., Mateus R, Hadgraft J., Lane M.E., 2011)

The opto-thermal impulse response is related to the optical and thermal properties of the sample, namely: optical excitation absorption, optical emission absorption and thermal diffusivity.

1.2.2 AquaFlux

The term transepidermal water loss generally refers to the total amount of water vapour lost through the skin. However, TEWL is a true reflection of the SC barrier function only when there is no activity of the sweat glands. TEWL is a consequence of the fact that the skin is dry at its surface and wet at its base. Thus, a concentration gradient exists within the SC, which results in a continuing diffusion of water from within the body through the skin into the environment. If the diffusion of the water through the SC is assumed to be passive (Blank, I.H., Moloney, J, 1984), then TEWL values will be proportional to the gradient of water concentration within the SC.

TEWL measurements have wide applications including: cosmetics testing (to evaluate moisturiser efficacy, irritation and barrier destruction by soaps, detergents and solvents)(Loden M, Lindberg M, 1994), dermatology (to test skin damage, the effects of drugs and other substances on the skin (Serup J, 1994)), neonatal research (SC formation in premature infants (Edwards C, Marks R, 1994)) and in the textile industry (to examine occlusive effects of fabrics)(Akin F, Lemmen J, 1997).

The AquaFlux uses the patented Condenser-Chamber method for measuring water vapour flux in general and TEWL in particular. Figure 1.6 below shows a cut-out view of the AquaFlux chamber.

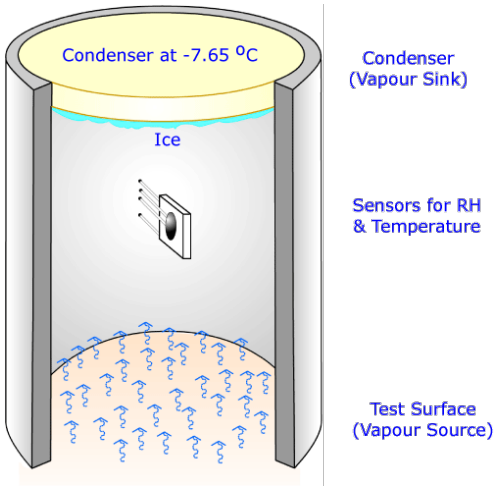

Figure 1.6: Cut-out view of the AquaFlux showing the closed chamber, condenser, sensor & the test surface. (Reproduced from [30])

The measurement chamber is a hollow cylinder whose lower end acts as a measurement orifice that is placed into contact with the test surface. Its upper end is closed with an aluminium condenser that is maintained below the freezing temperature of water by means of an electronic Peltier cooler (Xiao, P. and Imhof, R.E, 1998).

When in contact with the test surface, the chamber is closed and the air within it is protected from disturbance from ambient air movements. The condenser controls the humidity in the chamber independently of ambient conditions. It acts as a vapour sink by forming ice on its surface, thus creating a zone of low humidity in its immediate vicinity. By contrast, the test surface acts as a vapour source, creating a zone of higher humidity in its immediate vicinity. This humidity difference causes water vapour to migrate from source to sink by passive diffusion, leading to a linear distribution of humidity parallel to the axis of the chamber under steady conditions. The water vapour flux is calculated from measurements of this humidity gradient and Fick's first law[1] of diffusion (Imhof R.E., Berg E.P., Chilcott R.P., Ciortea L.I., Pascut F.C., 2002).

[1] Fick's first law relates the diffusive flux to the concentration under the assumption of steady state. It postulates that the flux goes from regions of high concentration to regions of low concentration, with a magnitude that is proportional to the concentration gradient (spatial derivative).

1.3 Introduction of the Chapters

This report is arranged into 8 chapters altogether. In this chapter, a general discussion was done on the skin mainly on the layers; Epidermis, Stratum Corneum, Dermis and Hypodermis. Subsequently, existing technologies measurement methods of skin hydration and TEWL using OTTER and AquaFlux were looked at.

In Chapter 2 a closer look is taken at the theory and techniques for skin measurement among others the optical sensors, radio frequency, thermal detection and capacitance. Then, a comprehensive look at existing capacitance & conductance based hydration measuring instruments is done. Finally the OTTER AquaFlux instrumentation is looked at in detail. The main findings of this chapter is that hydration of the skin can be measured using different instrumentation.

In Chapter 3, the theory of capacitance and its properties as an imaging medium is discussed in detail. Then, discussion focuses on the FPC-SMD capacitance kits used in the experiments for this report. Finally experiments and results of the use of the capacitance sensors are shown and this finding establishes the viability of the technology to be used as a hydration measurement instrument. Additionally, modifications that have been done to these kits to analyse skin images are also shown.

In Chapter 4, a comprehensive analysis of the capacitance sensor is undertaken; software techniques used in capturing the images, images processing techniques and data analysis. A specific program written in MATLAB to analyse the capacitance images data is discussed and its outputs are shown. To further strengthen the capacitance sensors readings, data showing comparison between AquaFlux and OTTER instrumentation is discussed. Co-relationships between capacitance sensor and AquaFlux and capacitance sensor and OTTER is shown.

Chapter 5 focuses on occlusion, moisturisers and other skin tests that have been carried out with the capacitance sensors. Measurements relating to 3D profiling, co-relation and quantified charts shows in detail how data from the capacitance images can be processed to show a variety of information rich data sets.

Chapter 6 is dedicated entirely on the study of scars and scabs using the capacitance sensor. Different types of scars are profiled using the capacitance sensor and then measured using the existing dedicated software written in MATLAB as discussed in Chapter 4.

Chapter 7 looks at RGB imaging and capacitance video imaging of the skin. Real-time video images are recorded of the skin. The main function is not only for measurements of the skin hydration but also for other materials measurements such as textile and membranes. Additionally an algorithm for skin location re-positioning was developed to find the exact location of the skin site on two different images.

Chapter 8 concludes this research report and looks at possible and additional work that will be carried our in the future.

With the conclusion of Chapter 1, Chapter 2 discusses the theory and techniques of skin measurement.

CHAPTER 2: SKIN MEASUREMENT TECHNIQUES

In non-invasive research methods of the skin surface, hydration quantification is an important area of study. At present, both OTTER and Aquaflux are *in vivo* skin measurements. Micro-relief of the skin surface holds vast amount of data when processed. The skin surface can be mapped and a topography of the surface created. On the most basic level, the surface can be compared with other samples to show consistency (or non-consistency) with an initial sample.

As discussed in Chapter One, one of the aims of this research is the measurement of skin surface hydration. In this chapter, a closer look is taken at the available techniques for skin measurement and the reasoning for selecting a particular technology for this research is explained.

2.1 Theory of Available Techniques

The following are some of the common techniques that could be used in skin measurement and quantification:

2.1.1 Optical Sensors

In an optical sensor a prism is used where a light source is reflected through the prism and the skin touches the prism on the second plane (direct in-line with the source light). As shown in Figure 2.1, the skin is illuminated and the optics lenses are used to focus the reflection into a camera. This image is passed on through a video signal to a frame grabber PCI/ISA card and the image is then stored in a computer.

Optical sensors are one of the most commonly available technologies used in fingerprint scanning. A similar concept with the same underlying principles is the use of a micro collimator. A micro collimator uses a LED to shine the skin surface. The resulting light reflected from the skin is passed through a group of tilted walls

fabricated with a multi-step etching process of silicon. The brightness of the skin image is adjusted and captured on a camera.

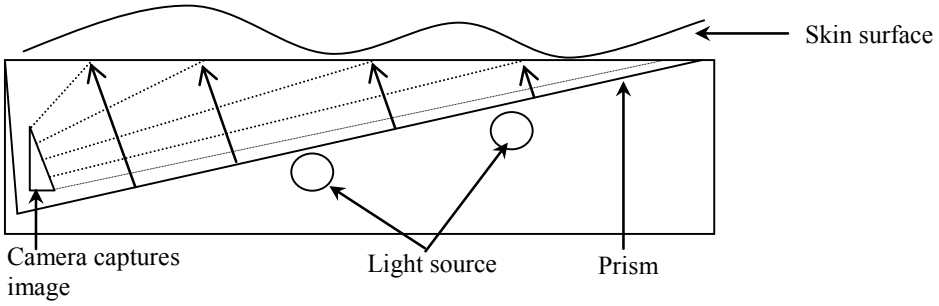

Figure 2.1: Diagrammatic layout of an Optical Sensor

Then, the skin relief[1] analysis can be done on the captured image. However, light source detection is frequently subject to moiré effect[2] and that skin is transparent to close and focused light (Creath K, Wyant J.C, 2002).

2.1.2 Radio Frequency

A low radio frequency (RF) signal is injected into the skin. The subsequent bouncing of the waves is then read by sensory array 'pixels' on a silicon panel that functions as tiny multiple antennas. The signal strength is dependent on the ridges and valley on the skin. The attenuation of the signal level is calculated by a sensory array and a skin image structure is produced.

Since there is minimal or no contact between the skin and the sensor, the skin remains relatively in its original form and the chances of occlusion[3] is minimised. Figure 2.2 shows the signal generator located on the left of the instrument which sends a radio frequency through the filter ring into the skin. The subsequent signal

[1] Is the overall pattern of the skin that allows the skin to move along with the limb movement and major surface parts of the human body.
[2] A pattern produced in optics due to two or more lines having approximately equal spacing. Commonly seen in camera pictures where group of lines appear as a solid coloured surface.
[3] Prolonged continuous contact with a surface results in the skin water being trapped in between the surface and the skin. This results in an increased reading in hydration measurements.

travels through the skin and moves towards the ground plane of the radio frequency instrument. The AC sensor detects the strength of the radio frequency.

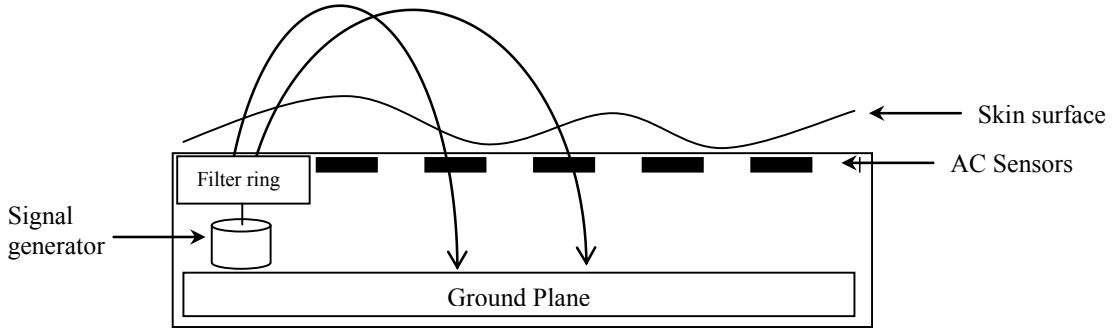

Figure 2.2: Diagrammatic layout of a Radio Frequency detector

2.1.3 Thermal Detection

In a thermal sensor, a small heating element is used to heat the skin surface and adjacent sets of thermal sensors are used to measure the heat reflected off the skin. Ridges and valleys of the skin surface will produce differential heat emission and the detectors will measure the differential heat gradient as patterns of the skin surface.

Initially, the skin passes over the heating element and the skin surface will be heated. An image of the skin surface is made based on the differentials in heat emission from the valleys and ridges of the skin surface.

Another type of thermal detector is a pyroelectric[4] detector. Here, a change in temperature will create a change in electrical polarisation. A current is only produced if there is a rise or fall in the temperature of the skin surface. If the surface temperature is constant, no current will be produced.

A major drawback of this technique is that consumption of power is high and accuracy drops in hot environments or hotter days. This is due to temperature

[4] Ability of certain materials to generate a temporary voltage when heated or cooled.

differential is not being as high between the ridges and the valleys (Dereniak E.L, Boreman G.D, 1998).

As shown in Figure 2.3, the charge plates generate heat and the resulting heat returns from the skin surface and is detected by the DC sensors.

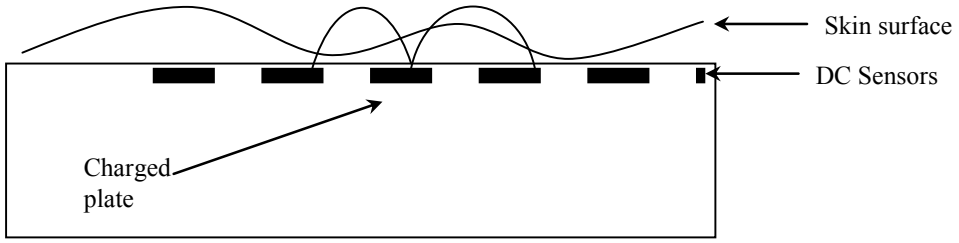

Figure 2.3: Diagrammatic layout of a thermal detector

2.1.4 Photo Imaging RGB Camera

The use of light that can be measured with photo imaging is another new technique in skin measurement. A photo image of the skin site is taken using a RGB digital camera and this image is the processed using special software to separate into red, green and blue filter. Then each colour change is measured to assess changes in the skin surface.

2.1.5 Capacitance Sensor

Capacitance is the ability to hold an electrical charge. The parallel plate capacitor is split and moved to a coplanar position; the fringing electric field will continue to create a field between the two plates.

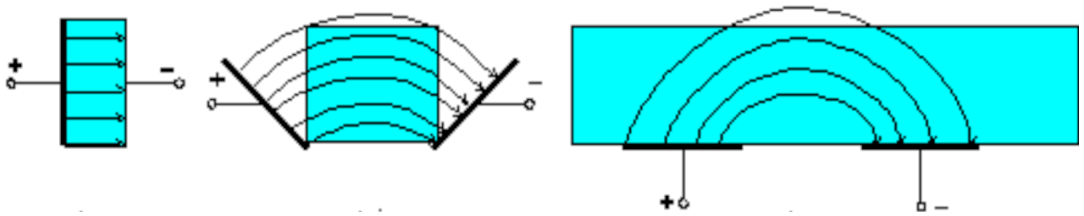

Figure 2.4: Two parallel capacitor plates are moved into coplanar position with fringing electric fields. Reproduced from [23]

Each set of a parallel plate is known as a cell and each cell in turn contains a feedback capacitance known as a sensor plate. A side-by-side array of alternating charged and sensor conductor plates are created. The alternating plates form the two plates of the capacitor, and any interference in between the plates causes the dielectric fields to change between the conductor plates. One set of conductor plates makes a single cell. The size of a single cell is larger than the width of one ridge[5] on the skin. The sensor detects variance in dielectric constants between the two to create the print image.

Each set of this conductor plates (or cells) contain their own electrical circuit thus making them tiny groups of semiconductor chips. The electrical circuit creates an inverting operational amplifier that alters the voltage being supplied. The altered voltage is relative to the inverting terminal input and the non-inverting terminal input is connected to a reference voltage supply and a feedback loop. This feedback loop is in turn connected to the amplifier output that includes two conductor plates. (H Singh, P Xiao, E.P Berg, R.E Imhof, 2006)

A set of these plates acts as a capacitor while the skin acts as the third capacitor plate. The varying distance between the capacitor plates and the skin changes the total capacitance of the capacitor. So, a space between the skin and the capacitor (e.g. valley) has lower capacitance compared to say a full contact with the skin (e.g. ridge). To scan the skin, the processor first closes the reset switch for each cell, which shorts each amplifier's input and output to "balance" the integrator circuit. When the switch is opened again, and the processor applies a fixed charge to the integrator circuit, the capacitors charge up. The capacitance of the feedback loop's capacitor affects the voltage at the amplifier's input, which affects the amplifier's output. Since the distance to the skin alters capacitance, a skin ridge will result in a different supply voltage output than a skin valley that is made up of micro-relief[6] structure.

[5] A ridge is an elevation of the skin mainly on the palms and soles and they correspond to one primary epidermal ridge (glandular fold) formed directly beneath each pore opening.
[6] A network of triangles and diamond shapes dotted with hair follicle and sebaceous gland openings. It allows the skin to expand or contract according to the overall skin movement.

The scanner processor reads this voltage output and determines whether it is characteristic of a ridge or a valley. By reading every cell in the sensor array, the processor can put together an overall picture of the skin map, similar to the image captured by an optical scanner.

Material with different dielectric properties can be in contact between these two plates. Water has high dielectric properties in comparison with other skin building blocks and therefore an increased presence of water can be measured.

Compared with thermal sensors, capacitor technology offers better image quality with a wider range of operating conditions.

Capacitive sensors are manufactured the same way as silicon materials and standard ICs. The low thickness of the ICs results in lower power consumption. For this research, the FPC-SMD Fingerprints Card Development Kit is used.

2.2 Existing Capacitance & Conductance based Hydration Measuring Instruments

2.2.1 Corneometer

The Corneometer measures changes in capacitance using a contacting probe that forms a capacitor with the skin under the test. Since the dielectric permittivity[7] of water is high compared with those of other skin constituents, the hydration of the skin in contact with the probe affects the capacitance sensed by the probe (Courage W, 1994).

The instrument is made up of a hand-held probe and a central processing unit, as shown in Figure 2.5 below.

[7] A measure of the ability of a material to resist the formation of an electric field within it.

Figure 2.5: Corneometer instrument and probe.

The probe head is made-up of a 7x7-mm size ceramic base with gold-plated conductor lines forming an interlaced grid pattern with spacing of 75µm and a surface area of 0.5 cm^2.

A view of the probe head with a cross section view is shown in Figure 2.6. The conductor tracks are protected by a separation glass where the test skin surface will be in contact. The glass cover is of 20µm thickness.

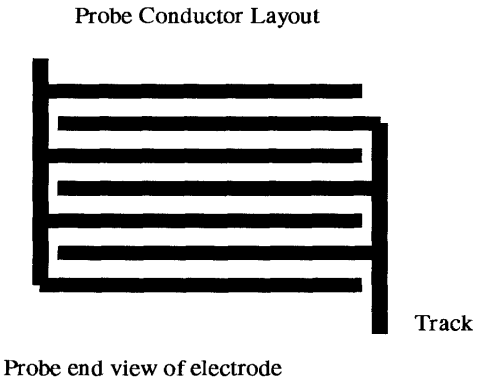

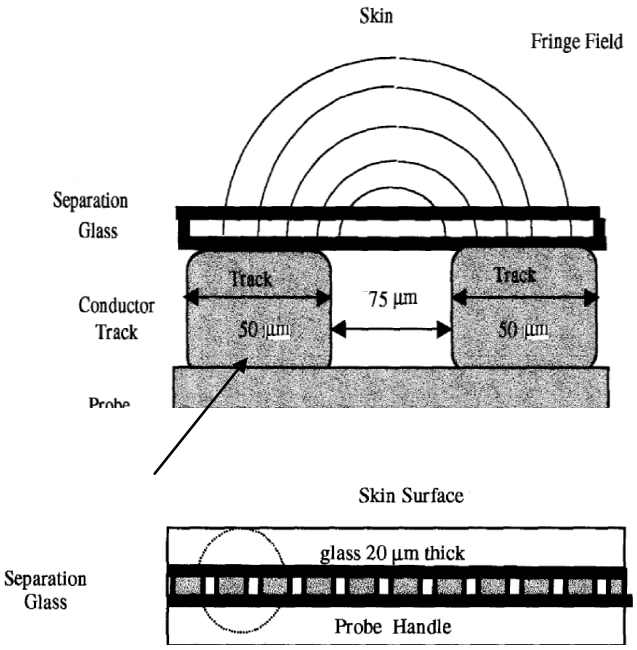

Figure 2.6: Corneometer probe head design; conductor track and cross section (reproduced from [40].

The track separation and the thickness of the glass cover limit the penetration depth of the electric field into the skin. Typically penetration depth is about 30-40 µm. This depth will result in both the hydration of the SC and part of the upper layers of the epidermis to be detected.

2.2.2 Skin Surface Hygrometer (Skicon)

The Skicon is not fully a capacitance measuring device. It uses use two techniques to measure the skin hydration. A 3.5 MHz capacitance and a separate conductance of the skin are measured by the probe (Courage W, 1994).

Figure 2.7: the Skicon is an instrument designed to measure skin hydration based on separate measurements of skin conductance and capacitance at 3.5 MHz (reproduced from [4]).

The probe consists of 2 concentric dry electrodes of 2 and 4-mm diameter, respectively, separated by a dielectric. The conductance between the electrodes is detected as changes of resonance voltage of a tuning circuit. When the probe is placed on the skin, a rapid initial increase in conductance occurs for a few seconds followed by a gradual increase, if the contact is maintained. The initial sharp increase reflects the hydration state of the skin, while the gradual increase is due to water build-up beneath the probe. It is claimed that there is a high correlation between conductance and SC hydration and according to the experimental results the hydration evaluated with this instrument seem to be those in the upper layers of the SC (Moseley H., 1985).

2.2.3 Nova Dermal Phase Meter (DPM)

The Nova Dermal Phase Meter shown in Figure 2.8 is another instrument that is designed to measure skin hydration using impedance[8] measurement from which capacitance is extracted.

[8] A measure of the total opposition to current flow in an alternating current circuit

The relationship between impedance and capacitance for this measurement is:

$$Z = (R^2 + (1/2\pi fC)^2)^{1/2}$$

where Z represents the impedance, f is the frequency of the applied alternating current, R and C represent the resistance and capacitance, respectively.

Figure 2.8: The Nova DPM with a probe head

The instrument is equipped with a probe with two concentric brass ring electrodes separated by an insulator (outer/inner ring ϕ 8.76/4.34 mm) as shown in Figure 2.9.

It measures impedance of the skin at pre-selected frequencies up to 1 MHz. Capacitance is calculated from the signal-phase delay. The values of the readout are in arbitrary units[9] of DPM. It is assumed that the penetration depth is limited to the upper part of the SC by the AC frequency and the geometry of the probe (Distante F, Berardesca E, 1995).

[9] A relative unit of measurement that shows the ratio of quantities based on a predetermined reference of measurement. Normally symbolised as AU or a.u.

Figure 2.9: View of the two concentric brass rings separated by an insulator.

2.2.4 The Fingerprints Card Sensors

The Fingerprints card sensor is an existing technology that allows for the detection of fingerprint ridges and valley using capacitance sensors. It is now a commonly used technology in airports, as a security check and in a multitude of companies where personnel access is controlled.

2.3 Photo Imaging Camera

For this research, the camera used is a Photo Physics Research LSBU camera model SONY DSC-W55. The camera has a 7.2 Mega Pixels with 3X optical zoom shown in Figure 2.10.

Figure 2.10: View of the SONY DSC-W55 camera used.

It also has a dedicated Dermlite II Epiluminescencemicroscopy light lamp that allows the skin surface to be illuminated for the image to be taken as shown in Figure 2.11.

Figure 2.11: View of the SONY DSC-W55 camera Dermlite II Epiluminescencemicroscopy light lamp installed.

2.4 Electrical Measurements

The technologies discussed in this chapter rely mainly on the dielectric constant or the lack of it in the keratin[10] layers and epidermal lipids[11]. Since the dielectric constant of stratum corneum is relatively low, the measurements are reliant mainly on the presence of water on the surface of the stratum corneum. The greater the water contents in the stratum corneum, the larger the dielectric constant.

Since the skin is the dielectric material in capacitance measuring, there is a proportional relationship between the skin and the dielectric constant. There will be varying degrees of reading based on the state of hydration of the skin.

In practice, owing to the absence of physical significance of this unit of measurement, this technique is confined to the measurement of variation in stratum corneum hydration between initial and final states (before and after).(Baran, Maibach, 2004)

2.5 OTTER Instrumentation

Opto-Thermal Transient Emission Radiometry (OTTER) is a form of infrared remote sensing technique; it uses a pulsed (or modulated) laser as heat source to heat up the sample and fast infrared detector to detect the consequent increase of blackbody radiation. OTTER is a very important means of Nondestructive Evaluation (NDE), which has been widely applied in industry and research (Imhof, R.E., Birch, D.J.S, 1984), such as

- Measurement of thermal properties
- Measurement of optical properties
- Measurement of thickness
- Measurement of thermal resistance

[10] A tough, insoluble protein substance that is the chief structural constituent of hair, nails, horns, and hooves.
[11] Any of a group of organic compounds, including the fats, oils, waxes, sterols, and triglycerides, that are insoluble in water.

- Material characterisation
- Flaw detection and characterisation.

The main advantages of OTTER are

- Remote sensing
- Non-contact, non-destructive
- Low probing energy
- Small probing area
- Spectroscopic in nature
- Direct measurement
- Signals related to sample's fundamental properties
- Unaffected to the geometry and movement of sample
- Quick and convenient to use
- Work on arbitrary surface.

The experiment is done in a controlled manner by conducting the experiments in a room with controlled room temperature and relative humidity.

2.5.1 Measurement Method

OTTER measures changes of heat radiation emitted by a sample after momentary near-surface heating by a laser pulse (Xiao P, Cowen J A, and Imhof R, 2001). Figure 2.12 shows a schematic diagram of OTTER apparatus. A Q-switched pulsed laser is used as the excitation source. The absorption of the laser in the sample causes heating in the near-surface region.

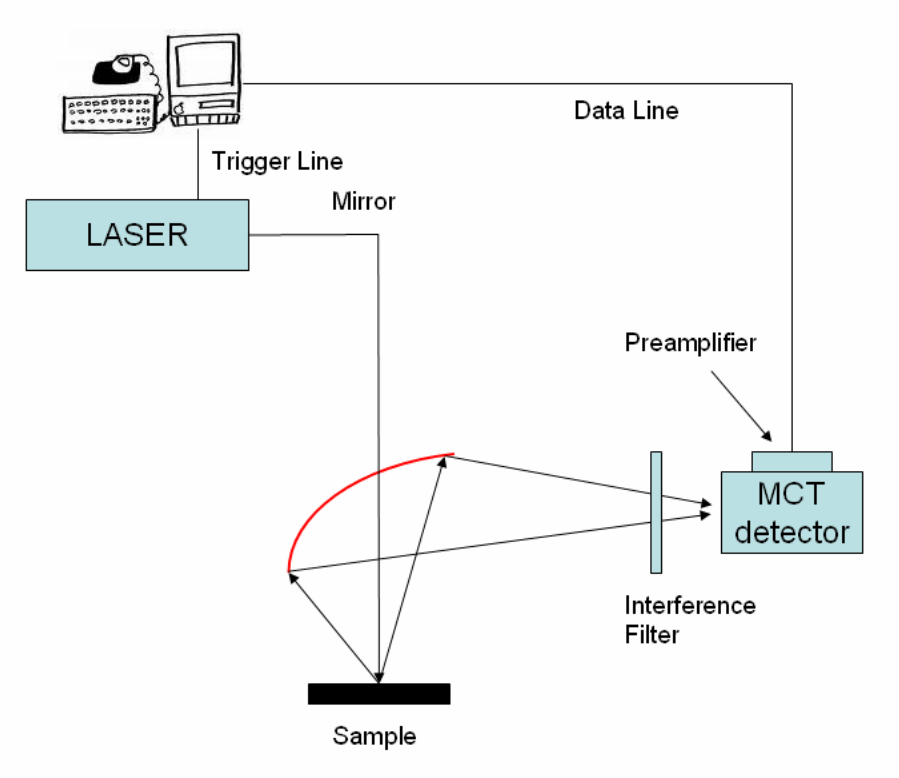

Figure 2.12: Diagrammatic view of OTTER. Reproduced from [7]

Heat radiation, in the mid-infrared ~5-15µm wavelength region is focused by an aluminium ellipsoidal mirror from the sample onto a high speed, liquid nitrogen cooled Mercury Cadmium Telluride (MCT) detector, whose signal is captured by a digitising oscilloscope.

A PC, linked to the transient recorder as digital oscilloscope through a high-speed parallel interface, is used for signal averaging, data storage, display and analysis.

A typical measurement consists of an average of 100 transients, collected at a laser pulse repetition frequency of ~4Hz. Signal averaging is essential to give adequate signal to noise ratios without damaging delicate samples. Interference filters are used to select narrow spectral bands within the black body thermal emission envelope for detection. For stratum corneum hydration measurements, interference filters of 6.05µm and 13.1µm transmission wavelength are normally used. At 6.05µm wavelength, strong absorption bands of water and amide coincide, whereas at 13.1µm wavelength, water is the only strong absorber. (Imhof, R.E., Birch, D.J.S, 1984)

The collected data from the OTTER is stored as individual files. One file representing a certain amount of readings is passed as a binary format.

2.6 AquaFlux Instrumentation

As explained in chapter 1, AquaFlux is an infrared remote sensing technology for non-contact and non-destructive surface analysis of arbitrary samples. Its existing application is measuring skin hydration, skin pigments, trans-dermal[12] drug delivery, thermal diffusivity and paint coating thickness. Its main benefits are in that it is a surface technology resulting in easy depth profiling, short measurement time, insensitive to colour and spectroscopic in nature. A normal configuration of AquaFlux consists of the below components:

1) Hand-held probe
2) Base unit
3) Data cables
4) Power supply
5) Software
6) Accessories

The AquaFlux relies on an "Active" closed chamber based on Nilsson's diffusion gradient measurement principle, the main difference being that it involves the continuous removal of water vapour from the chamber using a condensing surface opposite the measurement orifice.

2.6.1 Measurement Method

The AquaFlux uses the patented condenser-chamber method for measuring water vapour flux. Figure 2.13 shows the schematic diagram of the AquaFlux measurement chamber.

[12] Supplying a medication in a form for absorption through the skin into the bloodstream

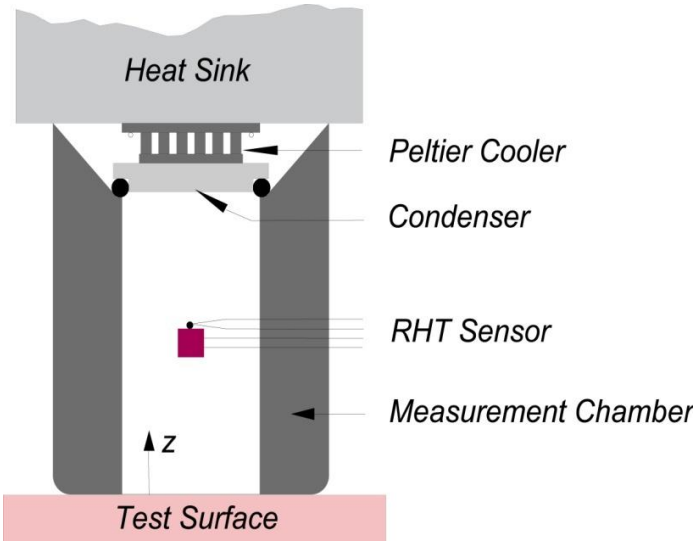

Figure 2.13: Cut-out view of the AquaFlux condenser-chamber. Reproduced from [16]

Looking at the above Figure, the lower bottom is open to contact with skin surface that will need to be measured. The upper end is sealed with an aluminum condenser and the temperature here is maintained at a constant -13.4 °C by means of a Peltier cooler and associated heat sink. A peltier cooler is a cooler that uses a peltier element (Thermo Electric Cooler-TEC). Peltier coolers consist of the peltier element itself, and a powerful heat-sink/fan combination to cool the TEC.

When the chamber is brought in contact with the skin surface, the chamber is sealed and the air within it is protected from disturbance from ambient air movement. Due to the internal dimensions of the chamber being very small, natural convection and other bulk air movements are brought down. In fluid dynamics terms, this requires the Rayleigh Number[13] to be below the critical value for its geometry. Under these conditions, passive diffusion remains the only transport mechanism for the water vapour entering the chamber (Imhof RE, Berg EP, Chilcott RP, Ciortea LI, Pascut FC, Xiao P, 2002).

[13] In fluid mechanics, the Rayleigh number for a fluid is a dimensionless number associated with buoyancy driven flow (also known as free convection or natural convection). When the Rayleigh number is below the critical value for that fluid, heat transfer is primarily in the form of conduction; when it exceeds the critical value, heat transfer is primarily in the form of convection.

The condenser controls the absolute humidity in the measurement chamber independently of ambient conditions. It acts as a vapour sink by forming ice on its surface, thus creating a zone of low humidity in its immediate vicinity. By contrast, the test surface acts as a vapour source, creating a zone of higher humidity in its immediate vicinity. This humidity difference causes water vapour to migrate from source to sink by passive diffusion, leading to an approximately linear distribution of humidity parallel to the axis of the chamber under steady conditions. The water vapour flux is calculated from measurements of this humidity gradient and Fick's first law of diffusion (Kamaruddin H.D, Koros W.J, 1997).

In the AquaFlux, the humidity immediately adjacent to the condenser is calculated as the thermodynamic equilibrium value for ice at the temperature of the condenser. The humidity gradient is determined from this value, together with the readings of RH & temperature from the sensor combination approximately half-way between the condenser and the measurement orifice.

2.7 OTTER/AquaFlux Experiment Results

One of the major functions of skin is to prevent the loss of body fluids. In general, water is lost in two ways, by diffusion and by sweating. However, at temperatures below 29°C, few sweat glands are active, therefore only diffusion plays an active role in the water loss through the Stratum Corneum. Normally, the water distribution within the Stratum Corneum is determined by a dynamic equilibrium with wet and dry boundaries respectively at the air and epidermis interfaces. Water continuously diffuses through the Stratum Corneum, driven by this water concentration gradient. The rate of water loss is determined by the concentration of water in the adjoining epidermis and the external environment, the diffusivity of water in the Stratum Corneum and its thickness.

This chapter presents the practical results gained from doing experiment on six different locations on the forearm mainly the bottom of hand, top of hand, bottom of finger, top of finger, lower arm and upper arm using the OTTER. From this experiment, two types of measurements are derived being the Hydration Gradient and the Surface Hydration.

A second experiment is done using the AquaFlux that looks at the TransEpidermal Water Loss (TEWL).

2.8 OTTER Experiments

2.8.1 Surface Hydration Measurement

Surface hydration is lowest on the bottom of the hand and highest on the upper arm. There is a gradual increase in the hydration level in between the lower hand and the upper hand, but the increase between the top of the finger and the bottom of the finger is marginal. These results are shown in the Figure 2.14.

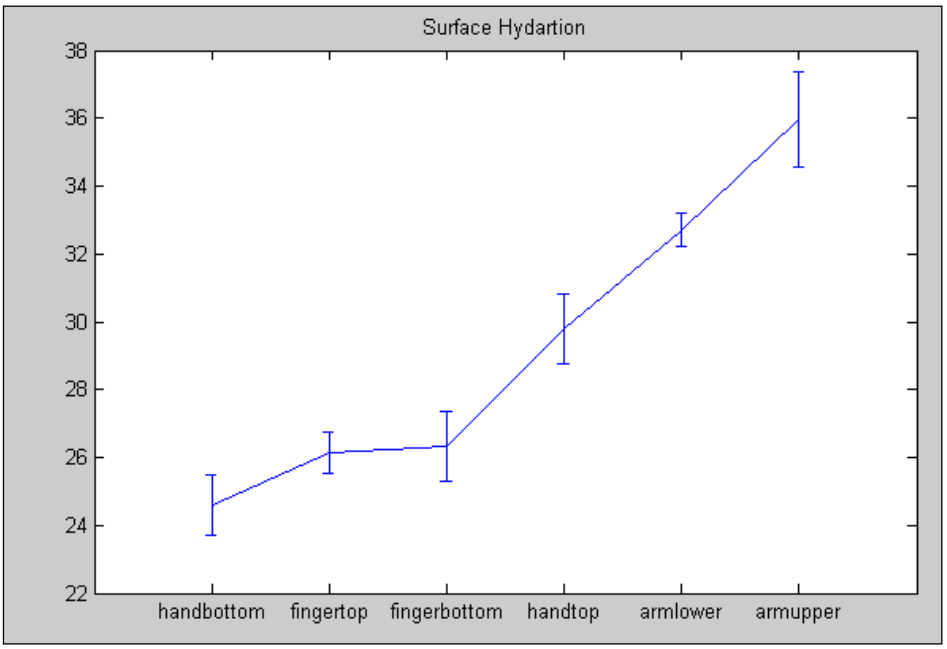

Figure 2.14: Surface hydration measurement of 6 locations of arm.

2.8.2 Surface Hydration Gradient Measurement

Gradient is the rate of change with respect to distance of a variable quantity, as temperature or pressure, in the direction of maximum change and hydration gradient shows the change in relation to the hydration level from the skin surface. The result for this test was derived from six different locations on the skin surface and the hydration gradients for the six different locations are shown in comparison to one another. These results are shown in the Figure 2.15. The subject is an oriental male aged 25 to 30 years. Five measurements were repeated for each of the site. The hydration gradient is lowest on the bottom hand and highest on the lower arm.

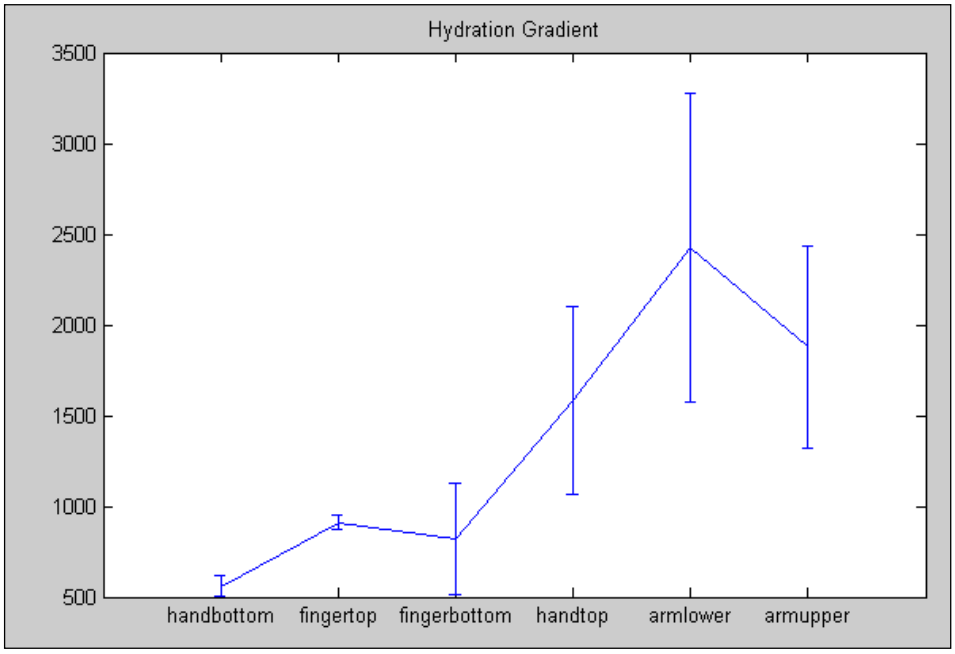

Figure 2.15: Hydration gradient measurements of 6 locations of arm.

2.9 AquaFlux Experiment

2.9.1 Trans-epidermal Water Loss Experiment

As discussed in point 1.3, water loss from the skin surface is measured in a chamber and this measurement is characterised in comparison in time to produce the chart in

Figure 2.16. For this experiment immersive hydration was done on an Asian volunteer's right hand middle phalange index finger for 10 minutes. Then after patting down the finger, measurements were done with the AquaFlux probe over a period of six minutes with an average time interval between readings of one minute. Average ambient temperature is 29.93^{0}C and average relative humidity is 36.57%.

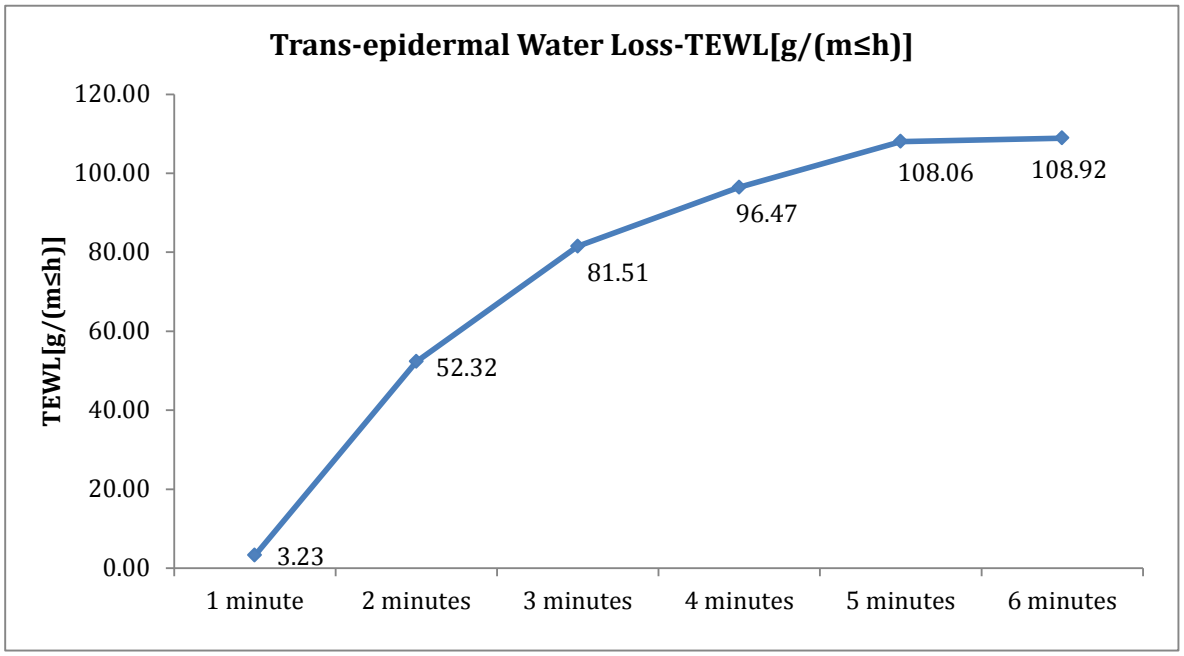

Figure 2.16: Trans-epidermal Water Loss from a hydrated index finger.

The trans-epidermal water loss between the first and second minute is 0.005% and increases steadily to 0.025% from the second to third minute, 0.163% from the third to fourth minute and slows down from fourth to fifth minute at 0.105% and 0.090% from fifth to sixth minute.

This test shows the gradual loss of water as measured by the AquaFlux.

2.10 Conclusion and Findings

In this chapter, existing technologies used in hydration measurement are discussed. It shows that there are many ways to measure hydration on multiple types of surfaces. Every measurement instrument has its own strength and weakness.

Due to limitation of the size of the probes and measurement methods, these technologies are unable to re-create a mapped image of the skin and thus are unable to show a visual view of the test skin site. An imaged map of the skin will better represent a cross section of the skin site and visually show the look of the skin.

Therefore, this research will look at developing and modifying existing capacitance sensor technologies to create a larger surface area capacitance sensor where more information of the skin can be analysed and a richer information base can be manipulated to gain more understanding of the skin sites.

The methods of OTTER and AquaFlux are some of the most accurate techniques to measure skin hydration and TEWL. However, due to limitation of portability in the case of the OTTER and speed in the case of AquaFlux, this research is developing a new technique employing capacitance sensors technology as a simpler, portable and quicker alternative where high precision is not a major requirement.

CHAPTER 3: SKIN IMAGING WITH CAPACITANCE SENSORS

Differential amounts of hydration in the skin can be recorded through a dielectric field that may be measured using the capacitance sensor (Leveque JL, 2003). Material with different dielectric properties will have an effect on the dielectric field. Since water has high dielectric properties in comparison with other skin building blocks, an increased presence of water can be measured using capacitance sensors.

3.1 Theory of Capacitance

Commonly, a capacitor is used to store (hold) this electrical charge. A capacitor is constructed of two conductive parallel plates separated by a non-conductive medium or the dielectric region. Assuming that the parallel plates are charged with +Q and –Q and that the voltage between the plates is V, the capacitance can be shown as:

$$C = \frac{Q}{V}$$

The unit of measurement used for measuring capacitance is farad, where 1 farad is equal to 1 coulomb per volt (Stauffer L, 2008).

The capacitor stores energy which is equal to the energy required to charge it and thus electrical energy is not dissipated.

If a small element of charge (dq) is moved across the two plates against the potential difference V=q/C; it will require the amount of energy dW.

$$\mathrm{d}W = \frac{q}{C}\mathrm{d}q$$

This energy fluctuates depending on the interference of the dielectric medium. (Adkins C.J, 2008)

3.2 Capacitance Imaging

Capacitance sensors instrumentation is a complex semiconductor device consisting of transistors, resistors and capacitors.

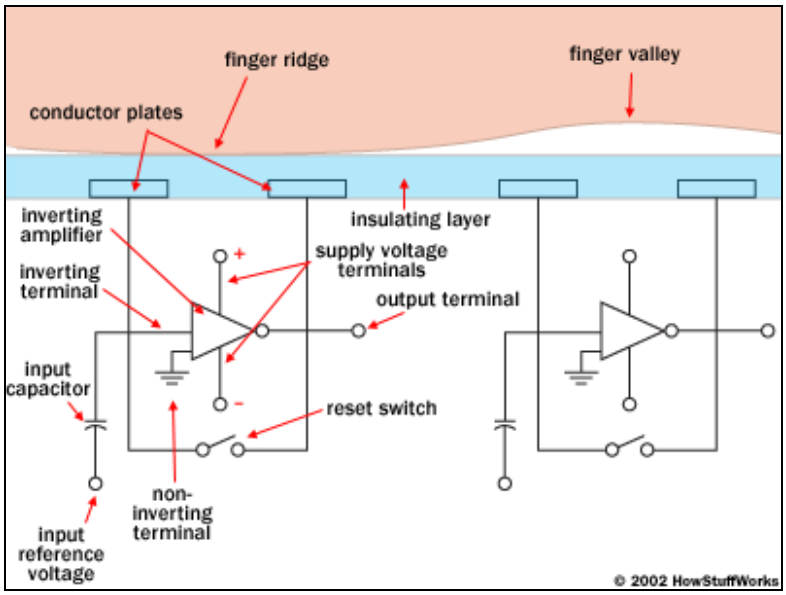

Figure 3.1: Diagrammatic view of a capacitive sensor with two semiconductor chips. (Reproduced from [24])

As shown in Figure 3.1, the conductor plates in the co planar position are connected to an integrator, an electrical circuit built around an inverting operational amplifier.

The inverting amplifier alters one current based on fluctuations in another current. Specifically, the inverting amplifier alters a supply voltage. The alteration is based on the relative voltage of two inputs, called the inverting terminal and the non-inverting terminal. In this case, the non-inverting terminal is connected to ground, and the inverting terminal is connected to a reference

voltage supply and a feedback loop. The feedback loop, which is also connected to the amplifier output, includes the two conductor plates (Webster's Quotations, 2008).

These two conductor plates form a basic capacitor, and the surface of the skin acts as a third capacitor plate, separated by the insulating layers in the cell structure and, in the case of the skin micro-relief valleys, a pocket of air (Walker C, 1990). Varying the distance between the capacitor plates changes the total capacitance (ability to store charge) of the capacitor. Due to this behaviour, the capacitor in a cell where there is higher moisture content underneath will have a greater capacitance than the capacitor in a cell under a valley with low or no moisture content.

Each amplifier's input and output to "balance" the integrator circuit. When the switch is opened again, and the processor applies a fixed charge to the integrator circuit, the capacitors charge up. The capacitance of the feedback loop's capacitor affects the voltage at the amplifier's input, which affects the amplifier's output.

Since the distance to skin and its moisture content alters the capacitance, a micro-relief will result in a different voltage output than where the skin is having full contact with capacitance sensor surface. A disturbance in the supply level is caused by the disturbance of the skin resistance that in turn causes a change in the current readout.

The possible range of change that can occur can be 0 to 255 corresponding to a gray-scale from white to black. A 255 gray-scale denotes no disturbances to the dielectric passage and allowing a complete black gray-scale to be registered. A 0 gray-scale will denote a complete restriction to the dielectric passage and

allowing a complete white gray-scale to be registered (Leveque, J.L, Querleux, B, 2003).

The scanner processor reads this voltage output and determines whether it is characteristic of a ridge or a valley. By reading every cell in the sensor array, the processor can put together an overall picture of the fingerprint, similar to the image captured by an optical scanner.

A large group of capacitors and their sensors are placed in an array to form a large imaging sensor. Each couple of capacitor plates acts as a single pixel than can be read and stored along with its neighbouring capacitor plates.

A single cell capacitance surface and the dielectric signal path is shown in Figure 3.2.

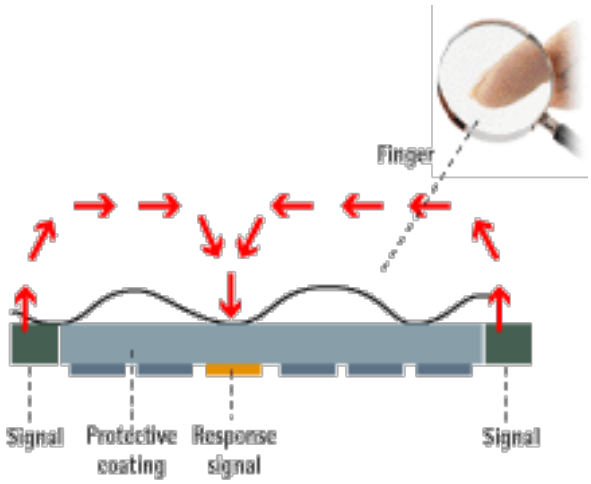

Figure 3.2: Diagrammatic view of a single cell capacitance surface and the dielectric signal path.

Capacitance sensors are manufactured the same way as silicon materials and standard ICs. The low thickness of the ICs results in lower power consumption.

For this research, the FPC-SMD 5410 Fingerprints Card Development Kit, the FPC6410 Fingerprints Card Development Kit and the FUJITSU's MBF-200 Capacitance Sensor are used.

3.3 The FPC SMD 5410 Development Kit

The FPC SMD 5410 contains a FPC SMD array swipe sensor chip, a processor board, a connecting cable, and a main development board. The swipe sensor is mounted on the processor board, connected through a 10 pin, 0.5mm pitch, and ZIF connector. The processor board, which is connected to the main development board through a connecting cable, has the ASIC (Application Specific Integrated Circuit) for biometric operations and ATMEGA162 for external communications. On the main board, there is an incoming 5V power supply and a serial port, for connecting the board and the computer through RS232 interface.

Extremely weak electrical charges are created, building a pattern between the finger's ridges or valleys and the sensor's plates. Using these charges the sensor measures the capacitance pattern across the surface.

A protective coating helps the FPC sensors to withstand and sustain static electricity (ESD) and general wear and tear.

The FPC-SMD has some inherent benefits. Method of capturing images used by the Fingerprint Cards is called the active or reflective method, and it brings several advantages.

1. Using the programmable logic internal to the capacitive sensor configuration, it is possible to read off and adjust the sensor reception to different skin types and conditions.

2. Another important benefit is that the strengthened signal communications between the fingerprint surface and the sensor plates allows the use of a strong,

protective coating layer, up to 25-30 times thicker on the sensor surface. This enables Fingerprint Cards to sustain up to and above the requirement for 15kV electrostatic discharge (ESD), as well as wear cycle tests for more than one million touches to the sensor.

3. For communications, a standard serial port (FPC5410) and a USB port (FPC6410) is included.

4. The FPC5410 has a surface area of 32 x 152 pixels[1] while the FPC6410 consists of 152 x 200 pixels.

5. Finally, the FPC-SMD can be controlled by using built-in hardware based commands. This does not limit the use to a specific programming language thus making it easier to program in a language of choice.

3.3.1 Modifications of the FPC-SMD 5410 Development Kit

For the initial purpose of this research, the FPC-SMD 5410 Fingerprints Cards Development Kit was purchased and used in the initial studies to determine the feasibility of using a capacitance sensor as a means of measuring skin hydration. Some modifications were necessary to allow a greater usability for skin imaging.

The sensor was re-mounted on a handheld probe and an additional flex data cable was used to lengthen the distance from the kit board to the sensor as seen in Figure 3.3. This allows a movable distance of about 3 feet from the kit board to the subject skin site.

Additionally, the capacitance sensor head is inserted through a polyethylene sponge to allow flexible movement on uneven skin sites. The surrounding head

[1] A picture element is the smallest addressable screen element or point in a display. The capacitance sensor can show an 8-bit image gray-scale point from 0 to 255 possible gray shades.

of the capacitance sensor is covered with a rubber tube to protect the electronic circuit board from dust, oil and water as shown in Figure 3.4.

Figure 3.3: FPC 5410 capacitance sensor mounted on a probe head.

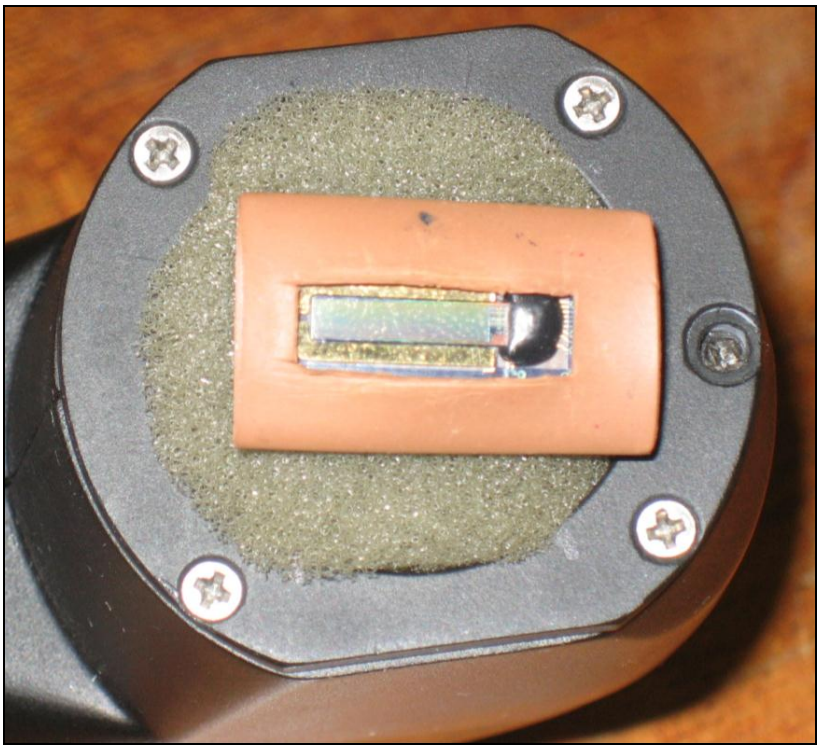

Figure 3.4: close up of FPC 5410 capacitance sensor mounting with cladding of a rubber tube to protect the PCB board.

3.4 Results using FPC-SMD 5410 Development Kit

The FPC-SMD 5410 development kit has been used for measuring the skin surface hydration. These tests were aimed to investigate the FPC-SMD 5410's capability of measuring the difference between a normal skin state and subsequently hydrated over time. To diminish possible scatter of data, primary experiments were performed on the same skin sites.

All the measurements are performed under normal ambient laboratory conditions, i.e. 21°C, and 40% relative humidity (RH), and all volunteers are acclimatised in the laboratory for 20 minutes prior to the measurements being done. Three different types of experiments were done on the skin surface mainly to test the device capabilities in measuring different types of hydration:

1. Immersive Hydration – where skin is immersed in water for a period of time before being tested.
2. Moisturiser Test – moisturiser is introduced to normal skin and then tested.
3. Occlusion – where normal skin is constantly kept on the device for a period of time without removing it from the device surface. At certain time intervals, images are captured.

3.4.1 Hydration Immersion Test Method

Method

The first test is done on the distal phalange of left index finger of a male Asian volunteer before dipping in water, and then dipping in water for 20 minutes.

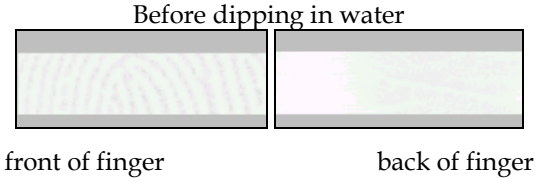

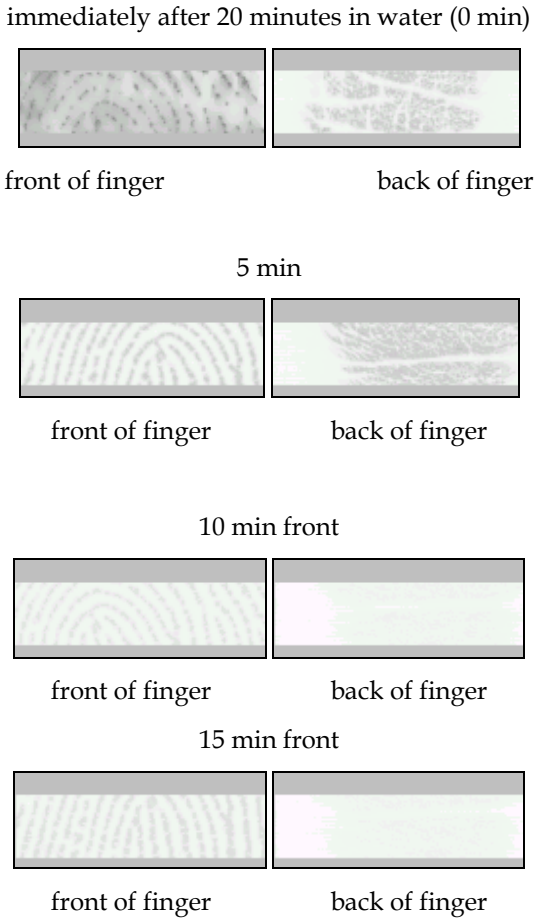

Figure 3.5: Images showing pre-hydrated and hydrated skin over time.

The first column of images in Figure 3.5 are showing the front of finger (fingerprints) and the second column of images are showing the back of finger where micro lines are the main 'landscape'.

The first two images on the top are before dipping in water. Subsequently, the index finger is dipped in water for 20 minutes and then patted dry with cotton and tested. Then at intervals of 5 minutes, a new image is captured. Between capturing the images, the finger is lifted off the device.

Results

An initial visual comparison shows that an increase in water presence can be seen in both the front and back of finger by variations of darkness. This is clearly visible from the second row images showing an increased presence of water level on the skin can be seen as a darker shade.

After 5 minutes, the shade intensity is reduced and after 10 minutes, it has nearly returned to its original (pre water dipping) condition. Based on prior tests done using the Aquaflux and the OTTER instrumentation, it is understood that the skin should return to its pre-soaking state after a period of time. However this is dependent on the age, type and properties of the skin of the subjects tested in these experiments.

3.4.2 Moisturiser Application Test

Method

A second test was done on the distal phalange of the right index finger of a male Asian volunteer with application of moisturiser.

A water-based moisturiser was applied to the skin and then wiped for any residual moisture. In this test, skin surface is compared as before and after the moisturiser only and no comparison is done over time.

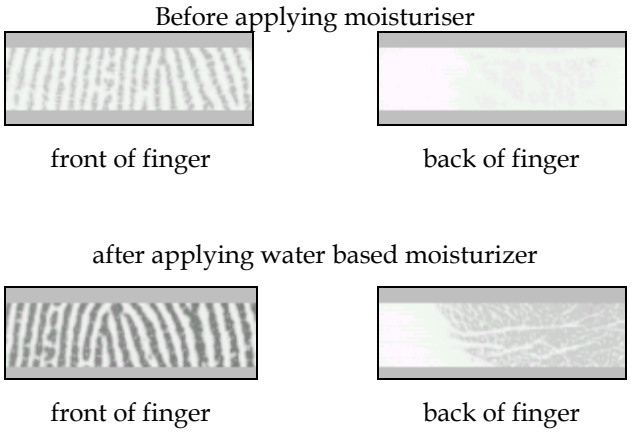

Figure 3.6: Images showing pre-moisturiser and moisturised skin

Results

An increase in intensity of gray is visible as compared to before application of moisturiser as seen in Figure 3.6. Micro-relief of the front of the finger is visible after application.

3.4.3 Occlusion Test

Method

The third test was done on the middle front phalange of the index finger of a female Caucasian volunteer. This test requires the finger to be maintained in the same position on the device for a period of time in order to allow occlusion and to be able to capture images with increased water presence.

The finger is kept stationary on the device and an image is taken every 5 minutes for 20 minutes.

Results

The result shows an increase presence of water over time. This increase is visible in the darkening of the images seen in Figure 3.7.

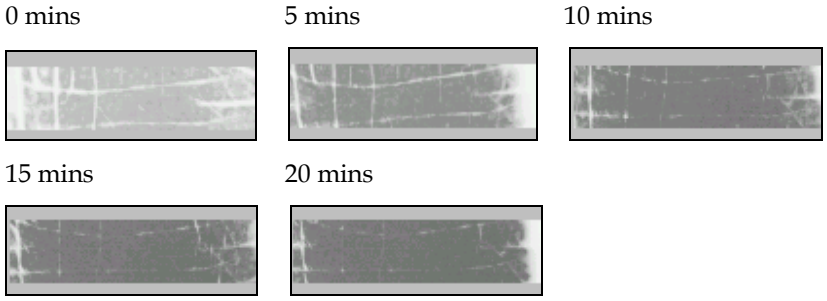

Figure 3.7: Images showing occlusion of skin surface over time

3.4.4 Additional Tests on non-Live Skin Surfaces

To further test the capability of the capacitance sensors reading, additional tests were done on non-live skin.

For the first test, the properties of snake skin's hydrophobic[2] and hydrophilic[3] behaviour were tested. The outer surface is scaly & hydrophobic while the inner surface is hydrophilic (Imhof RE, Xiao P, Berg EP, Ciortea L, 2006).

3.4.4.1 Snake Skin

An initial test is done to test if shed snake skin when hydrated can be analysed by capacitance sensors. The snake skin is obtained from PhotoPhyiscs Research Centre, London South Bank University and the source of the skin is of the Brazilian snake.

Method

A first measurement is done on dry snake skin with a thickness measuring 0.12mm. The tests are done at room temperature of 23°C and a relative humidity of 47%.

The snake skin is then submerged in water for 10 minutes. A reading is taken from the outer skin surface (hydrophobic) and under-skin surface (hydrophilic).

Results

The image results are shown in Figure 3.8 where a prominent water increase is visible in the hydrophilic skin surface compared with the hydrophilic surface.

Prior to hydration, the snake skin is completely dry thus registering only a low gray-scale (white) image.

[2] Hydrophobic – material (live or non-live) that have strong affinity or attraction towards water.
[3] Hydrophilic –material (live or non-live) that resist or having a lack of affinity towards water.

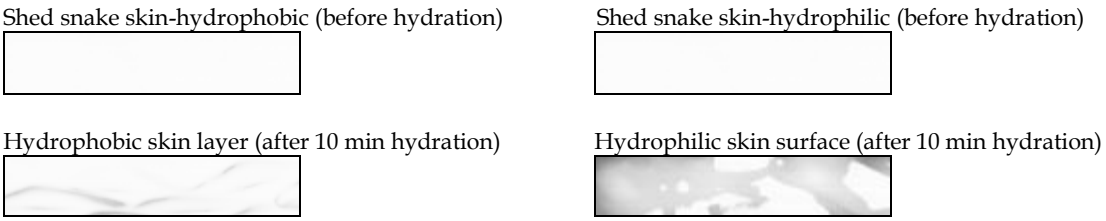

Figure 3.8: Image of hydrophobic and hydrophilic snake skin before and after hydration for 10 minutes.

3.4.4.2 In-vitro Stratum Corneum

These tests were done on an in-vitro[4] human Stratum Corneum (SC) sample which was then hydrated. The thickness of the SC is about 0.02mm. The tests are done at room temperature of 25^{o}C and a relative humidity of 48%. The FPC 5410 is used for these experiments.

Method

The Dry SC is dehydrated in a dehydration chamber for 48 hours prior to the test. Dry SC is measured first and then is submerged in water for 30 minutes. The SC is then patted dry and a measurement is taken. Consequently, measurements are taken every 2 minutes for 12 minutes and the images are reproduced in Figure 3.9.

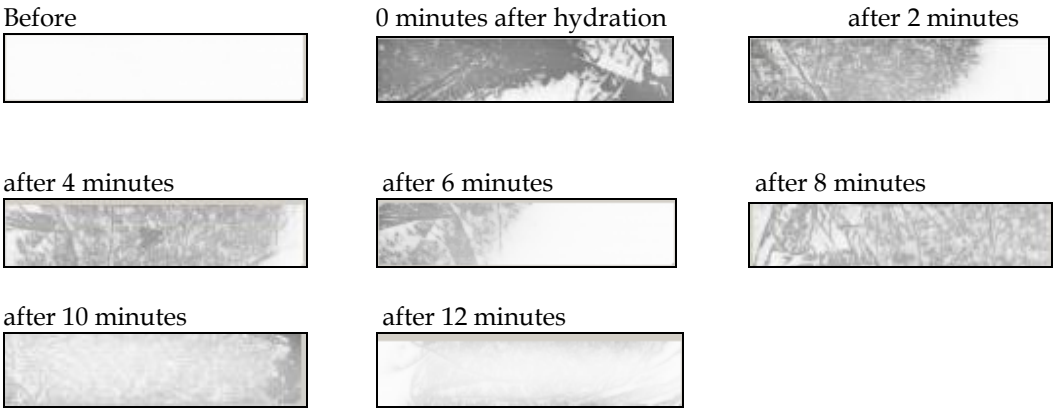

Figure 3.9: Image of dry stratum corneum before and after hydration for 10 minutes.

[4] studies conducted using components of an organism that have been isolated from their usual biological context in order to permit a more detailed or more convenient analysis than can be done with whole organisms.

Results

As Figure 3.10 shows, the pre-hydration has a lower gray-scale average at 37.56. After hydration, the hydration has increased to 92.48 and subsequently drops over time to a value lower than the pre-hydrated state at 33.67.

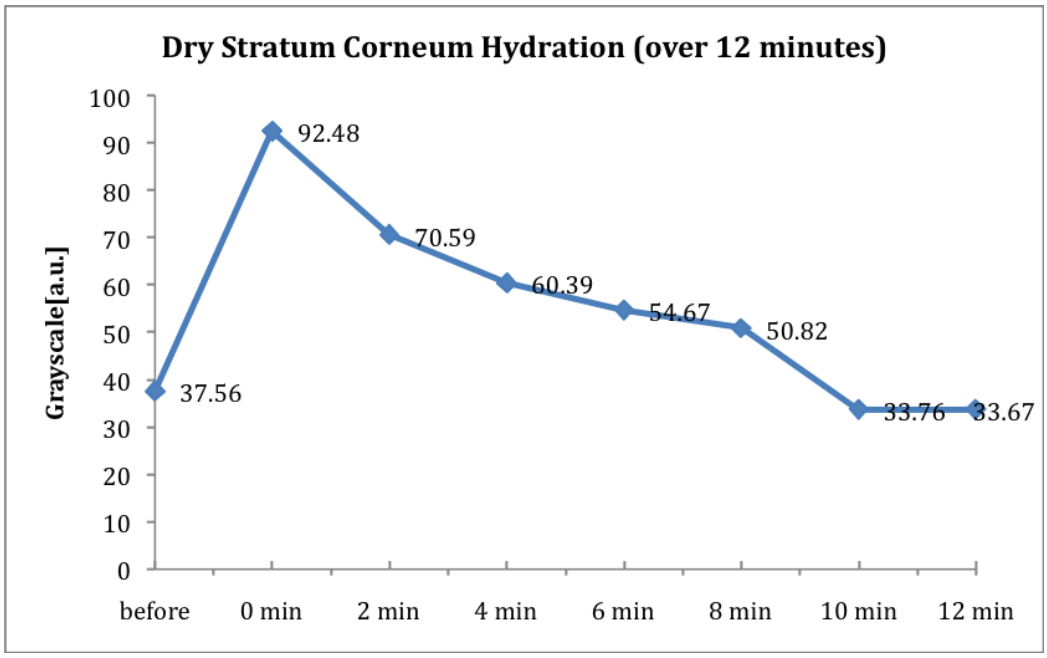

Figure 3.10: Graph showing pre-hydration and hydration measurement for 12 minutes of the in-vitro SC

3.4.4.3 ***Tissue, Cotton, Mix cotton and Paper***

These tests are done to ascertain if the FPC-SMD 5410 can detect different hydrated materials.

Method

Various materials are applied with 2 drops of water on the back of the surface to be tested. Application is by a glass pipette to drop 2 drops of water on the surface. For tissue paper, 2ply paper with 5 layers is used and only one drop of water is used.

The material is placed on a flat glass surface and the FPC5410 is used to take the reading. The process is repeated with the next material.

All experiments are performed with the same room temperature at 26°C and relative humidity at 36%. Figure 3.11 shows the results before and after hydration on various materials.

1.) Material: Wet tissue paper of 10 layer (2 ply x 5 layers)

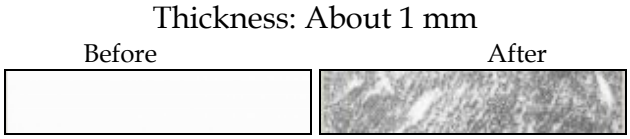

2.) Material: 100% cotton cloth

3.) Material: Cloth with 30% polyester 70% cotton

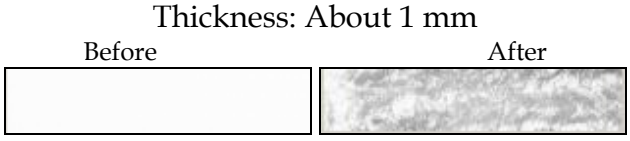

4.) Material: Paper (80g/m^2)

Figure 3.11: Capacitance images for four different types of non-organic materials before and after hydration.

Results

The results shows that pre-hydrated material have very little water presence and are registering a uniform measurement. After hydration, tissue paper has the highest amount of hydration at 77.26 average gray-scales, cloth with 30%

polyester and 70% cotton has the second highest hydration at 48.74 average gray-scales. 100% Cotton material shows a much level hydration at 41.25 average gray-scales while paper has increased minimally at 20.40 average gray-scales as can be seen from Figure 3.12.

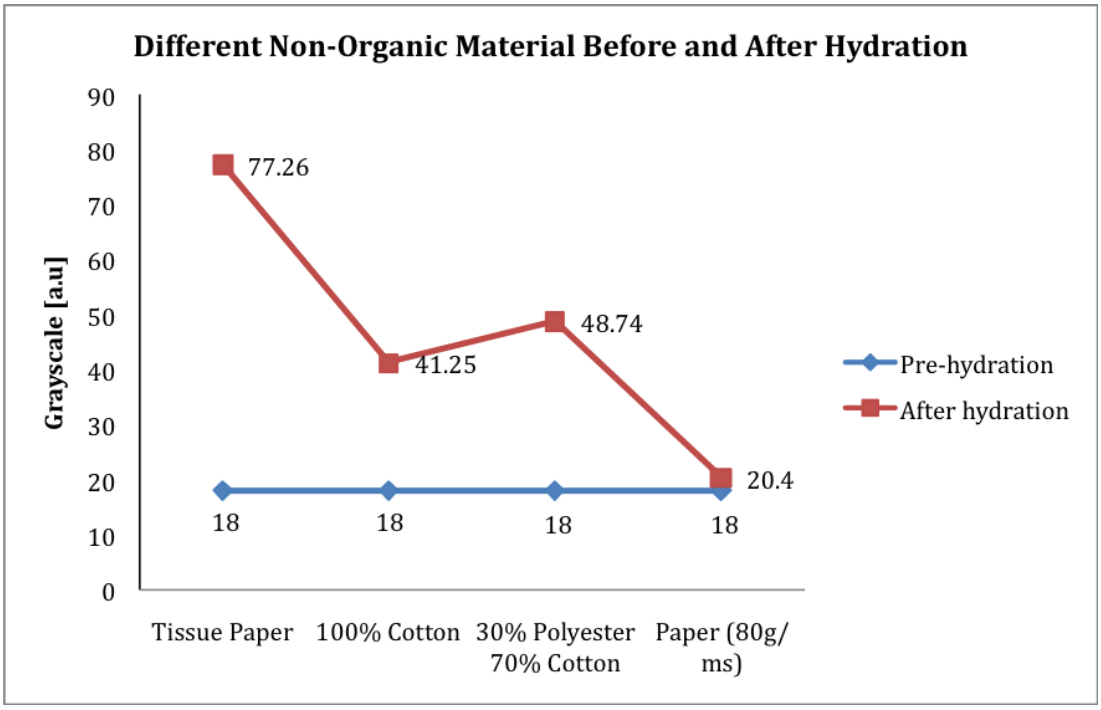

Figure 3.12: Comparison graph for four different types of non-organic materials before and after hydration.

3.5 The FPC-AMD 6410 Area Sensor Development Kit

Subsequently, the FPC-AMD 6410 Fingerprints Cards Development Kit was purchased and a dedicated program is written in Visual C++ to capture and store the images.

The FPC-AMD 6410 card is a fully integrated system with a USB connection. The capacitance sensor is mounted onto the processor board and access for test is through a recessed window on the front plastic panel.

A close-up image of a group of capacitor plates of the FPC-AMD 6410 can be seen in Figure 3.13. It is to be noted that the blemishes appearing in the image are not defects but debris of dust particles, remnants of sebaceous oil and water from constant contact with live skin and other surfaces during experiments.

Figure 3.14 further focuses on a single cell of a capacitor where the plates are visible in their co-planar position.

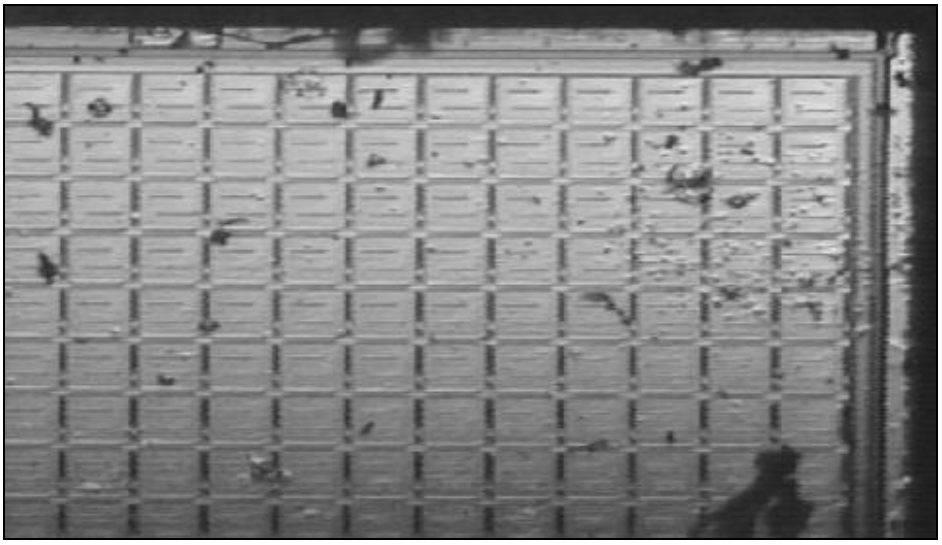

Figure 3.13: Close up array of capacitor sensors image taken with an electron microscope.

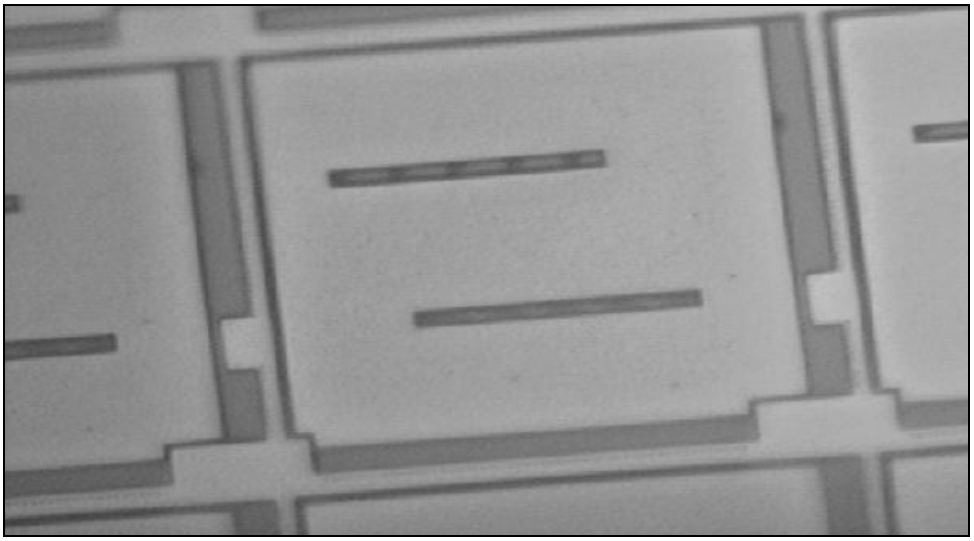

Figure 3.14: Close up of a single cell of capacitor with the plates in co-planar position on a capacitance sensor chip.

3.5.1 *Modifications of the FPC-SMD 6410 Development Kit*

Modifications were done on the sensor mainly to allow direct contact with skin and to allow flexibility in moving the sensor head on uneven skin. A Polyethylene sponge was used to mount the capacitance head to allow flexibility in movement as seen in Figure 3.15.

Figure 3.15: FPC 6410 capacitance sensor mounted on PCB Kit Board.

A conductive material is added around the capacitance sensor head to allow grounding of excess electrostatic discharge.

3.6 Results using FPC-SMD 6410 Development Kit

The FPC-SMD 6410 development kit is the second capacitance sensor used in this research. These tests were aimed to investigate the FPC-SMD 6410's capability of measuring the difference between a normal state skin and subsequently hydrated over time and to see the difference between FPC-SMD 5410 development kit and FPC-SMD 6410 development kit.

Three different types of experiments were done on the skin surface mainly to test the device capabilities in measuring different types of hydration:

1. Immersive Hydration – where skin is immersed in water for a period of time before being tested.

1. Moisturiser Test – the moisturiser consists of Parafinnum liquidum, methylparaben, butylparaben and aqua as the main contents. It is introduced to normal skin and then tested.
2. Occlusion – where normal skin is constantly kept on the device for a period of time without removing it from the device surface. At certain time intervals, images are captured.

With the FPC6410, a graph showing the gray-scale density is also produced. This quantification shows the change in gray-scale values for the experiments carried-out.

3.6.1 Hydration Immersion Test

Method

The subject is an Oriental male aged 40 to 45 years of age. The skin sites used for the measurements are untreated, but were wiped clean with ETOH/H_2O (95/5) solution. SC dynamic water distribution is achieved by immersing test skin sites in room temperature water for 20 minutes. The right cheek of the face is studied, and measurements are performed both before and periodically thereafter.

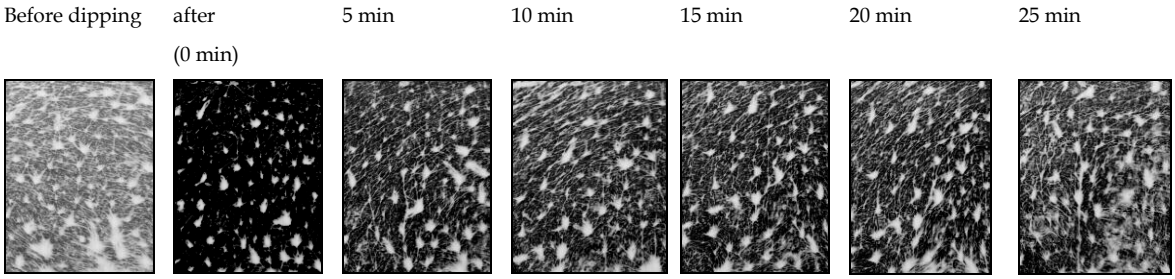

Figure 3.16: Images showing pre-hydrated and hydrated skin over time.

Results

In the above Figure 3.16, prior to immersion, the skin site has a low gray-scale level. After immersion the skin test area has darkened substantially.

The skin recovery can be seen over a period of 25 minutes. After these 25 minutes, the shade intensity has nearly returned to its original (pre water dipping) condition.

3.6.2 Moisturiser Application Test

Method

A second test was done on the upper volar forearm of a male Caucasian volunteer with application of moisturiser. A water-based moisturiser was applied to the skin and then wiped for any residual moisture. In this test, skin surface is compared as before and after the moisturiser only and no comparison is done over time. The capacitance images are shown in Figure 3.17.

Before applying moisturiser after applying water based moisturiser

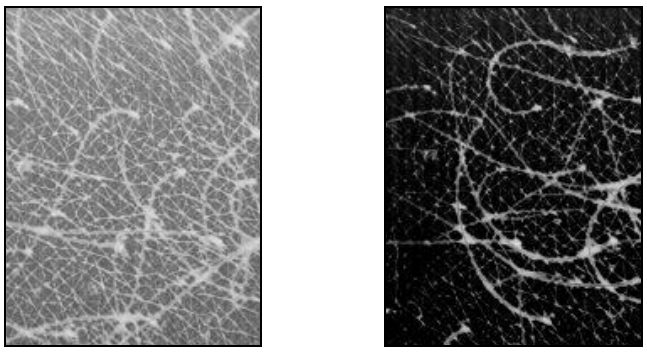

Figure 3.17: Images showing pre-moisturiser and moisturised skin

Results

An increase in intensity of gray-scale is visible as compared to before the application of moisturiser. The total pixel points on the FPC6410 are 30400 points (152 pixels width x 200 pixels length). In Figure 3.18, before the application of moisturiser, a larger amount of the gray-scale values of individual pixels are located between about 50 to 180 gray-scale producing a

typical bell curve. The highest amounts of pixels are in the middle consisting of about 500 pixels.

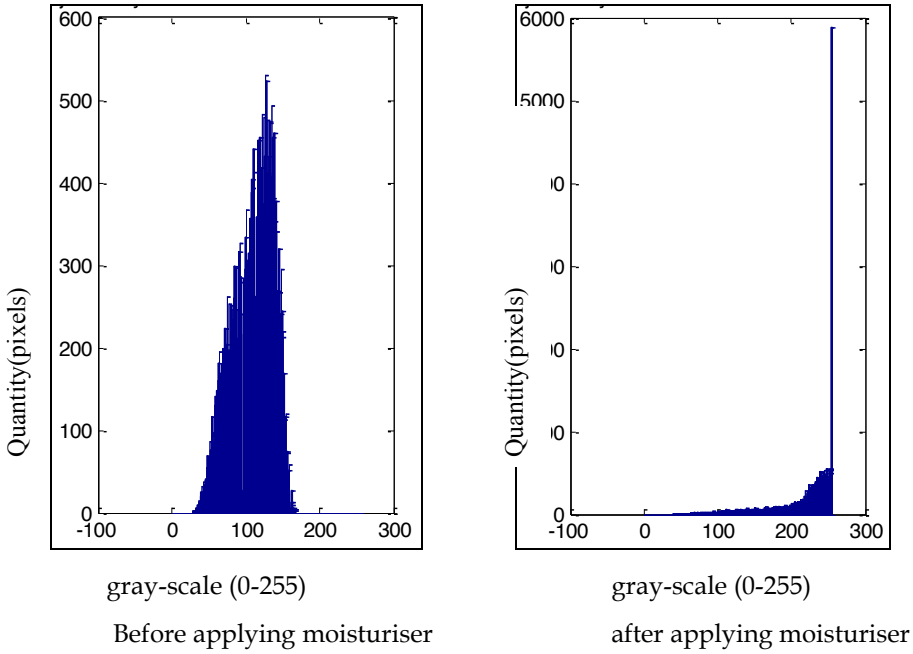

Figure 3.18: Graph quantifying gray-scale values of the pre-moisturiser and moisturised skin

After applying water-based moisturiser, the gray-scale value shifts towards the darker pixels. Now, the range is from about 50 to 255 gray-scales. The highest amount of gray-scale is the higher range nearing 255 with an amount of pixels reaching nearly 6000 pixels.

3.6.3 Occlusion Test

Method

The third test was done on the upper volar forearm of a male Caucasian volunteer. This test requires the volar forearm to be maintained in the same position on the device for a period of time in order to allow occlusion and to be able to capture images with increased water presence. The finger is kept stationary on the device and an image is taken every 1 minute for 5 minutes.

Results

The result shows an increased presence of water over time. This increase is visible in the darkening of the images seen in the above Figure 3.19.

The corresponding graph shows the quantification of the images in graph form. The first image has a normal bell-curve with gray-scale ranging from 30 to 200 gray-scale points.

The maximum points for range are averaging at 300 pixels per gray-scale. In the second image, the data has shifted towards the right showing an increasing gray-scale and the average pixels have dropped to below 300.

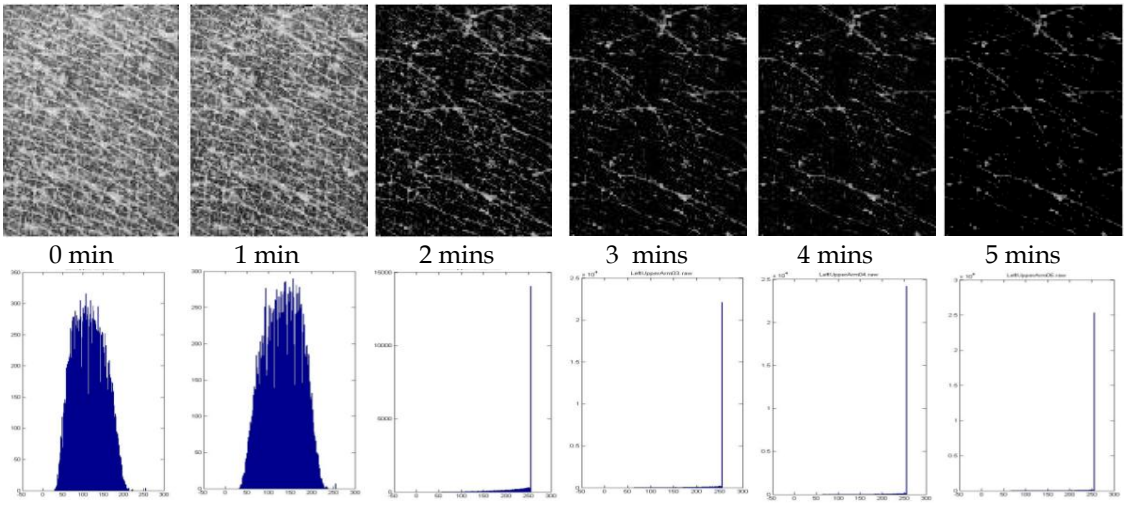

Figure 3.19: Images showing occlusion of the upper volar forearm skin surface over time with corresponding gray-scale density graphs below.

In the third image shown in Figure 3.19, since the image has gone darker, it is reflected in the graph by a larger amount of pixels (reaching about 14500 points) populating the higher gray-scale in the range of 250 gray-scale.

In the fourth, the lower gray-scale values has nearly disappeared and much of the gray-scale is above the range of 250 reaching 2.4×10^4.

The fifth image has a majority gray-scale of 250 and above and a total points in this range reaching 2.5 x 10^4 with about 6400 points ranging from 60 to 250 grayscale.

In the sixth image, the gray-scale above 250 has increased above 2.5 x 10^4. Although it's not visible in the graph, there are about 5400 points of gray-scale scattered throughout the 0 to 250 range as the higher end of the line is showing 2.5 x 10^4 (which amounts to 25,000 leaving behind 5400 points that are registered as a low horizontal flat line in the graph).

3.6.4 Banana Peel and Banana Fruit

This test is conducted on a banana skin and the banana fruit itself using the FPC6410 capacitance sensor. The banana was kept in the test environment for 5 hours prior to conducting the test.

The room's ambient temperature is 24^{o}C and relative humidity is 43%. Figure 3.20 shows the 3 images recorded of the banana. The top 3 sets of images are RGB photo digital camera with 2 megapixels while the bottom 3 sets of images are capacitance sensor images of the same site as the photo images.

Outer skin of banana | Inner skin of banana | Fruit surface

RGB Photo Images

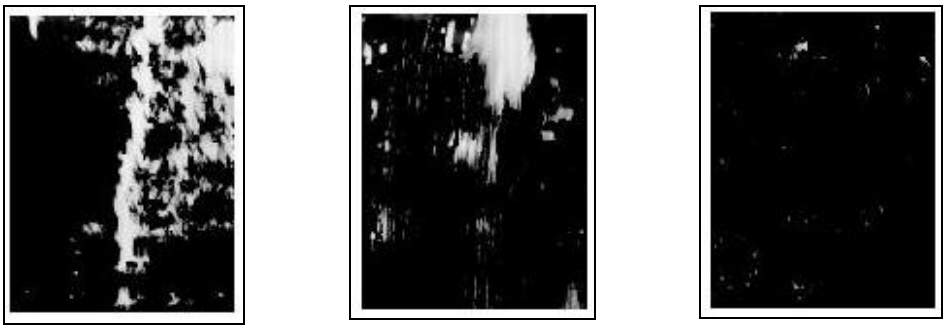

Capacitance sensor images

Figure 3.20: Images of skin surface of banana outer, inner skin and the fruit.

The first image shows an image of the outer skin surface, the second image being the inner skin of the banana surface and the last image of the exposed banana fruit surface.

A visual glance shows that the outer skin surface has lower hydration while the fruit surface has higher level of hydration and that the banana is highly hydrated.

In Figure 3.21, the quantification of the images shows similar results whereby the gray-scale of the outer skin is lowest at about 2.2×10^4 while the inner skin is nearing 2.5×10^4. The fruit surface has the highest level of hydration 3×10^4.

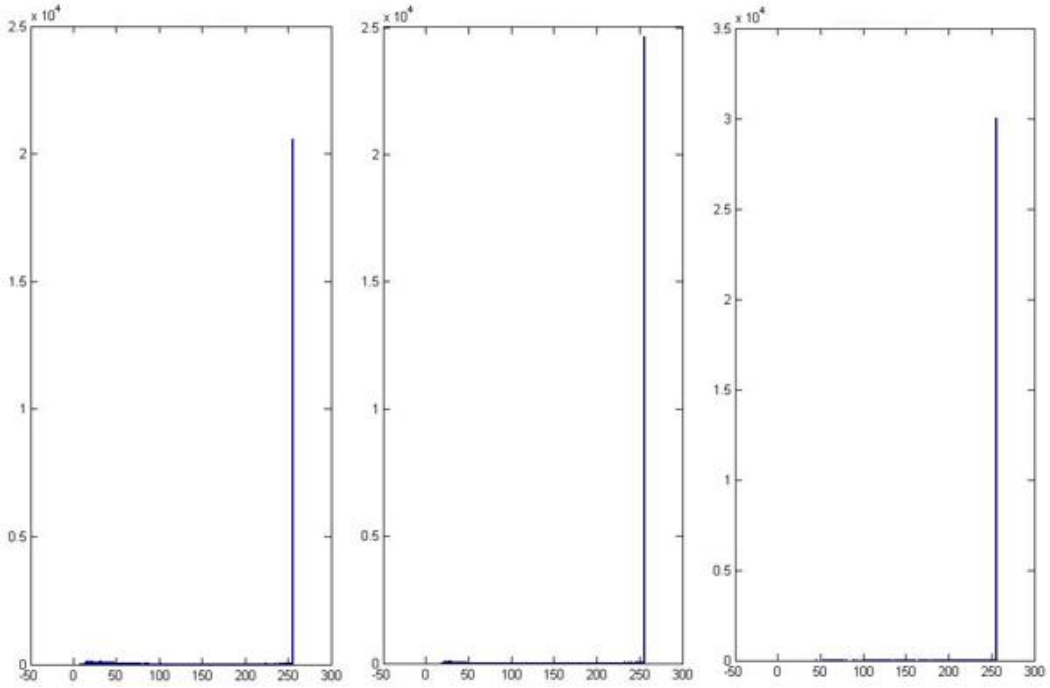

Figure 3.21: Graph showing the quantification of skin surface of banana outer, inner skin and the fruit.

These additional tests have further shown the capacity of the capacitance sensors in not only in reading live in-vivo skin but also a variant of in-vitro human skin, shed snake skin and fruit peel.

3.6.5 Multiple Skin Sites of the Human Skin Surfaces

Finally, multiple skin sites on the human body have been measured using the capacitance sensor to show variable differences in the human skin. The major sites that were measured were the forehead, cheek, neck, volar forearm, frontal bikini line, lower back pelvis (buttocks) and the lower leg.

Each of these sites was chosen due to its distinct uniqueness in the human skin surface. For the first test, four sites; the forehead, cheek, neck, volar forearm are measured on a female Caucasian subject aged 20 to 25 years old and is shown in Figure 3.22.

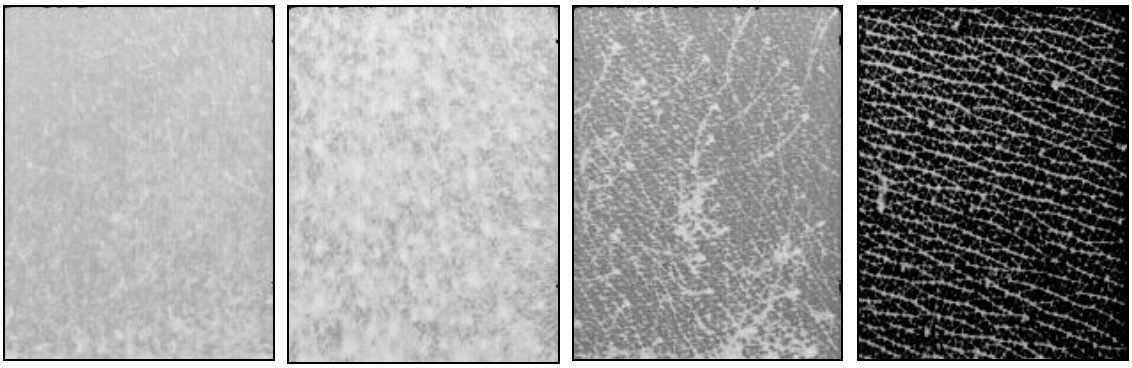

Forehead Right Cheek Right Neck Right Volar forearm

Figure 3.22: Imaging using capacitance sensor of different skin sites of the human body.

Quantitative analysis of these skin shows that the cheek has the lowest hydration at 67.82 grayscale. The forehead has a slightly higher value at 70.39 grayscale and the neck is higher at 101.88 grayscale. The Volar forearm has the highest hydration level at over 176 gray-scale values. This can be seen in Figure 3.23 below.

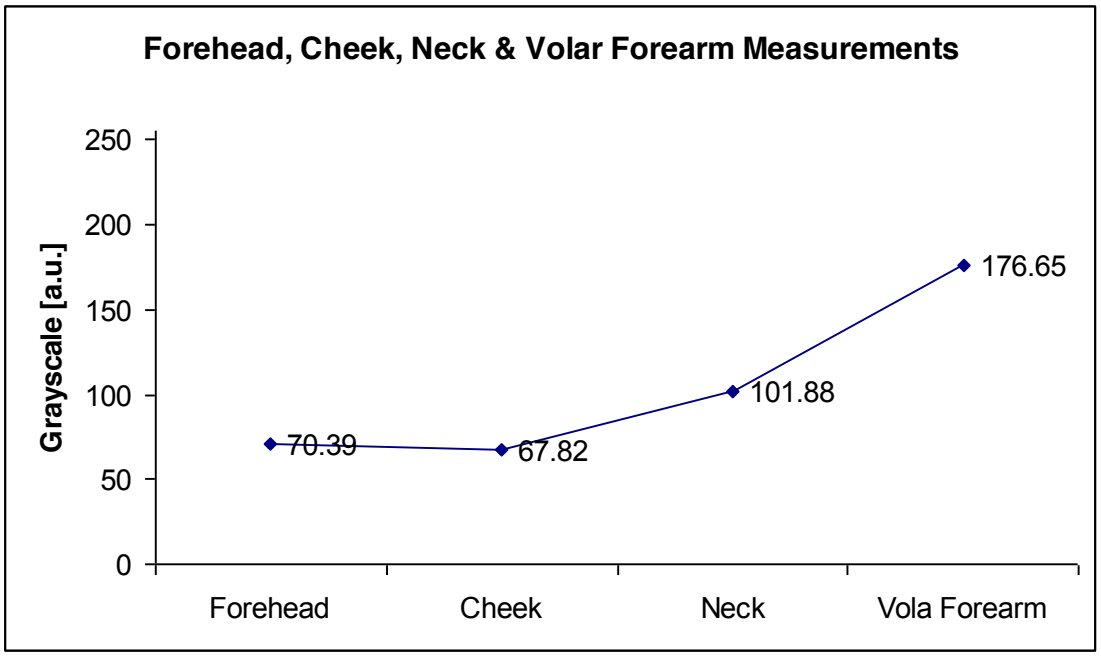

Figure 3.23: Line chart showing gray-scale values of four skin sites of a female Caucasian aged 20 to 25

.

The next two sites measured are the frontal bikini line, lower back pelvis (buttocks) and the lower leg of a female Caucasian aged 40 to 45 years old. The

image of the bikini line shows shaved are of the skin and location of the hair follicle is showing and white as seen in Figure 3.24.

The second image shows the buttocks area and skin surface shows a major difference that other skin sites in the form of larger and wider micro-relief lines. The last image is of the lower leg showing a more uniform, hydrated skin surface.

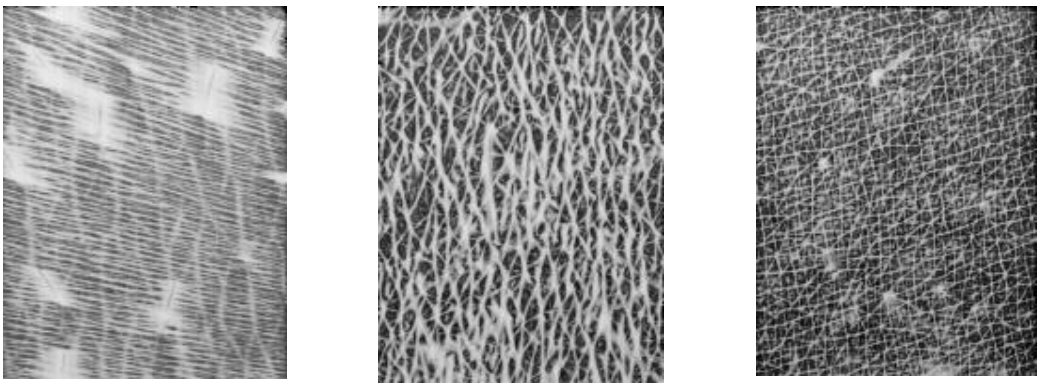

Frontal bikini line lower back pelvis (buttocks) lower leg

Figure 3.24: Imaging using capacitance sensor of different skin sites of the human body.

The data measured from these images is shown in Figure 3.25 and it can be seen that the bikini line has the lowest hydration levels, the buttocks has a higher level of hydration meanwhile the lower leg has the highest hydration from the three sites measured.

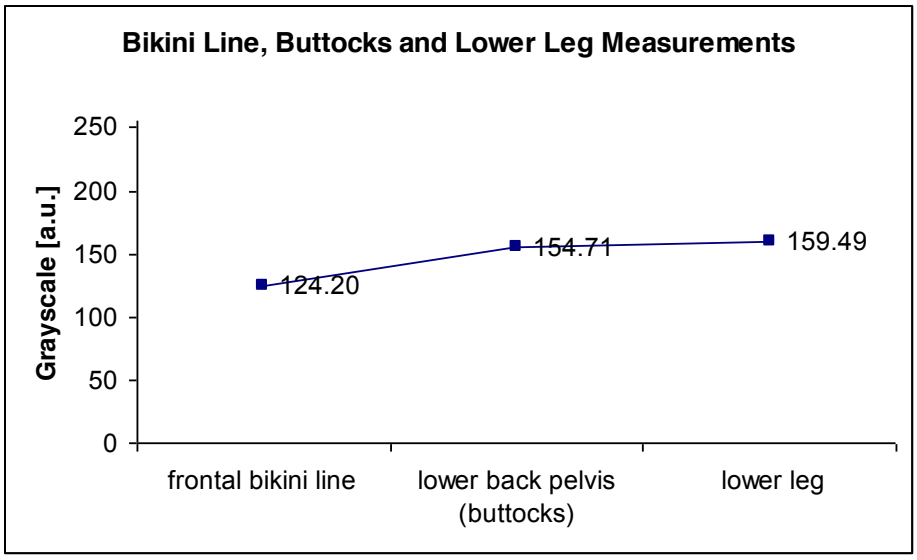

Figure 3.25: Line chart showing gray-scale values of three skin sites of a female Caucasian aged 40 to 45

3.7 The Fujitsu MBF-200 Capacitance Sensor

Finally, a more robust and highly sensitive sensor the MBF-200 developed by Fujitsu Corporation was used to analyse the skin. This sensor has the capability to measure images in video format where the changes in hydration can be measured as a video file.

As seen in Figure 3.26, the width of the sensor is 1.3cm while the length is 1.5cm. A USB connector is used to carry signals from the sensor to the computer application for processing and display.

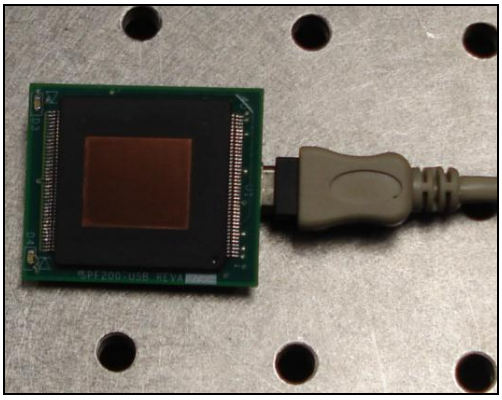

Figure 3.26: View of the Fujitsu MBF-200 capacitance sensor with an attached USB connector cable.

3.8 Conclusion and Findings

The capacitance sensor technology has shown promising results in measuring hydration in in-vivo skins, in-vitro skins and a multitude of other material both organic and non-organic.

The FPC-5410 capacitance sensor was modified to suit it to skin measuring. The sensor head was re-mounted onto a handheld probe so as to allow for easier handling and measurements of skin surface. Additionally the head was

supported with polyethylene sponge to allow for greater movement according to skin contours.

It has been observed that the capacitance sensor along with the program written has been successful in imaging and measuring hydration of not only detecting hydration of the skin but also hydration on other materials such as cotton, tissue, paper, snake skin and fruits.

Additionally, the capacitance sensor has also shown promising results in differentiation between different types of skin showing different structure of localised skin area such as forehead, cheek, neck and volar forearm. Quantification of the measured image has been attained by finding the average gray-scale value of all the points within the image.

It has been found that the capability of the capacitance sensor in both imaging and then on measurements from the data allows for a visual and data based results. This can be seen from images in Figure 3.24 showing distinct patterns of skin of three locations and then in Figure 3.25 showing the average hydration measurement values of the same sites.

In chapter 4, more detailed analysis of the measurement data will be done to show the effectiveness of measurements using capacitance sensors.

CHAPTER 4: DATA ANALYSIS OF CAPACITANCE SKIN IMAGING

The FPC6410 was adopted as the default capacitance sensors for future experiments due to its larger contact surface area that is in contact with the test area compared to the FPC5410 swipe sensor.

The area sensor chip of the FPC6410 unit has an array of 152 by 200 capacitive sensors, which generates a 30400 pixels in black and white skin capacitance image with a 50x50um special resolution. In the images, each pixel is represented by an 8 bit gray-scale value, 0~255, with 0 represent white (low capacitance) and 255 represent black (high capacitance) (Xiao P, Singh H, 2007).

The FPC6410 Development Kit contains standard software written in Visual C++ with functionality to capture and store the image in RAW format. A RAW format image is a file where the data has been processed minimally from that of the sensor.

The file does not contain any additional header information as it is normally done in other graphics format files. Each element or pixel in a RAW format file is an individual 8 bit (1 byte) data. As each pixel is represented, the RAW file represents closely a high truer image of the actual site (*Steinmueller U, Gulbins J, 2006*).

```
120  250  118  ..............................
 69   78  230  ..............................
.............................................
```

In the diagram above, six values on the X-axis from the top left of a file are shown. It's representation in byte format in a RAW file format is shown below.

```
01111000  11111010  01110110  ..............
01000101  01001110  11100110  ..............
.............................................
```

The original program supplied by FPC was modified to incorporate additional functionalities mainly:

1. Time based capturing of the image (time intervals in seconds).
2. Looping of the images being taken against time.

4.1 Software Techniques Used in Image Capturing

The FPC area sensor verification system consists of the following system components:

1. A host processor
2. A fingerprint processing device
3. A fingerprint capturing device [area sensor]

The purpose of the host processor is handling the management of templates created for recording the images, user interface and issuing commands for recording image.

The fingerprint-processing device then performs all calculations needed to enrol/verify the recorded image. It also acquires the fingerprint image from the fingerprint sensor.

This means that there is no direct interaction between the host processor and the fingerprint-capturing device (sensor).

The interface between the host and the processor is a parallel data/address-bus. Figure 4.1 shows a diagrammatic view of capacitance sensor system process layout.

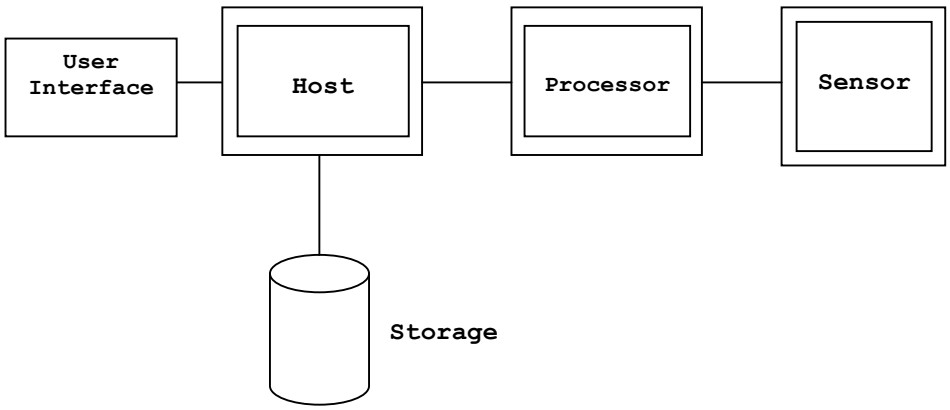

Figure 4.1: System Layout from the Capacitance Sensor to the User Interface

The user interface allows the user to record an image by applying the capacitance sensor to the test site and selecting the 'Capture' button on the application. The processor will capture the image and the values are passed to the Host which will then store the image in a .RAW format.

As shown in Figure 4.2, the user has a few options to select from the User Interface. The image can either be captured as a single .RAW file or using the Loops option the user can specify the Time intervals(in seconds) and the total amount of loops required.

Subsequently, the recorded image is stored as a RAW file and can be accessed with a multitude of applications for processing including Adobe Photoshop, IrfanView and dedicated programs designed in Mathworks's MATLAB.

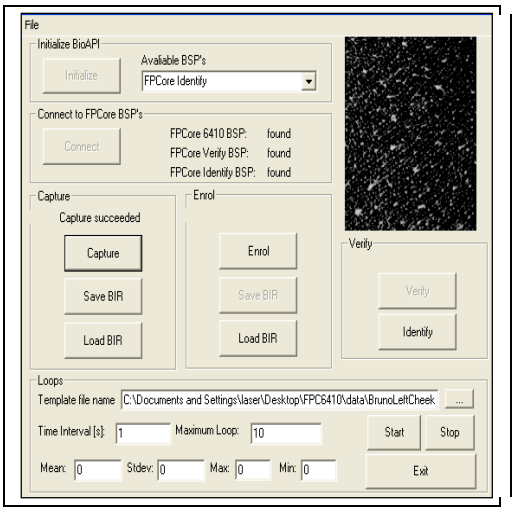

Figure 4.2: User interface of the FPC6410 showing the options available to the user

For this project a specific program is written in MATLAB to allow the extraction of information from the RAW file data. Using this program, the extracted information can be analysed for closer details of gray-scale, quantification of the image and for generating 3D skin surface profile.

An assumption is made where all the pixels whose gray-scale values are above the threshold have a good skin contact. By capping their gray-scale values, 3D skin surface profiles can be produced.

When an image is recorded by the capacitance sensor, the gray-scale image is displayed in the user interface window and the raw image file is stored in the selected folder. Figure 4.2 above shows a sample image of the left cheek of a male Caucasian aged 20-25.

In addition to recording a single image, the program has been modified to capture images in time interval and in loops that can be specified by the user. The images are

recorded individually and stored as different files in order to allow processing and analysis of individual file images.

With the capability of time interval loop, the capacitance sensor can be placed directly on the subject test area for a period of time for continuous time interval imaging. This technique is useful where occluded images of the skin site need to be recorded separately and the images are stored the image as separate files for analysis later.

4.2 MATLAB

4.2.1 Definition

MATLAB is a high-level interactive programming language that allows rapid development of code to test and effectively process large volumes of data for scientific and engineering purposes. Typical uses include:

- Math and computation
- Algorithm development
- Modelling, simulation, and prototyping
- Data analysis, exploration, and visualization
- Scientific and engineering graphics
- Application development, including Graphical User Interface building[54].

4.2.2 MATLAB Interface

MATLAB is an interactive application where users can input commands and instructions directly into a Command Window and the commands are carried out in real-time. Commands may also be written as traditional programming language coding through an editor. The program can then be saved as a MATLAB format (.m) file and then processed.

One of its main strength as a development tool is that it contains easy to use tool boxes that allow manipulation of data based on numerical algorithms. In addition, processed data can be easily plotted in graphs and charts format using simple plotting techniques using these toolboxes.

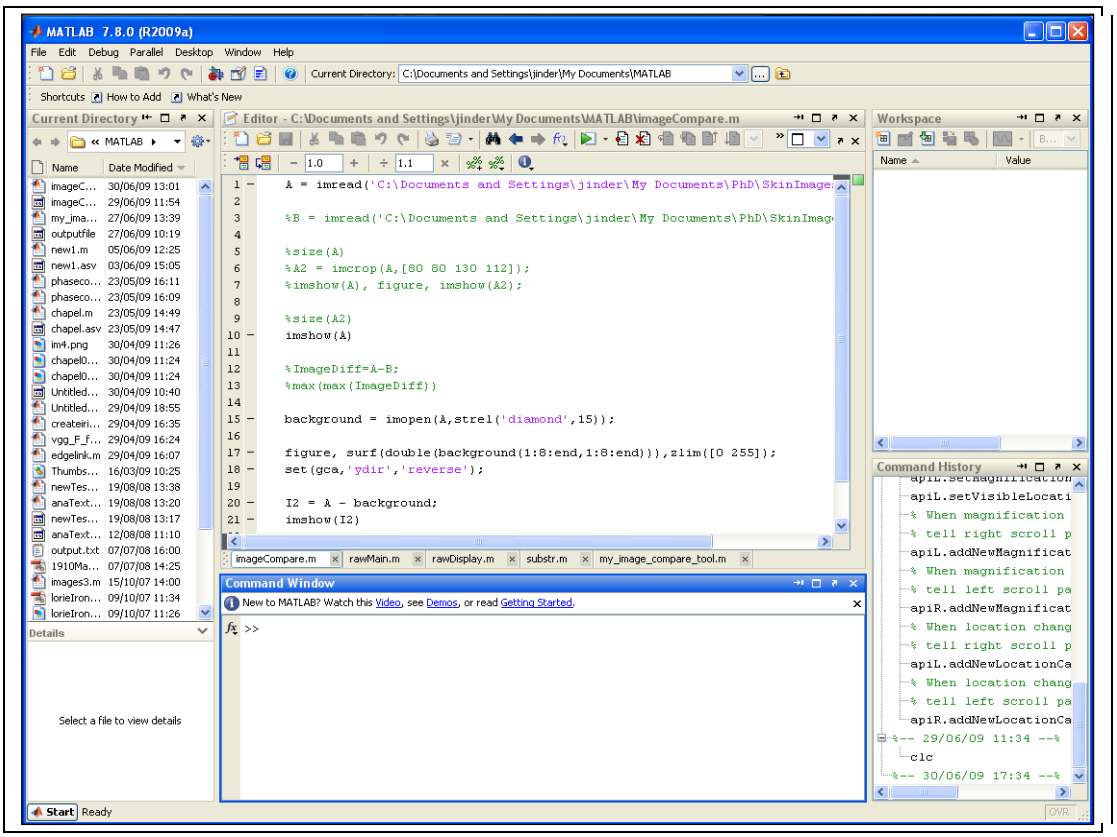

Figure 4.3: Image of a Mathworks MATLAB window showing the Current directory, Editor area, Details, Command Window, Workspace and Command History.

In Figure 4.3 above, MATLAB has a conventional style window where on the menu options are standard graphical-user interface based.

4.3 Image Processing

4.3.1 Three Dimension Profiling

A three dimensional view of the image is rich in information and has the capacity to

display a clearer image of the skin profile compared with a 2 dimensional image. Additionally, a colour scheme is used whereby a closer to the surface pixel is coloured red while deeper valleys are coloured light blue. There is a range of spectrum colours from red to blue in between to show different depths of the micro-relief and skin surface indentation (Singh H, Xiao P, Berg EP, Imhof RE, 2008)

Figure 4.4 show a site of the skin selected to be processed with the dedicated image processing program written in Mathworks MATLAB. The site is immersed in water for 20 minutes and the subsequent RAW image taken immediately after immersion.

The third image has been taken 25 minutes after the immersion. These images are in RAW format and have been taken using the FPC-SMD Fingerprints Card software prior to processing.

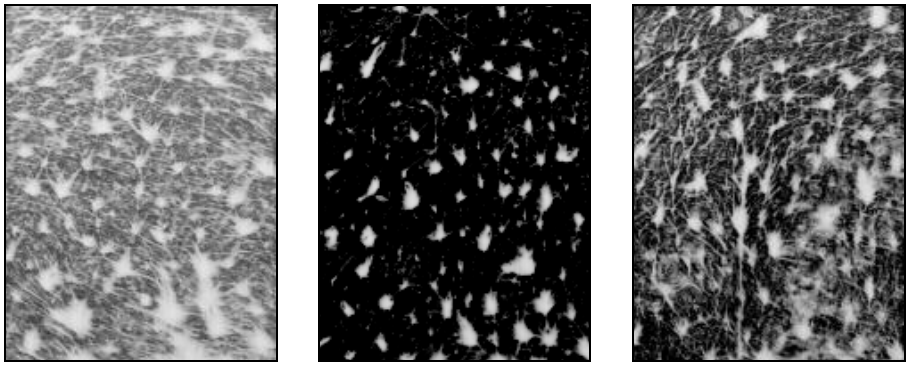

Figure 4.4: RAW image of the face skin surface before and after immersion in water

In Figure 4.5, the three images are of the first site processed by the MATLAB program and show a 3D profile from the RAW file as seen in Figure 4.4. (H. Singh and P. Xiao, 2008)

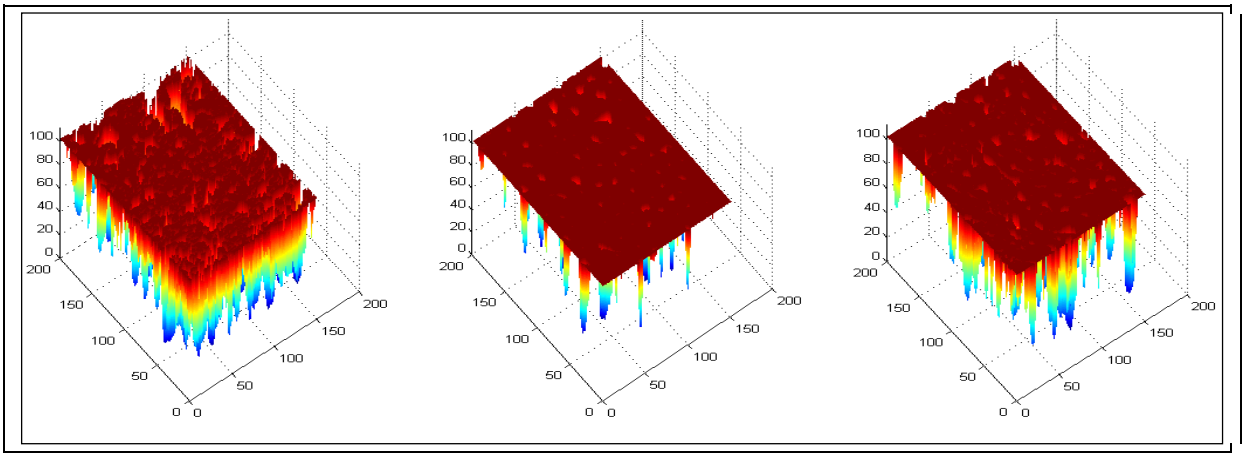

Before After (0 min) 25 min

Figure 4.5: 3D Profile of the face skin surface before and after immersion in water

4.3.2 *Data Analysis*

In analysing the data, the average grayscale value and its standard deviation of an image are calculated by averaging all the pixel values which are above a certain threshold.

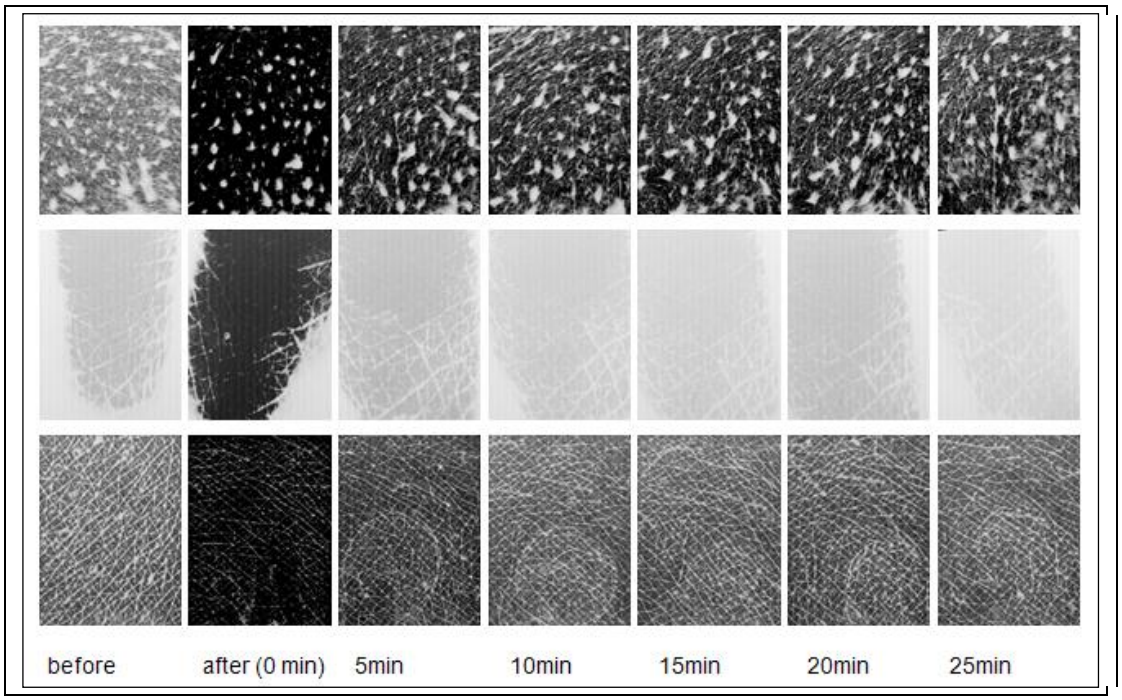

Figure 4.6: The capacitance images of three different skin sites (from top: face, thumb and volar forear) before and after a 20-minute immersive hydration.

The capacitance images of the three different sites show varying degrees of gray-scale as seen in Figure 4.6. The values of the gray-scale of each of the image are then calculated by the MATLAB program and a line chart showing the quantified values is then generated as shown in Figure 4.7.

The results show that the thumb skin site has the most significant hydration increase during the immersive hydration; it is also the quickest to recover to its normal hydration level. While face and volar forearm skin sites have also hydration increases, the face skin site is the slowest to recover. The different dynamic water distributions reflect different skin sites' different characteristics, such as SC water holding/binding capabilities, thickness, porosity and its barrier functions.

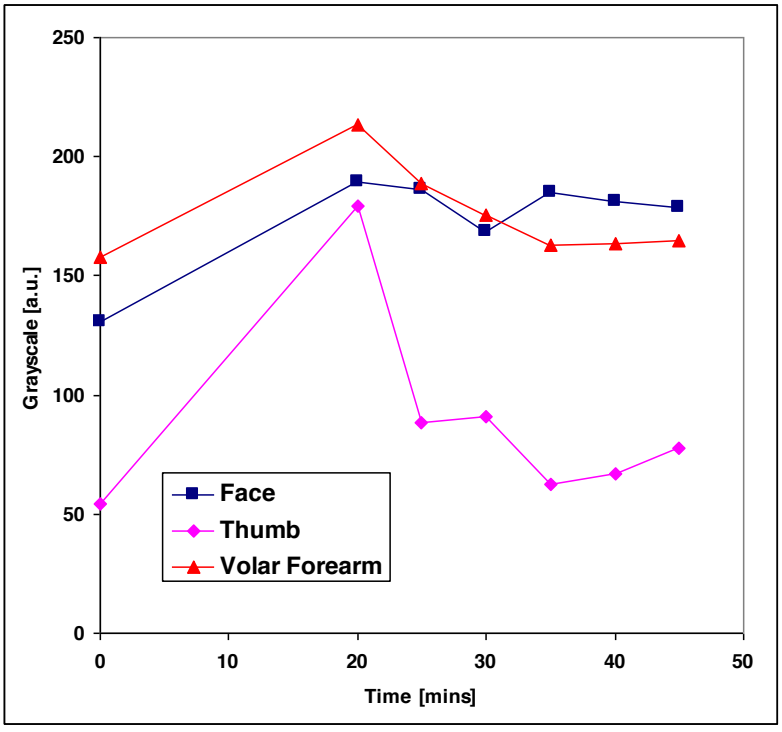

Figure 4.7: The capacitive images of three different skin sites (from top: face, thumb and volar forearm) before and after a 20-minute immersive hydration.

Assuming all the pixels whose gray-scale values are above the threshold have a good skin contact, by capping their gray-scale values, 3D skin surface profiles can be produced. Figure 4.8 shows the 3D skin surface profiles of three skin sites before and

after the immersive hydration by using the image data shown in Figure 4.6.

The first column in Figure 4.8 shows 3D skin surface profile of 3 sites prior to hydration. Each of the skin sites shows different characteristics as recorded by the images. The second column shows the 3D skin profile after 20 minutes hydration. All three sites are highly hydrated with varying degrees of gray-scale. In the third column, images have been recorded after 25 minutes since hydration. The most prominent change can be seen in the second row where the image of the thumb is recorded.

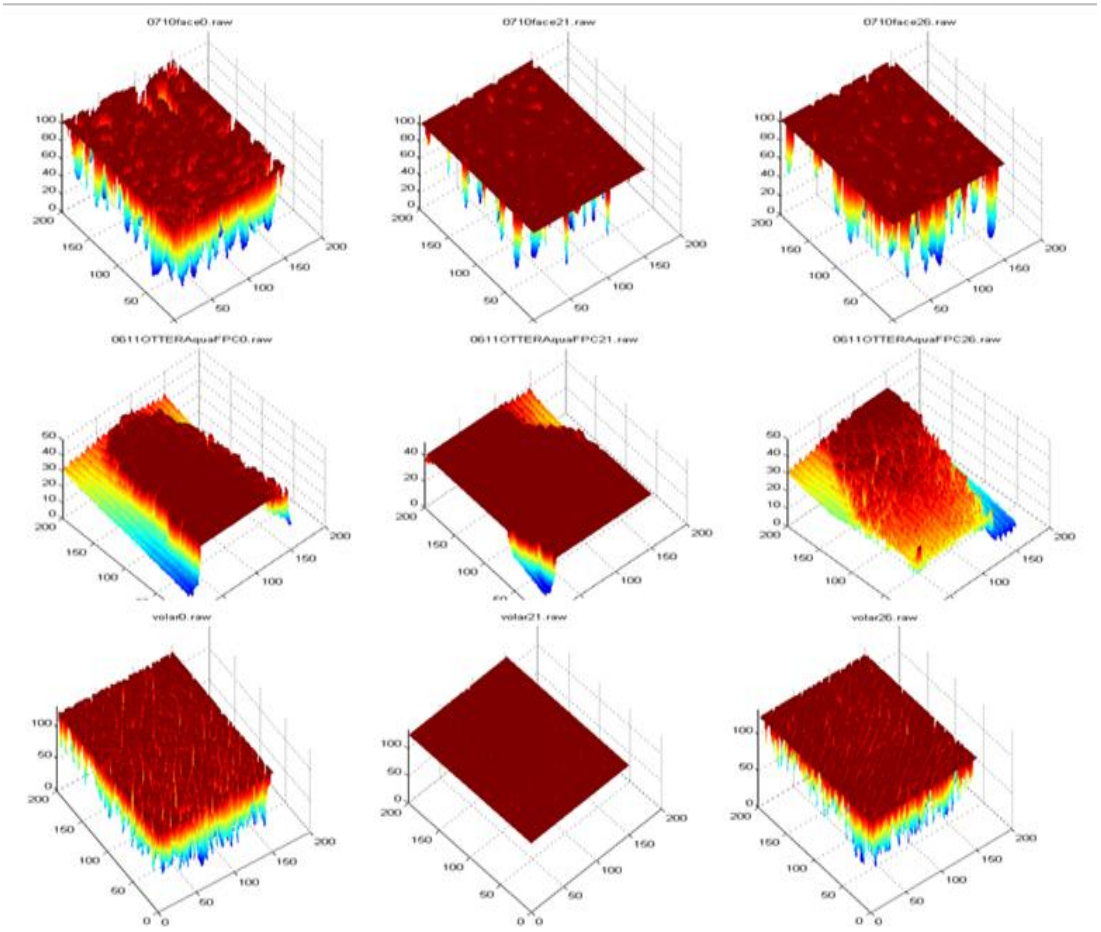

Figure 4.8: The 3D skin surface profiles of three different skin sites (from top: face, thumb and volar forearm) before and after a 20-minute immersive hydration.

4.3.3 Data Analysis with OTTER and AquaFlux

To further validate the gray-scale values from the capacitive skin images, tests were also performed using the opto-thermal transient emission radiometry (OTTER) and the AquaFlux condenser-chamber TEWL method measurements at the same time.

Figure 4.9(a) shows the skin surface hydration results before and after the immersive hydration and Figure 4.11 show the TEWL value results. The skin surface hydration results are generally in agreement with the gray-scale value results.

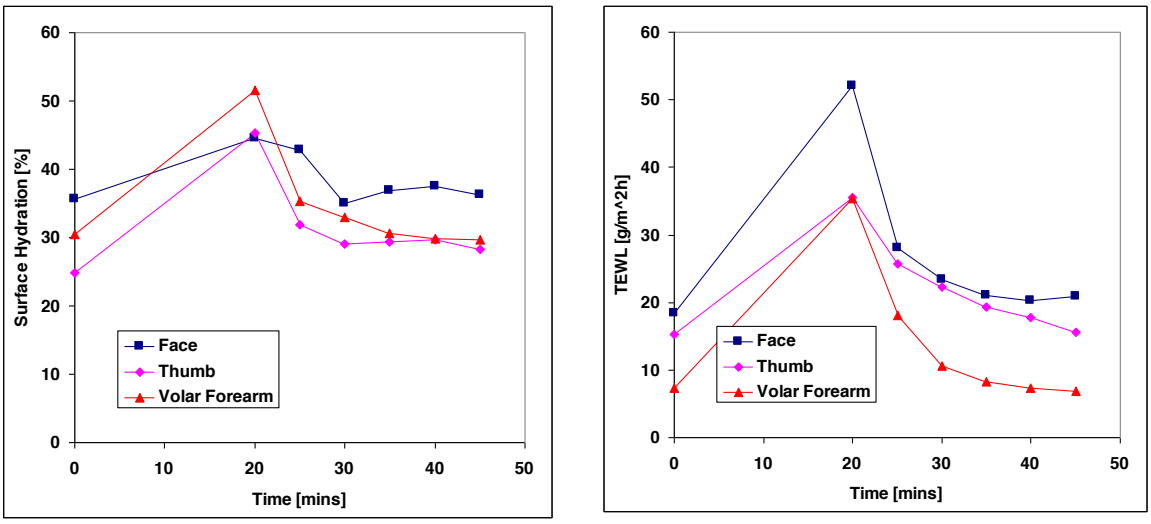

(a) SC surface water concentration *(b) SC Trans-Epidermal Water Loss values*

Figure 4.9: SC surface water concentration and SC TEWL values of three different skin sites.

In the above Figure 4.9(a), the SC surface water concentration of three different skin sites is measured using the OTTER. An initial reading is taken and after a 20-minute immersive hydration, 6 readings are taken every 5 minutes.

Figure 4.9(b) is showing the stratum corneum trans-epidermal water loss (TEWL) values of three different skin sites before and after a 20-minute immersive hydration by using condenser-chamber TEWL method.

Both SC surface water concentration and SC TEWL values show increase; and then a

drop towards recovery of the skin within the experiment duration. Subsequently, correlation between the gray-scale values of the capacitance sensor is established against the surface hydration of the OTTER; and then against the TEWL values of the AquaFlux.

Figure 4.10 shows the correlation between SC surface hydration [%] and gray-scale values and Figure 4.11 shows the correlation between gray-scale values and TEWL values.

Different skin sites clearly have a different correlation which reflects the different SC characteristics. With data from Figure 4.10 conversion from the gray-scale values into hydration levels can now be done.

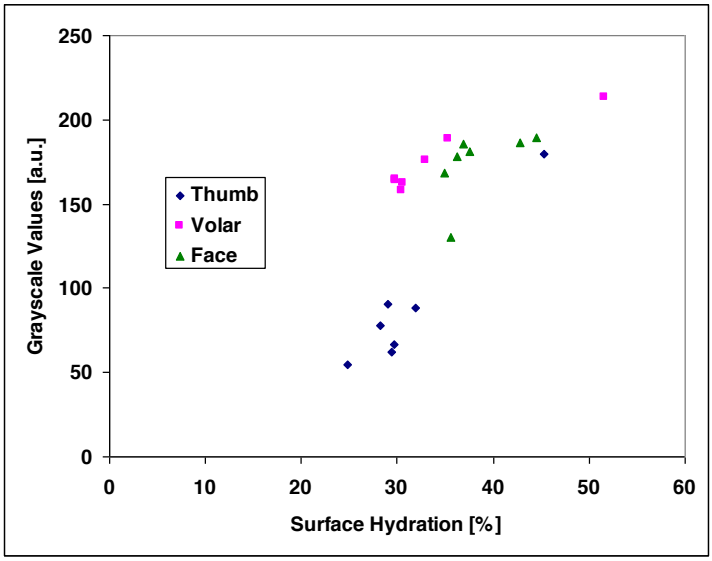

Figure 4.10: The correlation between SC surface water concentration and gray-scale values.

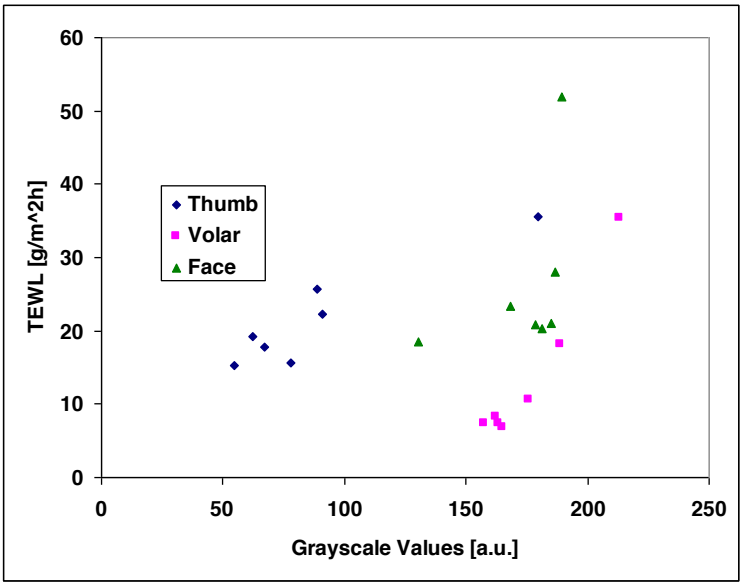

Figure 4.11: The correlation between gray-scale values and TEWL values.

The gray-scale values of the SC capacitive images show that different skin sites react differently to the immersive hydration even under identical conditions.

With these capacitive images, the skin surface 3D profile can be generated and show changes in the hydration level before and after the immersive hydration.

Comparing with opto-thermal transient emission radiometry (OTTER) results and condenser-chamber TEWL (trans-epidermal water loss) method results, calibration can also be done for the gray-scale values of the images.

4.3.4 Further Data Analysis of the Capacitance Image

The dedicated MATLAB program is also generating data analysis of the gray-scale of the skin, the total points used in a particular image, sum of value of all gray-scale values between 0 to 255, the standard deviation of the particular image, entropy or statistical measure of randomness that can be used to characterise the texture of the image, gray-scale values width, micro-relief of the skin surface and the image threshold.

The images of a dry skin site are recorded and then the skin was occluded for 1300 seconds (21 minutes). Then a second reading is taken at 1300 seconds as shown in Figure 4.12.

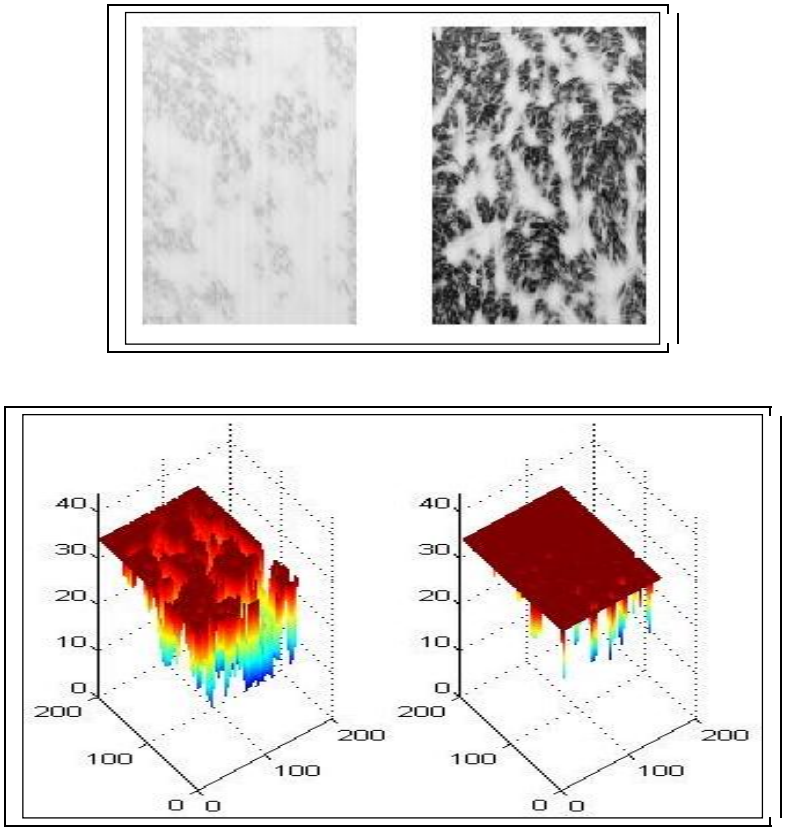

Figure 4.12: Two skin sites (pre-occlusion and occluded skin) with 3D skin profile.

The images are then analysed with the MATLAB program and the data analysis is shown in Figure 4.13.

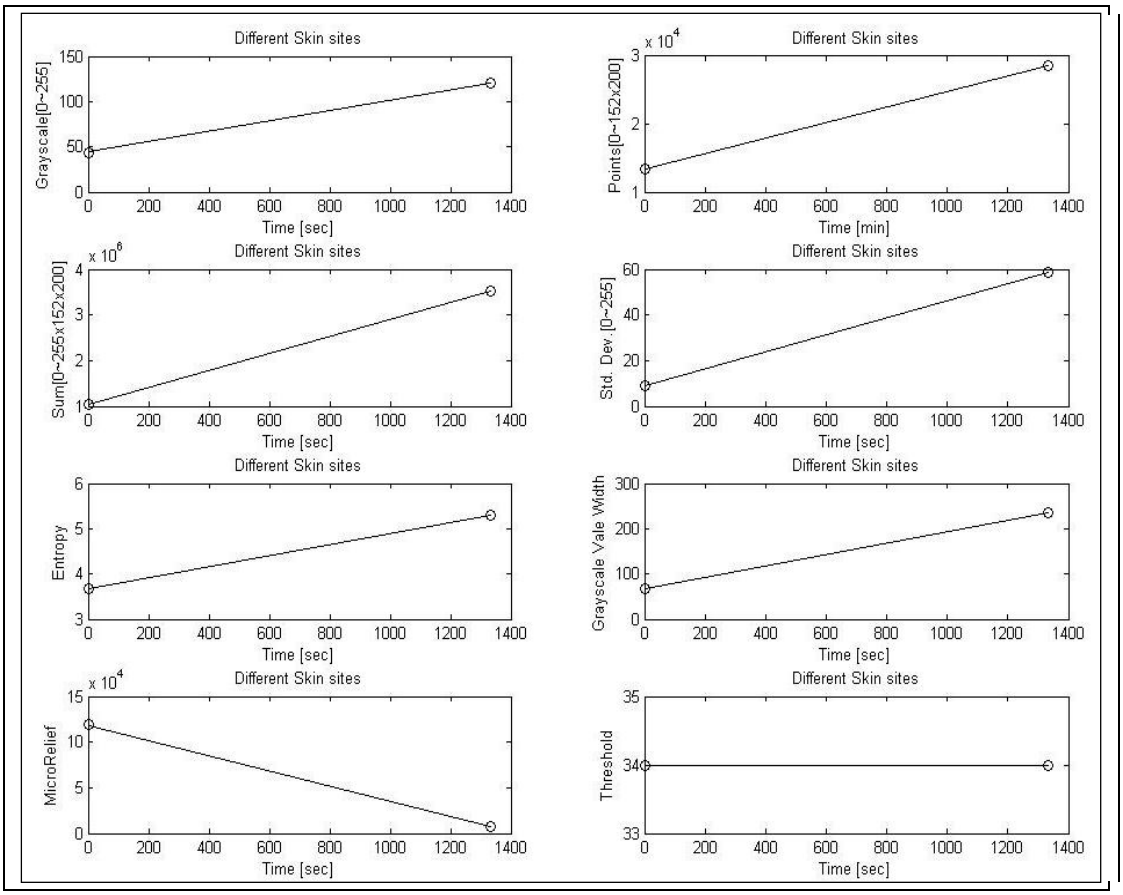

Figure 4.13: Data analysis of two skin sites (pre and occluded skin) showing multiple results analysis.

Gray-scale Chart

The first graph shows the average gray-scale values of each of the image taken as seen in the formula below:

$$\bar{x} = \frac{1}{n}\sum_{i=1}^{n} x_i = \frac{1}{n}(x_1 + \cdots + x_n).$$

Where x_1 to x_n are the values of each pixel (152 pixels in width and 200 in length totalling 30400 pixels). However the n value is the total number of pixels that were used and does not represent the total value of all the pixels. This is done to weed out

pixels whose values are below the threshold of the calculation (i.e. non contact point and micro-relief).

All the needed pixels value are added and then divided by the total pixels taken into consideration. After progression over time, the gray-scale value graph can be seen rising.

Points Chart

The second graph on the top right shows the total amount of points that were used in the image. The total points that can be used are 30400(3×10^4) as shown by the Y axis. The amount of points in use steadily rises over the duration of the time.

Sum Chart

The third graph shows the sum of all the pixels value in use added together. The formula below describes adding each value of x the total n (30400 pixels). n represents the total pixels in use. Each pixel is added toproduce the total summation of all the pixels.

$$\sum_{i=m}^{n} x_i = x_m + x_{m+1} + x_{m+2} + \ldots + x_{n-1} + x_n.$$

At 0 second, the total sum is about 1×10^6 and increases to about 3.5×10^6.

Standard Deviation Chart

The fourth graph shows the standard deviation of the gray-scale values. Standard deviation measures variability of statistical population of the data.

$$s = \left(\frac{1}{n-1} \sum_{i=1}^{n} (x_i - \bar{x})^2 \right)^{\frac{1}{2}}$$

s is the standard deviation of x(the gray-scale values of each point) and n represents the total pixels in the image.

Entropy Chart

In the fifth graph E = entropy(I) returns the value E, which is a scalar value representing the entropy of gray-scale of image I. Entropy is a statistical measure of randomness that can be used to characterize the texture of the input image. Entropy is defined as:

$$sum(p.*log2(p))$$

where p contains the histogram counts returned from 'imhist' function of MATLAB. The value of entropy increase over time as more of the gray-scale values increases and spreads across the image.

Gray-scale Value Width Chart

The sixth chart simply shows the gray-scale value width range from the first image taken to the last image. As can be seen in this chart, the gray-scale value has increased from about 80 gray-scales to about 250 gray-scales during this time period.

Micro-relief Chart

The seventh chart shows the micro-relief changes of the skin surface. The micro-relief is measured by capping all values below 20 gray-scales. A drop in this range over

time shows that the micro-relief is being hydrated and that the space occupied by the micro-relief in the capacitance image is being reduced.

Threshold Value Chart

The eighth graph shows the threshold[1] value of the total image and is consistent based on the capping of the gray-scale values.

The increase in gray-scale is seen in the graphs generated in Figure 4.13.

There is an increase in values consistent with the gray-scale increase as seen in Figure 4.12 except for the micro-relief of the skin that shows a decrease in value.

4.4 Conclusion and Findings

In this chapter, the work of writing program to process data extracted from the capacitance sensor is discussed. Formulas used in extracting and manipulating the data are shown.

It has been noted that the capacitance sensor, when applied on the skin for a period of time will naturally allow occlusion of the skin. This is because the surface of the capacitance sensor is in direct contact with the skin site and therefore surface water has no means of escape into the surrounding environment.

This will result in the water occluding between the skin surface and the capacitance sensors head. This property of the capacitance sensor coupled with the software capability to measure images in a time loop allows for good study area of occlusion of the skin.

[1] The point that must be exceeded to begin producing a given effect or result or to elicit a response

It has been found that a 3D surface image profile can be created using the dedicated MATLAB program. Additionally, the water loss can be seen from the hydrated surface as shown in Figure 4.5.

The correlation between SC surface water concentration and gray-scale values; and the correlation between gray-scale values and TEWL values has been established.

Further detailed experiments and research on occlusion using capacitance are looked at in Chapter 5.

CHAPTER 5: OCCLUSION, MOISTURISER AND OTHER SKIN MEASUREMENT

Occlusion is the complete impairment of passive trans-epidermal water loss at the application site. The main influence on the skin under occlusion seems to be the retention of water that is detectable by the trans-epidermal water loss and the increase of water holding capacity. (Fluhr, Elsner, Berardesca, Maibach, 2005)

As noted in Chapter 4, occlusion is achievable with the capacitance sensor as the contact surface of the sensor head with skin allows for impairment of the water loss from subject skin site.

To analyse the feasibility of occlusion tests with the capacitance sensor, multiple tests were conducted with the FPC6410 capacitance sensor. A comparison was also done with RGB Digital Camera imaging to see if the occlusion could be recorded by means of photographic images.

5.1 Occlusion with the Capacitance Sensor

For the first test, the capacitance sensor was applied on the left volar forearm of an oriental female aged 20-25 years. An initial image was measured and the capacitance sensor is maintained on the skin site to allow occlusion for 5 minutes. The occluding of skin will result in higher hydration levels that are trapped between the skin and glass surface of the capacitance sensor surface.

Then a second image is measured as shown in Figure 5.1.

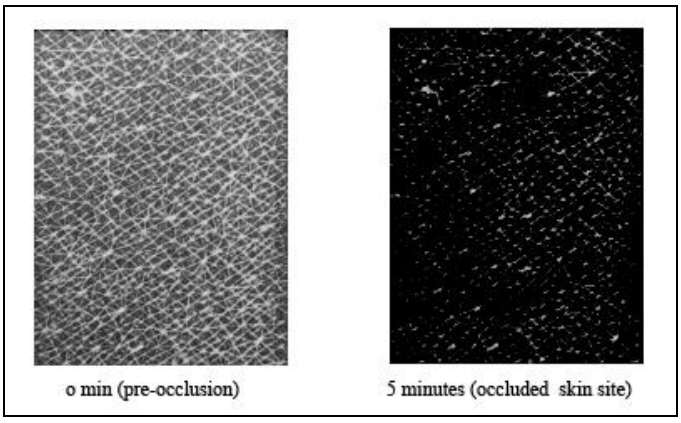

Figure 5.1: Capacitance image of the left volar forearm of an Oriental female aged 20-25 before and after occlusion for 5 minutes.

The image recorded prior to occlusion shows the skin surface with normal gray-scale ranging from 20 to about 230 points as shown in Figure 5.2. After occlusion for 5 minutes, the gray-scale level has increased vastly and the image now shows gray-scale values in the range of 250 to 255 points with pixels amount ranging at about 2.7×10^4. A small amount of gray-scale is visible below 0.1×10^4 ranging from about 80 to 250 gray-scales.

The 3D profile image showing the water concentration between the pre-occluded and occluded skin in Figure 5.3 shows a vast increase in occlusion. Variability of degrees exists in the depth of the pre-occluded 3D profile showing a normal non-occluded skin. However the same depth is nearly eradicated in the occluded 3D profile as the contact surface between the capacitance sensor and the skin is occluded.

This inhibits the depth of penetration of the capacitance dielectric field thus showing the nearly complete occluded surface area between the skin site and the capacitance sensor.

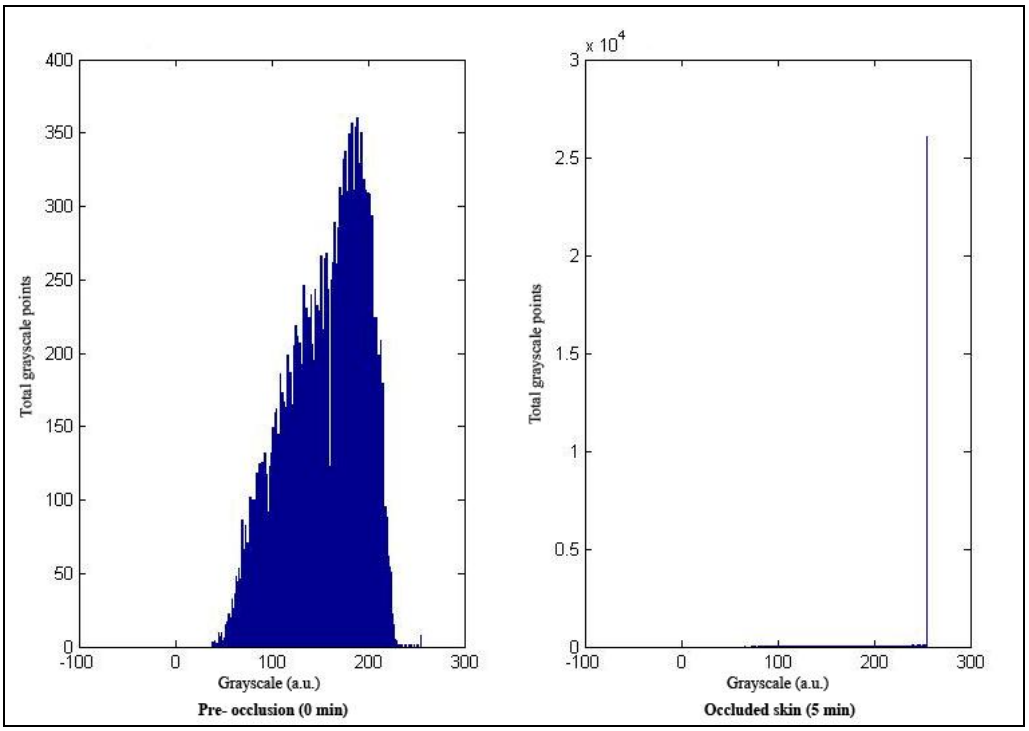

Figure 5.2: Quantification comparison of the image of left volar forearm of an Oriental female aged 20-25 before and after occlusion for 5 minutes.

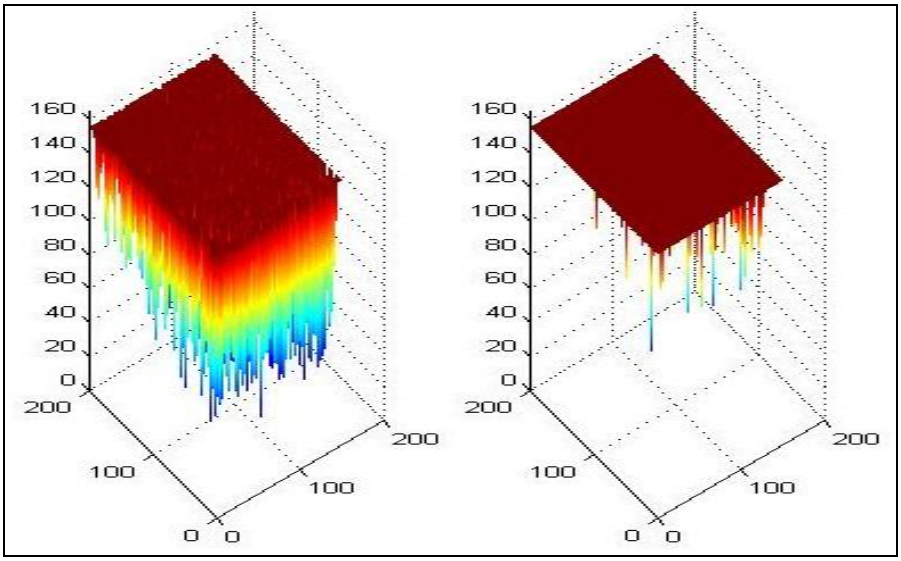

Figure 5.3: 3D profile image of the left volar forearm of an Oriental female aged 20-25 before and after occlusion for 2 minutes.

On looking at the co-relation between the two images; a shift towards the upper gray-scale values of the occluded skin site can be seen in Figure 5.4. As seen from this Figure, the co-relation at the higher values (higher occlusion) over 100 gray-scale shows that there is a major shift towards the occluded skin (after 5 minutes).

This means that more of the surface area is now having a higher gray-scale as compared to the pre-occlusion measurement.

There are a small number of 0 to 100 gray-scale pixel points which are consistent with lower end of the gray-scale as seen in the chart in Figure 5.2.

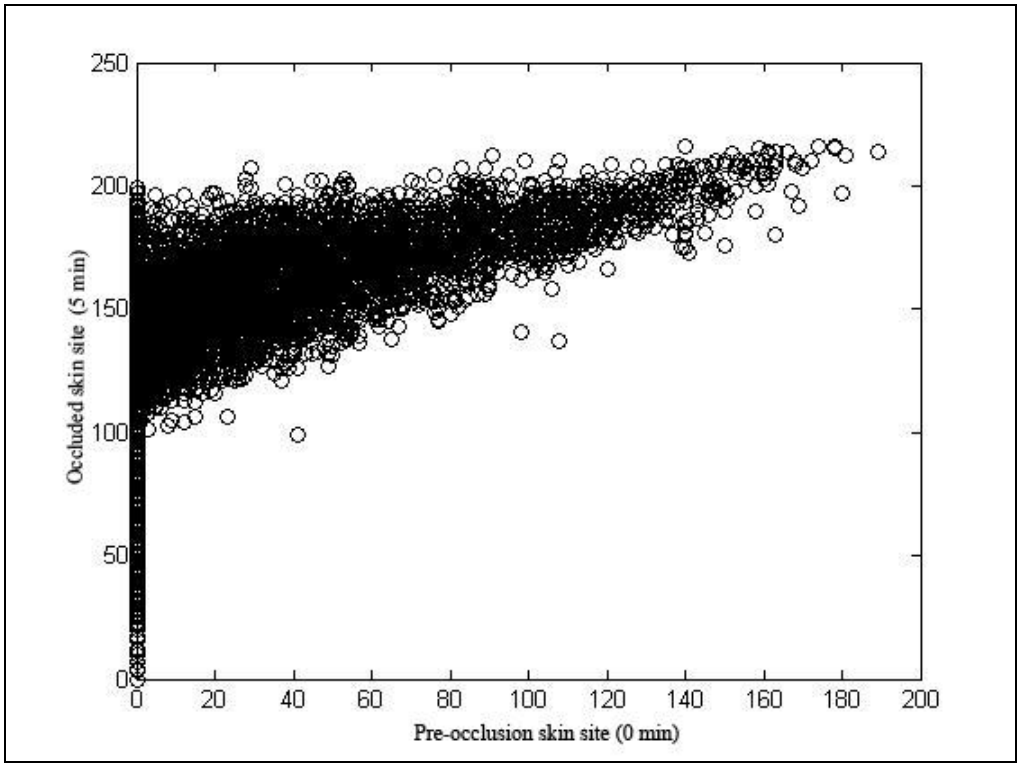

Figure 5.4: Co-relation between the image of left volar forearm of an Oriental female aged 20-25 before and after occlusion for 2 minutes. Pre-occlusion is on X-axis while occluded skin is Y-axis.

For the second occlusion test, the left frontal neck of an Asian male aged 35 to 40 is occluded and an image is recorded every one minute for three minutes as shown in Figure 5.5. The 3D profile for each of the image shows the surface is being occluded.

However a more prominent change can be seen in the depth image view where at 0 minutes, there is a higher reach (shown in red, yellow and blue) while in the consecutive images, the depth recedes until 3 minutes whereby it is at it lowest reach with a highly occluded surface.

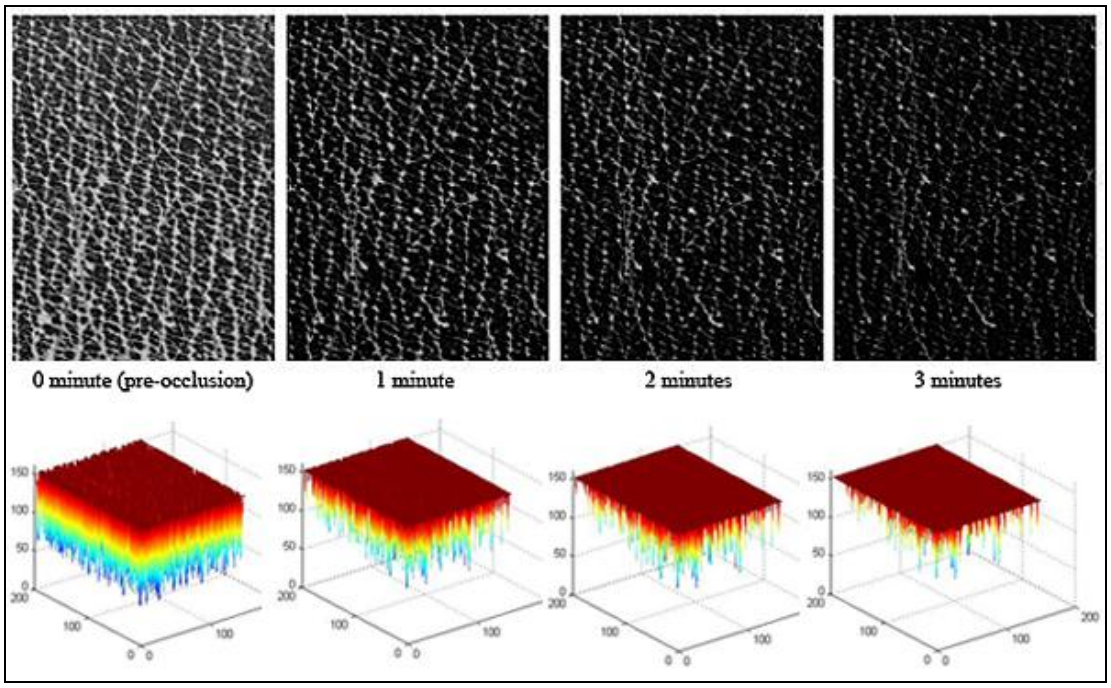

Figure 5.5: Occlusion for 3 minutes of left frontal neck of an Asian male aged 35 to 40 with corresponding 3D profile of the occluded skin site.

The gray-scale quantification can be seen in Figure 5.6 where the first recording has a gray-scale below 200 points and within the first minute has reached about 210 points.

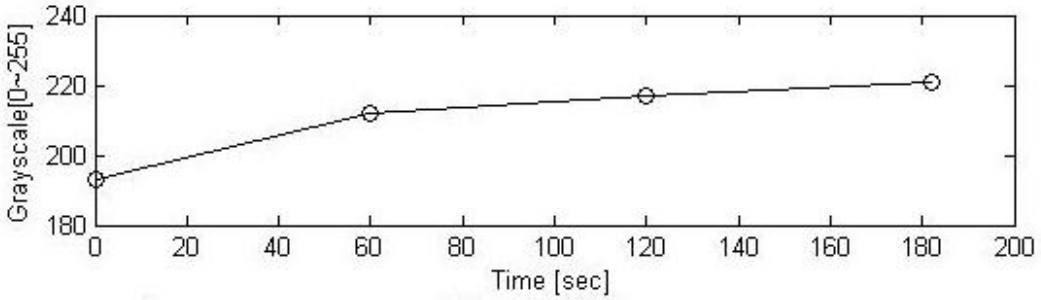

Figure 5.6: Occlusion gray-scale graph for 3 minutes of left frontal neck of an Asian male aged 35 to 40.

Within the second and third minute, the increase has slowed as the occluded area between the skin and the capacitance is saturated.

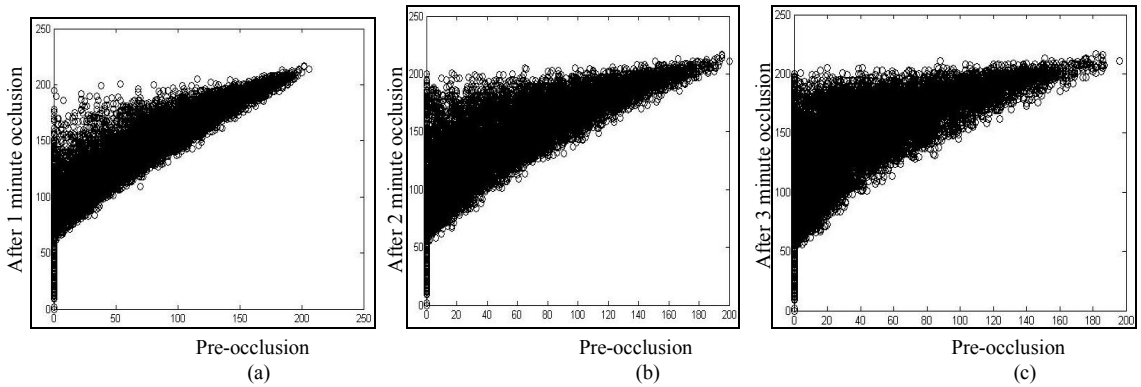

Figure 5.7: Occlusion co-relation between pre-occlusion and after 1 minute (a); occlusion and pre-occlusion after 2 minutes (b); occlusion and pre-occlusion after 3 minutes (c) .

In Figure 5.7(a) the co-relation between the pre-occlusion and after 1 minute occlusion shows a shift towards the higher gray-scale after the one minute occlusion. Figure 5.7(b) shows the co-relation is further decreasing in the higher gray-scale after 2 minutes occlusion as the surface water increases thus producing a much darker image.

In Figure 5.7(c), further saturation of the surface water occurs in 3 minutes as compared to the pre-occluded skin site thus resulting in a higher shift towards gray-scale nearing 200 points.

5.2 Comparison of Occlusion with capacitance sensor and RGB Camera Imaging

The skin site with a scab on the ankle is tested at 0 minutes and the capacitance sensor is maintained on the site for 30 seconds. Then a second image is automatically taken by the software and this is repeated every 30 seconds for 120 seconds while maintaining the capacitance sensor on the skin site without being moved to allow continuous occlusion.

After a time gap of 20 minutes to allow recovery of the skin site, the same test is repeated on the same site with RGB imaging using a SONY DSC-W55 Digital Camera and the results are seen in Figure 5.9

A gradual increase in gray-scale darkness is visible from 0 second to 120 seconds. It is noted that after occlusion for 120 seconds, the edges of the scab have become profoundly clear and the scab's border is much more prominent. Also, in Figure 5.8, the corresponding RGB images are shown against capacitance images for the duration of the time of measurement. There is no marked difference between the RGB images visually. This is due to the inability of RGB imaging in detecting hydration of the skin.

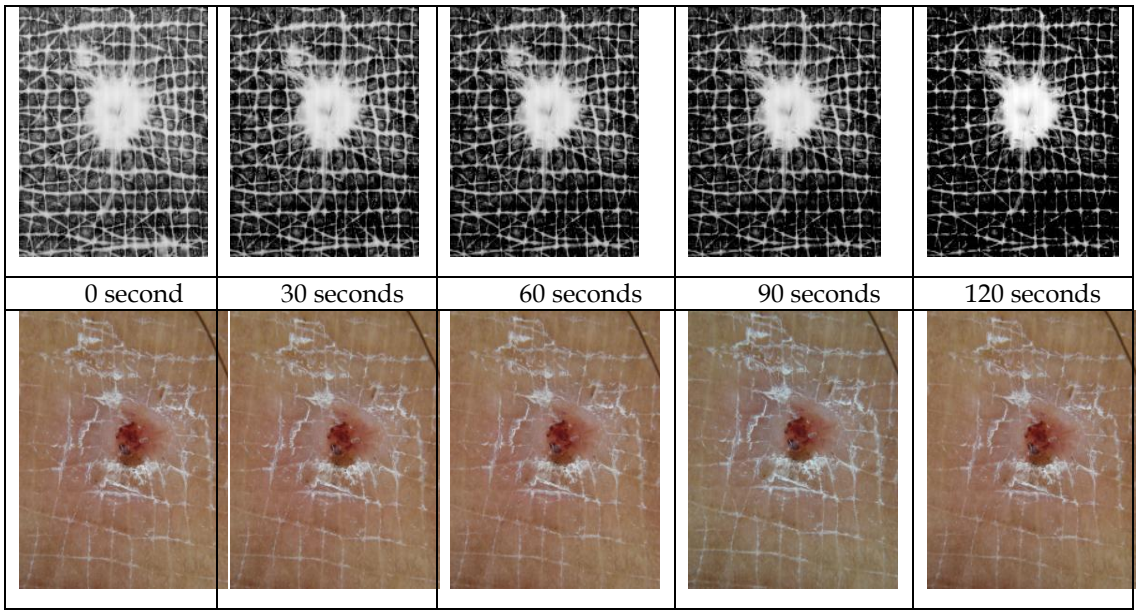

Figure 5.8: Skin capacitance images of scab on left ankle front, RGB Imaging with SONY DSC-W55 Digital Camera over 2 minutes.

The gray-scale average values increase is shown in Figure 5.9 where the average rises from 58.511 to 69.929 within 120 seconds. Major increase occurs within the first 30 seconds.

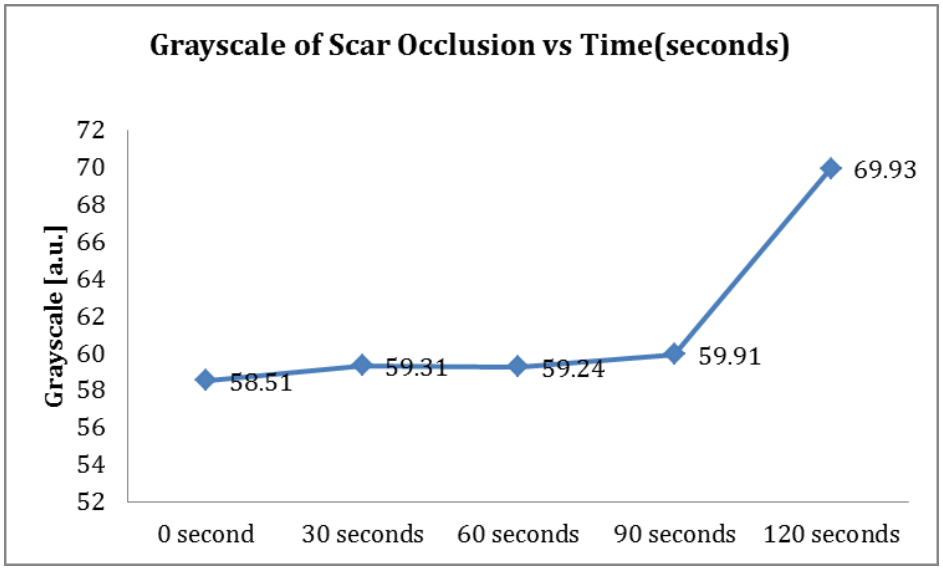

Figure 5.9: Tabled data and graph showing average gray-scale increase with time for the occluded skin site.

5.3 Moisturiser Treatment and Measurement

Dry skin is one of the most common symptoms of dermatological disorders and it is usually treated with the application of moisturisers. Moisturisers are categorised as hydrophilic and lipophilic. Hydrophilic moisturisers are low molecular weight thus penetrating the SC where they subsequently act as humectants[1]. (Caussin, 2009) Most commonly, glycerol is used as the low molecular weight to assist water retention.

Lipophilic moisturisers either penetrate into the lipids and provide increased barrier to water loss or they remain on the skin surface preventing evaporation of water from the SC. A substance is lipophilic if it is able to dissolve much more easily in lipid than in water.

[1] A substance used to help retain moisture mainly to absorb ambient water. Often it is a molecule with several hydrophilic groups.

In this experiment, a hydrophilic moisturiser is used to test the skin site in a room at 23.3°C and relative humidity at 46%. The moisturiser contains glycerol as the low weight molecules and is applied on the volar forearm of a female subject aged 25 to 30 years. Prior to application of the moisturiser, a measurement is taken and after application of the moisturiser, the test area is patted down and a measurement is taken. After one minute, another measurement is taken every 2 minutes up-to 7 minutes (Figure 5.10).

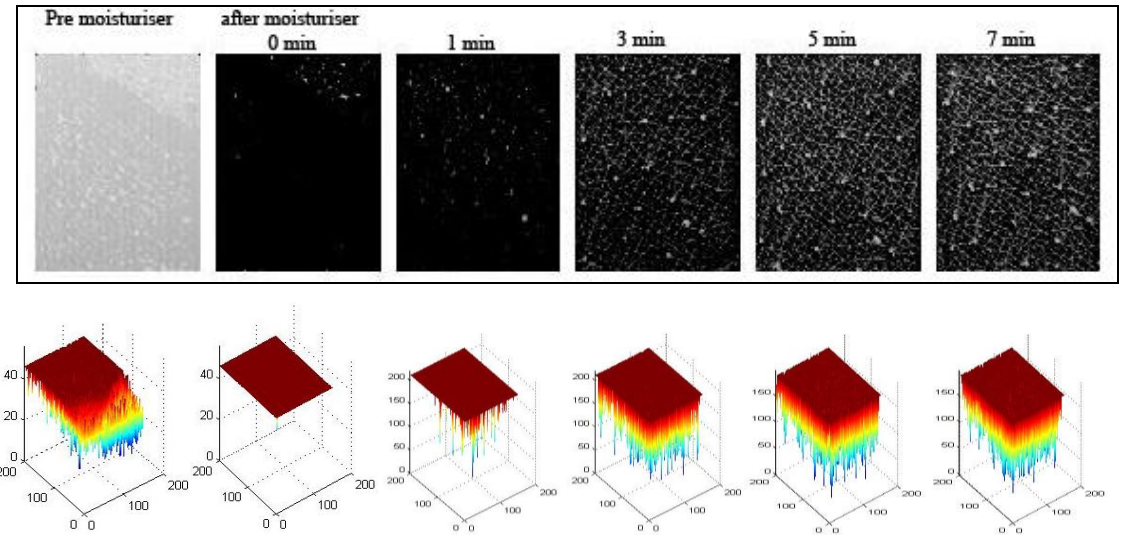

Figure 5.10: Pre-moisturiser and after application of moisturiser on the skin site monitored for 7 minutes showing both capacitance images and the 3D profile images.

As shown in 5.5 above, Glycerol or glycerin is a frequent addition to moisturising lotions and skin creams. From both the visual image and the 3D profile, it can be seen that the pre-moisturiser skin is relatively dry.

After moisturisation, there is a high increase in hydration show in the 3D image taken immediately after application of moisturiser. There is very little depth profile at this phase; and after 1 minute depth profile is visible showing a return to normalisation for the test skin site. After the third minute up-to the seventh minute, there is a rapid increase in the depth profile. During this test for 7 minutes; the

moisture loss is gradual and recovers towards the normal skin image of the pre-moisture skin.

The line chart of the capacitance images (Figure 5.11) below shows that prior to moisturisation the gray-scale average value is below 80 and immediately rises to about 190 after the skin site has been moisturised. There is slight increase after 1 minute interval reaching about 200 and after 2 minutes drops gradually reaching slightly below 200 points after 7 minutes.

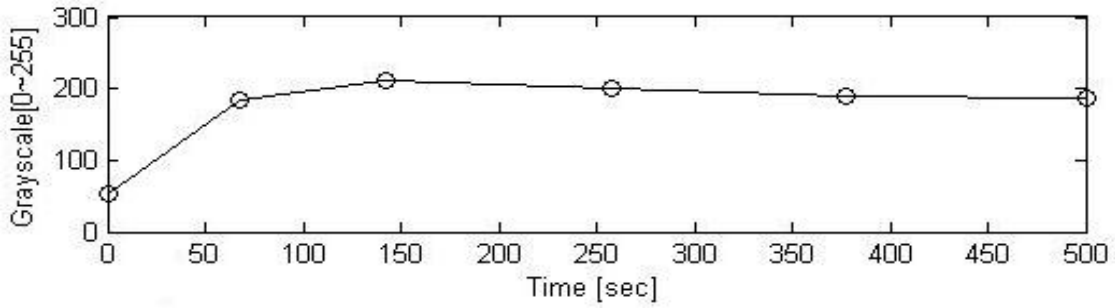

Figure 5.11: Quantification in line chart of the pre-moisturiser and moisturised skin for 7 minutes.

Total gray-scale can be further analysed from the Figure 5.12 where pre-moisturiser chart shows a bell-curve between 0 to 90 gray-scale ranges. The highest point for a gray-scale is about 1550 points.

On the pre-moisturiser skin a variable scale from 0 to 100 is present showing the water present on the skin is not able to produce a darker gray-scale as it lower in quantity.

Immediately after moisturisation (0 min), the gray-scale has increased to 250 and above with points in this range reaching 3×10^4. There are a small amount of points spread evenly from 60 to 250 gray-scale. This shows that there is a larger concentration of water on the skin surface caused by the moisturiser and water is spread more evenly on the surface within the range of 60 to 250 gray-scale.

By 1 minute, the gray-scale above 250 have further increased to nearing 255 but the total points in this range has dropped to about 2.8 x 10^4 points. The lower end gray-scale has further spread from 50 to 250 gray-scales. The moisturiser coupled with the effect of natural hydration of the skin has a larger variation of gray-scale but water is being lost from the skin surface resulting in the drop of the overall higher scale to about 2.8 x 10^4 points.

At 3 minutes, the gray-scale at 250 has further dropped to below 16,000 points; and the lower end gray-scale between 50 to 250 is further increasing and can be seen in the rising of the values towards the higher gray-scale.

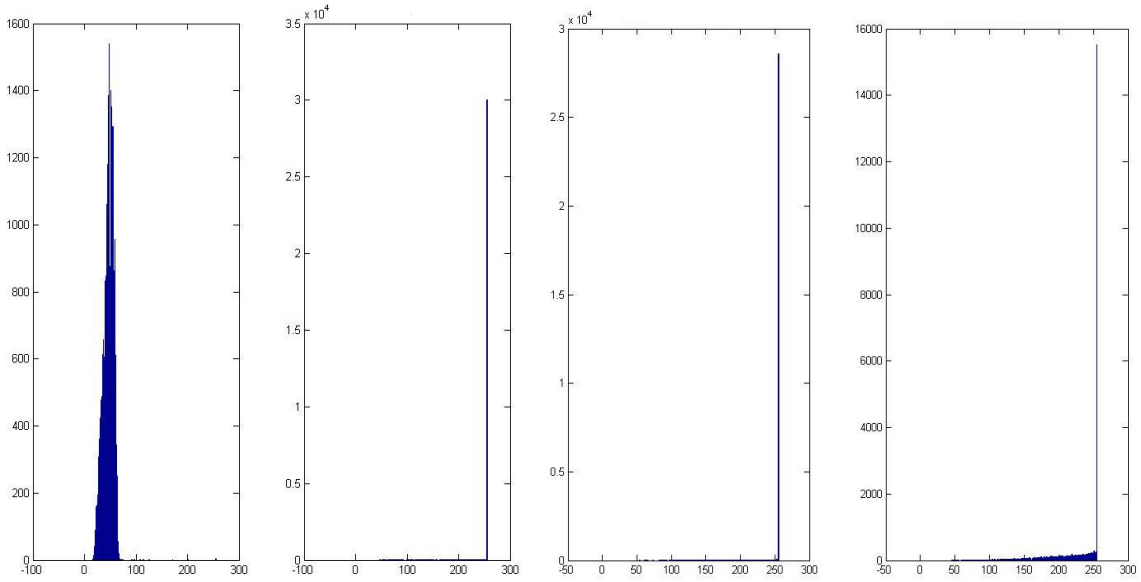

Pre-moisturiser 0 min 1 min 3 min

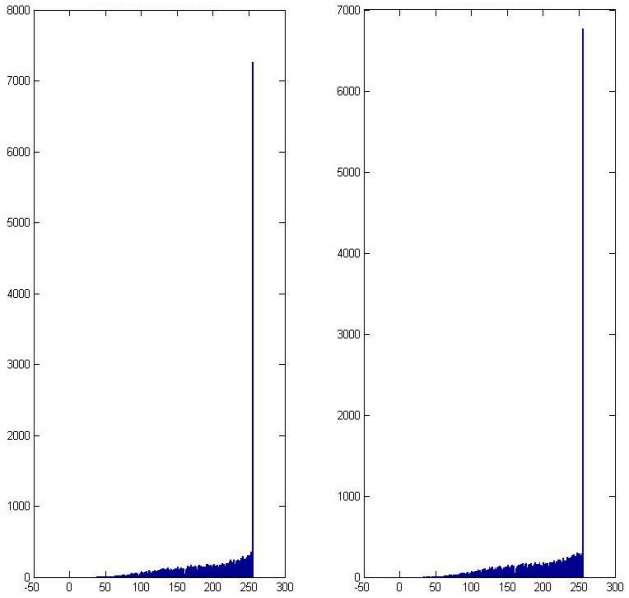

5 min 7 min

Figure 5.12: Line graph showing gray-scale points accumulation for the first 4 readings.

At 3 minutes, 250 gray-scales have dropped to about 7200 points indicating a recovery towards pre-moisturiser skin condition. The lower end gray-scales between 40 to 250 is increasing further to about 500 points.

By the seventh minute, the gray-scale at 250 have further dropped to below 700 points and a consistent increase in the lower gray-scales. At the seventh minute, it can be seen that larger amount of the gray-scale is moving towards the lower end scale. This shows that the skin is in the process of returning to it's original pre-moisturiser condition.

5.4 Depilation of Multiple Skin Sites with Waxing Strips

Waxing strips are used as a method of hair removal. Typical waxing strips are treated with either wax or chemicals to remove hair. A chemical based wax strip was used for this experiment. The main ingredients of the wax strips are triethylene glycol rosinate, glyceryl rosinate, silica and isopropyl myristate.

The strip is applied by warming the strips first; by holding between the palms for about a minute. Then the strip cover is removed and the wax side is placed against the skin. After a light massaging movement over the strip, it is pulled away backwards in a rapid single movement.

Three skin sites; the right front upper foot, left dorsal forearm and the right volar forearm were selected for depilation with wax strips. Measurement was done both before and after waxing the skin site.

An initial visual inspection as in Figure 5.13 showing a varying difference between the three skin sites selected for waxing. After waxing, all three skin sites show a visible visual difference.

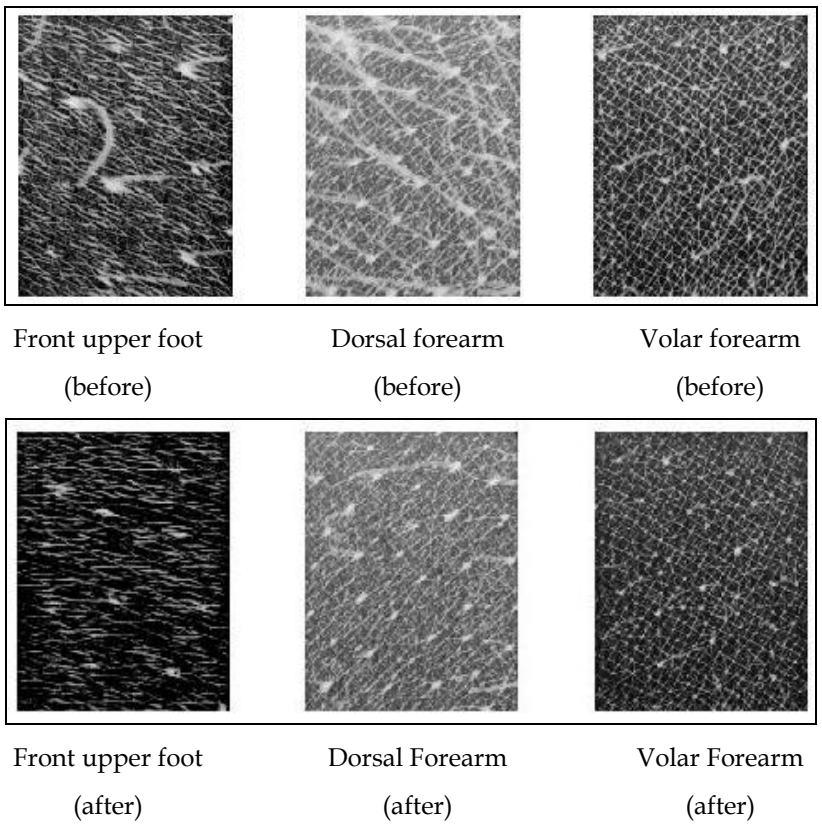

Figure 5.13: Three skin sites showing different visual images both before and after waxing.

The 3D depth profile is noted to have not changed much as compared to other types of tests such as hydration and occlusion. This is mainly due to no additional hydration is being added to the skin site. The main action of the wax strip is to remove hair follicles but some small amount of stratum corneum is also being stripped depending on the strength of the wax used. A 3D profile comparison between the three different sites is imaged in Figure 5.14.

Overall surface change is visible and this can be seen from gray-scale data as shown in Figure 5.15.

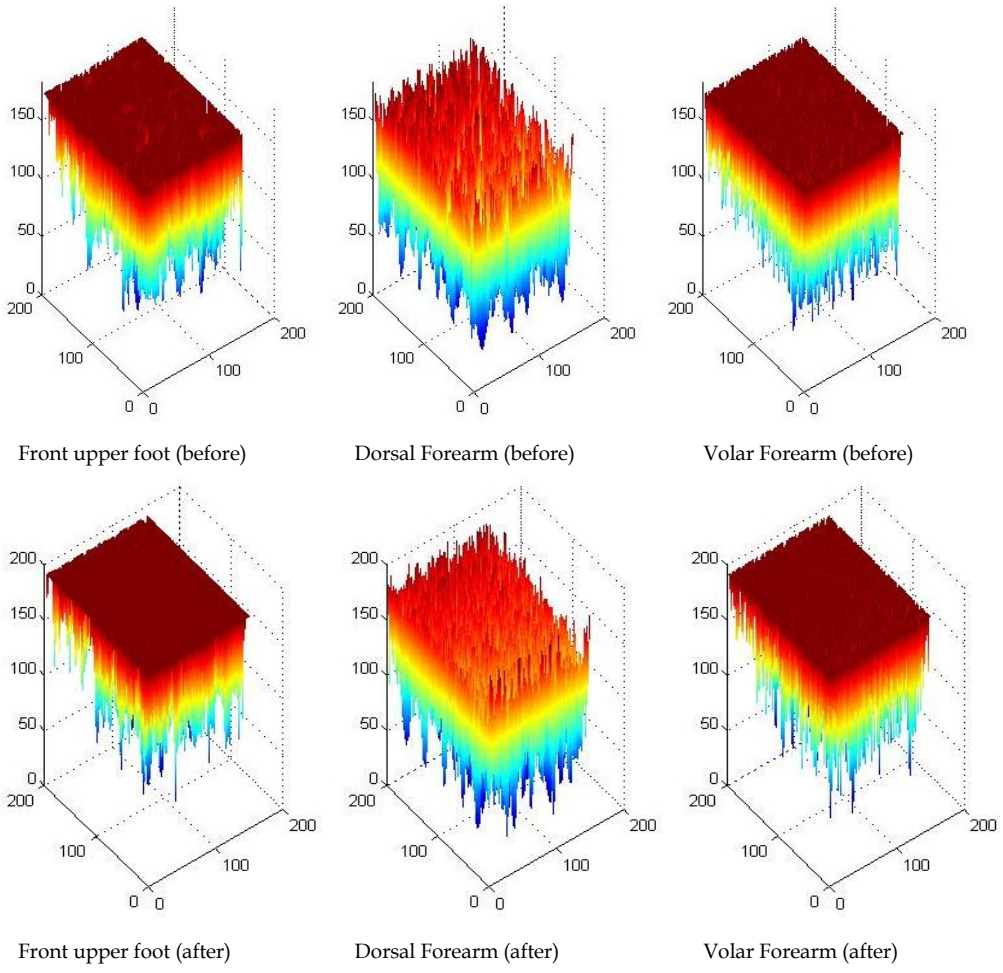

Figure 5.14: 3D profile of three skin sites pre-waxing and after waxing shows different visual images both before and after waxing.

The gray-scale values of all three sites have increased. The gray-scale of front upper foot has increased from 210 to 235 and the gray-scale of dorsal forearm has increase from 180 to 200. The volar forearm gray-scale has increased from 210 to 220.

An initial visual inspection of the skin image shows that with the loss of hair after depilation (characterised by lower water concentration and showing as major white lines in the image), a larger skin surface is now having contact with the capacitance sensor thus allowing more water to have contact with the capacitance sensor surface.

In a study done by H.Y. Ando and A. Escobar (1983), depilation of the skin causes the loss of Stratum Corneum cells and the thinning of the SC layer thus exposing the inner hydrated skin.

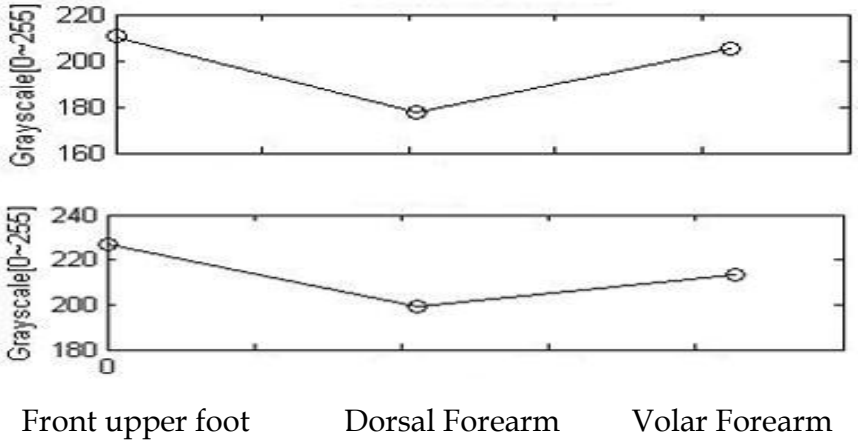

Figure 5.15: Gray-scale of three skin sites pre-waxing and after waxing.

5.5 Dry Skin Treatment with Oil and Measurement

A dry skin area on the front of the right lower leg of an Asian volunteer aged 35 to 40 is identified and a measurement is carried out with the capacitance sensor. Then the skin site is treated twice with mineral oil (Johnson's Baby Oil); once

immediately after the first measurement and then again the next morning with a time interval of 24 hours. The measurement is done about 6 hours after the second application. There is a 24 hours gap from the first measurement to the second measurement.

The visual result shows (Figure 5.16) more uniform and thinner micro-relief lines as compared to the pre-treatment measurement.

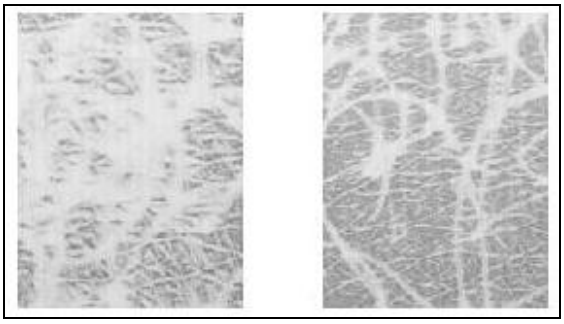

Dry skin After mineral oil treatment

Figure 5.16: Gray-scale of dry skin prior to treatment with mineral oil and after treatment.

The 3D profile image (Figure 5.17) shows a much more uniform surface after treatment with mineral oil. However, the depth profile remains roughly the same before and after the treatment. This shows that water content of the skin has not changed much from before and after treatment.

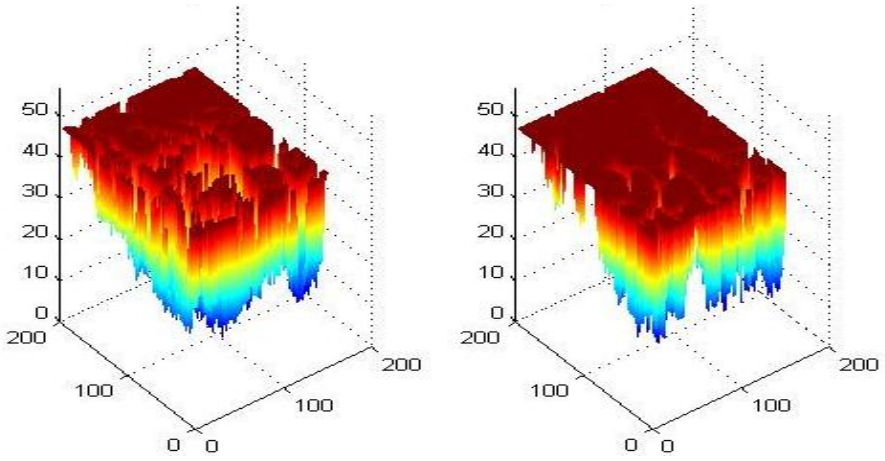

Dry skin After mineral oil treatment

Figure 5.17: 3D profile of dry skin prior to treatment with mineral oil and after treatment.

A look at the total points of gray-scale shows that prior to mineral oil treatment, most of the gray-scale points are grouped below 100 gray-scale and reaching a total of about 1100 points as shown in Figure 5.18. After treatment with mineral oil, the total points have dropped to 500 and shifted more towards higher gray-scale indicating a more uniform distribution between 0 to 100 gray-scales.

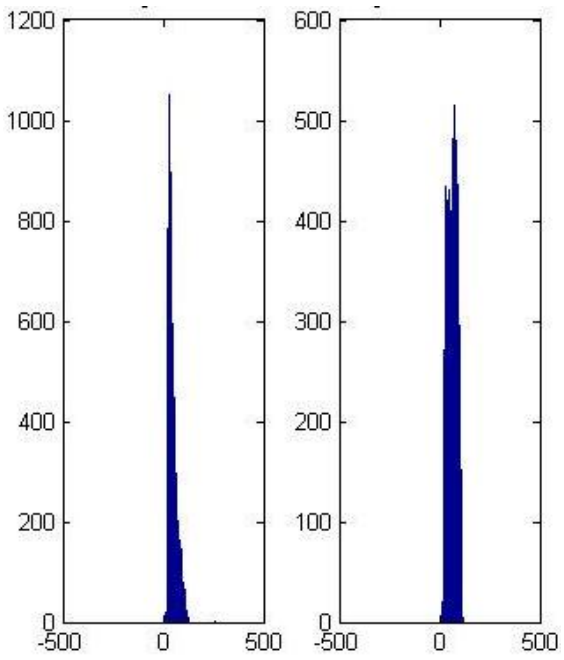

before oil application after oil application (24 hours)

Figure 5.18: Graph showing dry skin prior to treatment with mineral oil and after treatment.

This shift from higher points with lower spread over gray-scale compared to after treatment with lower points and a bigger spread of gray-scale goes to show that there is uniformity in the hydration of the skin surface.

5.5.1 Further Tests on Mineral Oil Application

A new test side was added to the example above that is the skin on the front of the leg and is shown in Figure 5.19. Again, visual inspection of the 2D image shows that the skin micro-relief lines have become much finer.

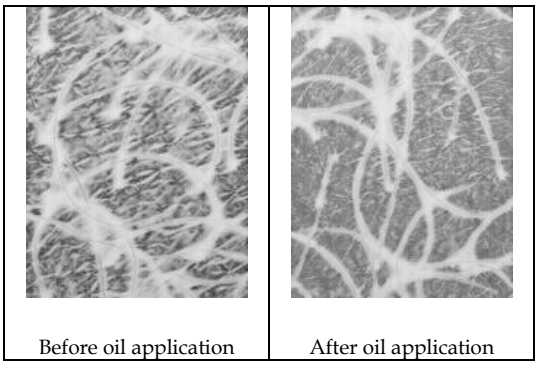

Figure 5.19: Capacitance images showing dry skin prior to treatment with mineral oil and after treatment.

The dry skin characteristics have shown an improvement visually as the surface of the skin has become more uniform.

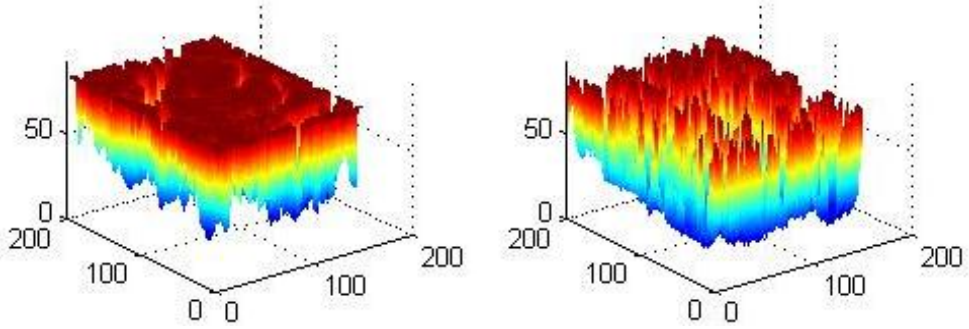

Left Leg Front (before) Left Leg Side (before)

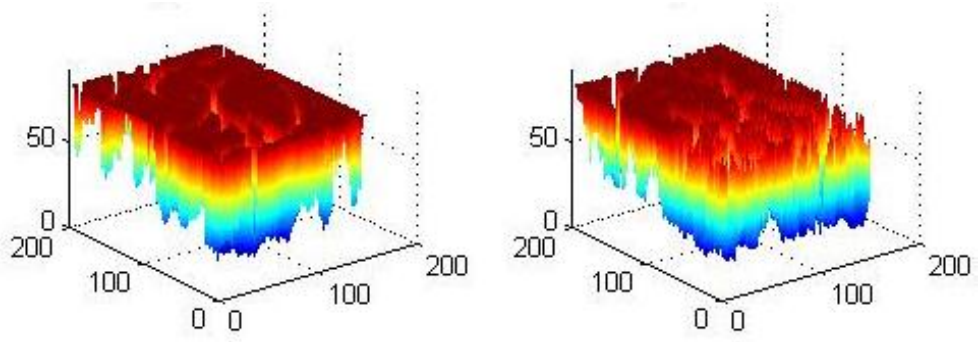

Left Leg Front (after) Left Leg Side (after)

Figure 5.20: Capacitance Skin capacitance images of before and after mineral oil application on dry skin of the leg on Asian volunteer shown in a 3D profile

Figure 5.20 shows 3D imaging of the same skin site shown in Figure 5.16 and 5.19 put together. The lower 2 images are after 24 hours has lapsed since the application of oil on the skin surface. The 3D images show a more robust view of the skin surface and the micro-relief lines depth is clearly visible.

5.5.2 Further Analysis with MATLAB Imaging Program

Figure 5.21 shows the average gray scale values generated for all the images. It can be seen that the gray scale average drops after the treatment of the skin site with mineral oil. This is mainly due to the skin is now more hydrated than before the application of mineral oil.

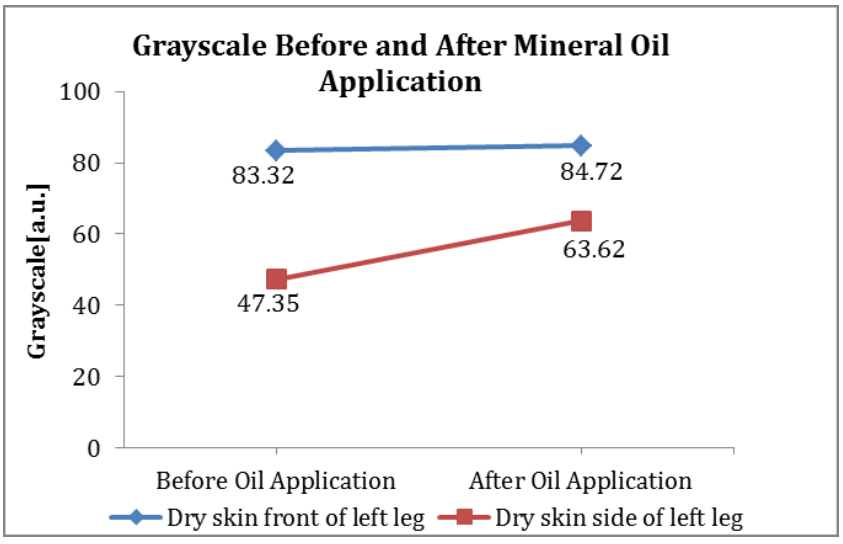

Figure 5.21 Grayscale of dry skin before and after mineral oil application

Figure 5.22 shows further imaging using MATLAB filters, averaging and standard deviation. The first image shows the average values of the 9 neighbouring pixels. The second image shows the possible disks on the skin surface.

Here any area that has 2 pixels on all sides of the selected pixel will be marked. Larger amount of noise (or inconstancies on the skin surface) will be marked with more disks.

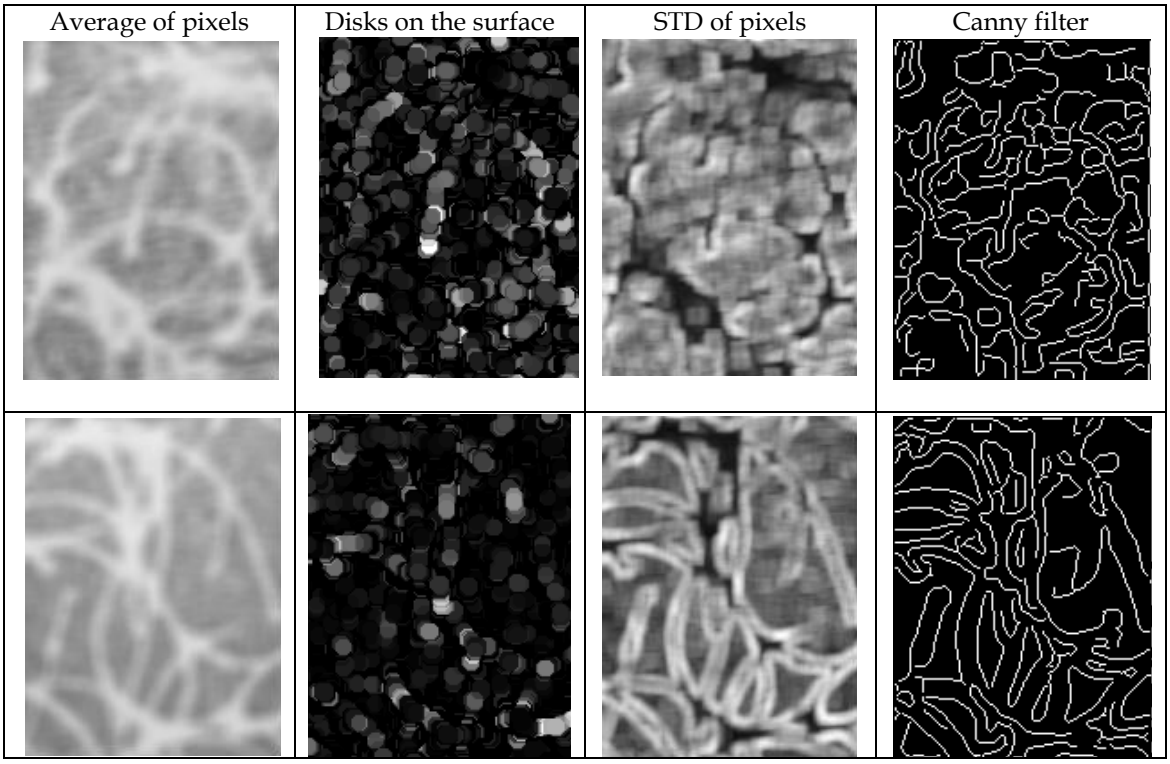

Figure 5.22 Skin capacitance images of before and after mineral oil application on dry skin of the front of leg on Asian volunteer shown with Matlab filters.

The third image shows the standard deviation of 9 neighbouring pixels. The more consistent the surface area, the better the images appears. In the first case of the dry skin, the surface area shows inconsistent surface whereby even the hair shaft is blended with the surrounding area (as the dryness of the skin is closely similar to the hair follicle). In the second image after oil application, the surface of the skin is clearly marked and the hair shafts are delineated.

The final image is a Canny filter that outlines major lines within an image. The image generated with Canny filter shows that much of the background noise can be removed and in the case of after oil application, the image shows mostly the outline of the hair shafts. The process used to generate these images are discussed in Chapter 4.

In Figure 5.23, similar filter images are shown for the side of left leg of the same volunteer.

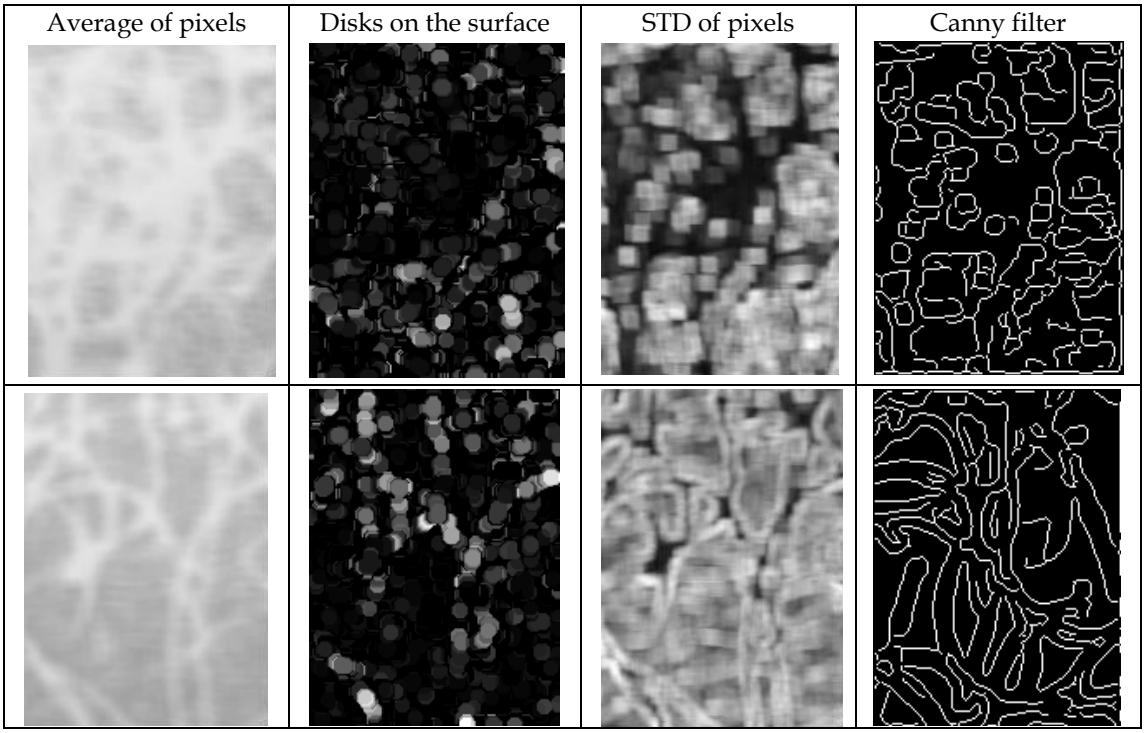

Figure 5.23 Skin capacitance images of before and after mineral oil application on dry skin of the side of left leg on Asian volunteer shown with MATLAB filters.

Mainly the STD image and Canny filter shows more uniform images after application of oil on the dry skin.

As seen here; a dry and/or scarred skin surface is easily detectable on the capacitance sensor. After occluding the scarred surface, its border is more prominent and can be measured with high accuracy.

The disk filter shows the co-joining areas more clearly and isolating the dry area from the surrounding hydrated areas. The STD filter can clearly isolate the uniform areas from the surrounding non-uniform areas thus showing more accurately the hydrated skin with clear borders against the dry skin.

5.6 Conclusion and Findings

In this chapter, the feasibility of measuring occlusion using the FPC6410 capacitance sensor was established. After analysis of the data attained from the capacitance sensor, it was noted that in occlusion measurement, a shift towards a higher gray-scale is evident in the measurement. Co-relation is established between pre-occlusion and occluded skin and this relationship shows that there is a shift towards that the occluded skin.

A comparison was done between the capacitance sensor images and RGB imaging of a camera that shows the capacitance has a good measurement capability as compared to the RGB imaging.

Tests were also done with applying moisturiser to the skin and it shows that the capacitance sensor has the ability to measure and show the loss of hydration over time effectively.

It has also been found that depilation of the skin can be measured using the capacitance sensor. Loss of hair after depilation can be seen visually on the skin sites and further measurement can be done with 3D imaging showing a change in the skin.

Using filters in MATLAB, the skin surface can be seen from different aspects such as line formations, disks surface and through standard deviation values. This form of imaging allows for better understanding of the skin that may not be seen from a standard capacitance image.

The capability of the capacitance sensor coupled with the imaging process of the skin is researched in detail in chapter 6.

CHAPTER 6: IMAGING AND MEASUREMENT OF SCARS AND BODY ART USING CAPACITANCE SENSORS

Scars are caused by the destruction of the dermis thus resulting in fibrous tissues to replace the damaged tissues. It is a natural healing process of the body. A multitude of reasons can be the cause for a scar (e.g. accidents, surgery or disease). Scar tissues are not similar to the normal skin and normally have lesser propensity in losing water due to the inability of sweat gland and hair follicles to grow. Scar tissues are also of inferior functional quality as compared to the surrounding normal skin.

In the analysis of scars, both the FPC5410 and FPC6410 capacitance sensors were used.

6.1 Classification of Scars

Classifying a scar is important in ultimately choosing which treatment modality best fits. Factors contributing to scar formation include pigmentation/vascularity[1], thickness (scar height), pliability, surface texture, and surface area. Accurate and reliable tools have been developed to measure each of these features subjectively and objectively. (Idriss N, Maibach H.I, 2008)

In a very broad scale, scars can be classified as:

6.1.1 Keloids

Keloids are thick irregular clusters of scar tissues that are normally rounded. They may grow beyond the border of the wound. Keloids are formed by collagen that is produced by the body when the wound heals. They may occur anywhere on the body and are more common on a dark-skinned person.

[1] Vascularity – a condition where veins are visible and prominent. Mainly occurs due to low body fat, high blood pressure and low water retention in the body.

The scar can occur up to one year from the time of the initial wound to the skin.

6.1.2 Hyperthropic scars

Though similar to keloids, they normally are confined to the original boundaries of the injury thus may have an elevated and thick scar. Occasionally, hyperthropic scars have a red tint to it and develops within weeks of the injury.

6.1.3 Contractures

Contractures are an abnormal occurrence that happens when a large area of skin is damaged and lost, resulting in a scar. The scar formation pulls the edges of the skin together, causing a tight area of skin. The decrease in the size of the skin can then affect the muscles, joints, and tendons, causing a decrease in movement.

6.1.4 Adhesions

Another type of scarring, called adhesions may form between unconnected internal organs. Adhesions may cause complications during certain surgeries.

Scars cannot be removed completely, thus the need for a regime of care to minimise and reduce the size of the scars. It is therefore necessary that maintenance of the scar is done and measurements are taken as comparison of the percentage of improvement over time (Brodland D, 1998).

In most cases, measurement of scars are normally done using the visual eye and also aided by a measuring device such as a ruler. The need for a better, more accurate and image based technology is a sure step in the direction of better management and measuring of scars.

Analysis has shown that from the skin capacitance images, any abnormality of the skin resulting from a loss of hydration can be imaged.

6.2 Theory

As has been established in the previous chapters experiments, the image gray scale values are associated with skin hydration, the higher the skin hydration, the higher the image gray scale value will be, and vice versa.

To quantify the skin hydration level, and to compare the results from different skin images, the average gray scale values are used. The average gray scale value of an image is calculated by averaging all the pixel values which are above a certain threshold; in this case, it is set at 20. Using the threshold, pixels with a bad contact can be eliminated from the average gray scale value calculation, and yield better results.

As mentioned earlier, scars has lesser propensity in hydration and thus a marked difference can be seen between a scar and the surrounding healthy hydrated skin. The average gray scale value of a scar in comparison to the surrounding healthy skin can be taken by imaging the scarred area and a healthy area.

Apart from the greyness, the images can also show the fine structures of skin, called micro relief. Figure 6.1 shows some sample of scabs[1] and scars imaged with the FPC6410 capacitance sensor.

Due to scars natural properties of being less hydrated and having lower micro relief lines, a prominent image can be seen with capacitance sensors.

[1] A crust discharged from and covering a healing wound.

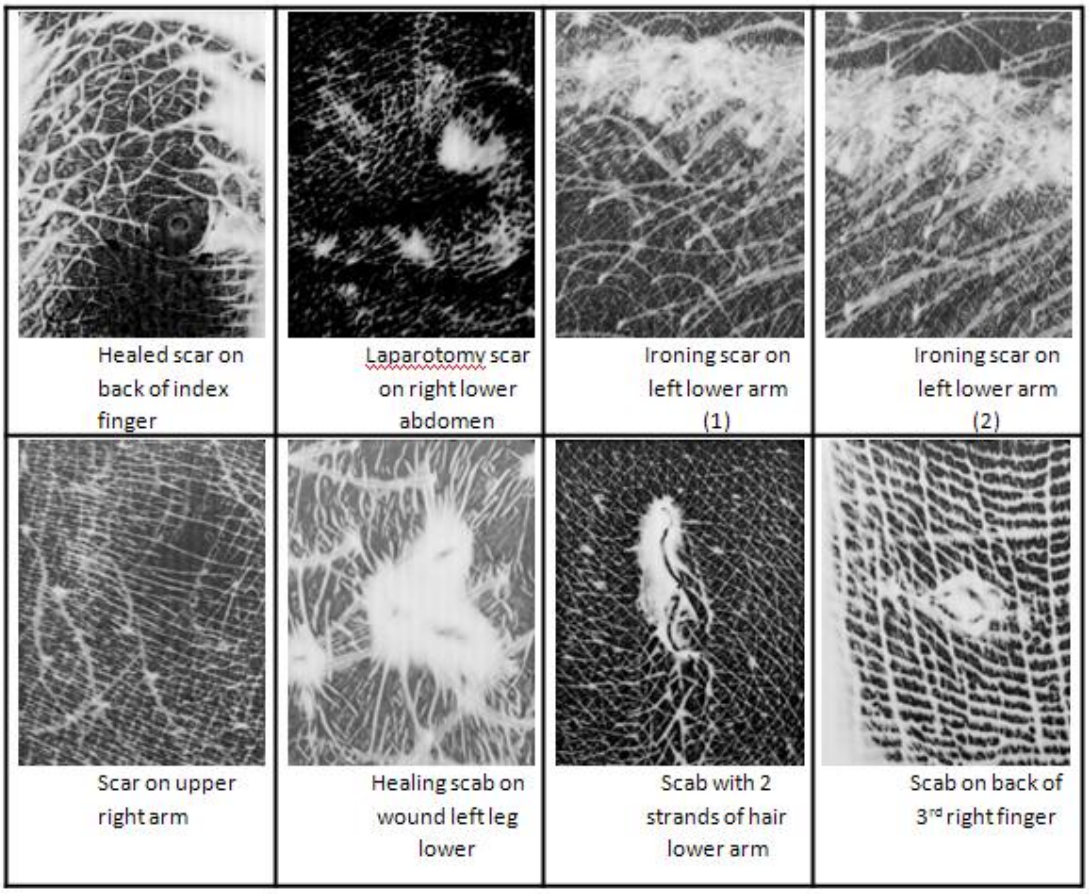

Figure 6.1: Skin capacitance images of scars and scabs on 8 sites on different volunteers.

6.3 Measurement, Imaging and Discussions

In measuring scars using the capacitance sensors, 3 major types of scars; keloids, hyperthropic and contractures have been selected. Also, images of a healing wound over a period of 26 days to show if a scar will develop have been taken.

6.3.1 Keloid

As a comparison, a digital image (Figure 6.2) of the scar is taken with a camera prior to it being subjected to scanning by the capacitance sensors.

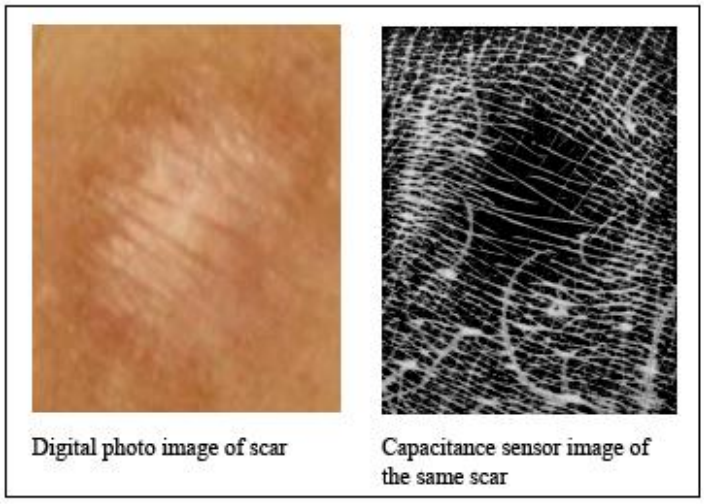

Figure 6.2: Showing a digital camera image and the same scar on the right upper arm imaged with FPC6410 capacitance sensor. Subject is an Oriental male aged 40 to 45 years.

The camera image is similar to what one will see when looking at the scar visually. Figure 6.1 shows the image taken using the capacitance sensors. This image though is in a gray-scale, gives a clearer image of the scar and raised micro-relief lines on the hyperthropic scar are clearly visible.

As can be see in the above images, the digital camera colour image is not able to show the finer details of the visibility of the micro-relief from the capacitance sensor is prominent compared the visual image.

The close grouping of the micro-relief lines around the scar shows the raised area bordering normal skin. The capacitance image also show other details such as hair follicles and sweat pores as white lines and dots.

Shown in Figure 6.3 is another image of a keloid scar that is comparatively smaller in size.

Figure 6.3: A scar below the Index finger of the right palm. Subject is a Caucasian female aged 20-25 years.

6.3.2 Hyperthropic

Here in Figure 6.4, a hyperthropic scar that is more than a few weeks old is captured using a digital camera and compared against an image produced by the capacitance sensor. It is noted that only part of the scar is captured by the capacitance image.

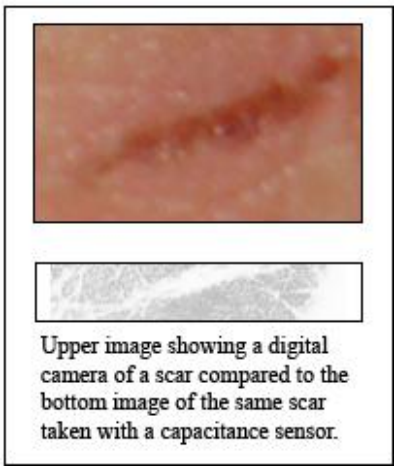

Figure 6.4: A fresh hyperthropic scar at the back of the thumb on right hand. Subject is a female Caucasian aged 35 to 40.

The red surface of the scar is a characteristic of a hyperthropic scar. It shows as white values on the capacitance sensors image as the scar surface is less hydrated in comparison to its surrounding skin area. The edges of the scar are much finer on the capacitance sensor image. The bottom left of the photo image shows a whiter surface

which consequently appears as a low hydrated region (shown as white) in the capacitance image.

6.3.3 Contractures

An image of a contracture is harder to capture on a non visual device as the 'landscape' of this scar is much flatter thus hiding much of the damage as it may be visible to the naked eye.

However imaging with a capacitance sensor (Figure 6.5) shows that a good image can be reproduced, and that a prominent image of the scar can be studied more effectively.

Figure 6.5: Showing a digital camera image and the same contracture scar imaged with FPC6410 capacitance sensor. Subject is an Oriental male aged 40 to 45 years.

6.3.4 Healing Wound Imaging

This experiment was conducted over a period of 11 days. For the purpose of this experiment, the smaller surface area capacitance sensor FPC5410 was used. Images were taken on day 0 (the initial cut day) shown in Figure 6.6, day 1 and subsequently everyday for 10 days shown in Figure 6.7.

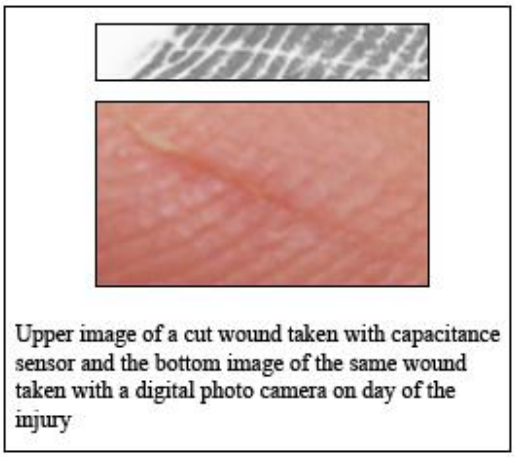

Figure 6.6: Showing a digital camera image and the same cut wound imaged with FPC6410 capacitance sensor. Subject is an Asian male aged 35 to 40 years.

A visual image was only captured for day 0. The wound was a straight cut caused by a blade. From early observation, it is believed that the cut probably reached the dermis layer as there was presence of blood.

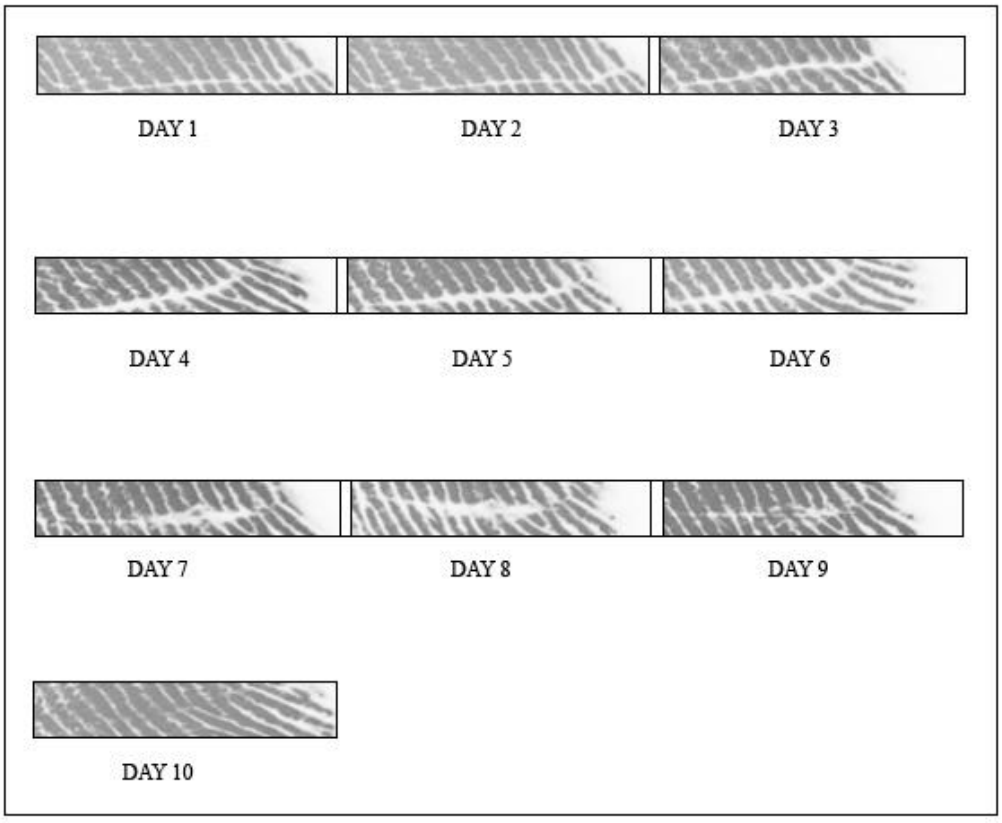

Figure 6.7: Showing a digital camera image and the same cut wound imaged with FPC6410 capacitance sensor. Subject is an Asian male aged 35 to 40 years.

A gradual improvement over the 10 day period is documented by the capacitance sensor. It is also noted that on day 7 and 8, the thickness of the scar has increased. This is due to the dried scab on the surface has fallen off exposing a much drier inner skin that hydrates and closes the wound within the next 3 days. Day 10 shows the skin has recovered with minimal damage or formation of a scar.

The images produced over the period of time shows the practical application of the capacitance sensor for management of scars.

6.4 Occlusion of Scar

Scars can be occluded to produce a better image and more precise measurements. Figure 6.8 shows occlusion of a scab over a 4 minute period that is achieved by keeping the skin with constant contact with the capacitance sensors surface. As the skin surface is deposited with water, the images gray scale increases especially around the surrounding area of the scar. This gives a better and sharper image and since much of the micro-relief lines are now minimised, quantification of the scar is more prominent.

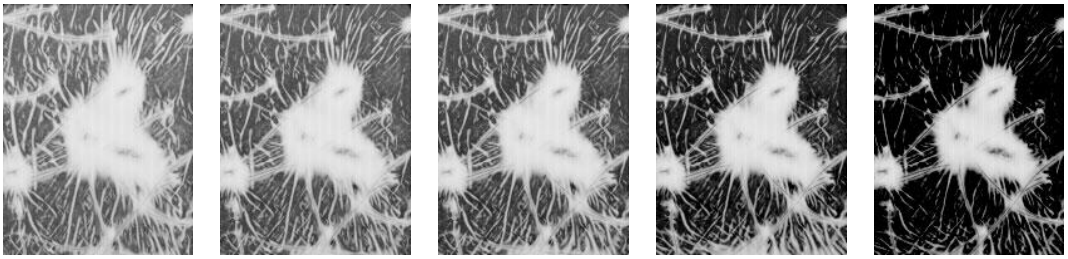

Figure 6.8: Occlusion of a scar over a period of 4 minutes

The clarity of the scab increases as the surrounding skin is being hydrated while the scabs surface hydration remains the same. The image is then quantified showing the gray-scale values against the 4 minutes duration as seen in Figure 6.9. It is seen that as the skin surface occludes, the gray-scale values rises correspondingly.

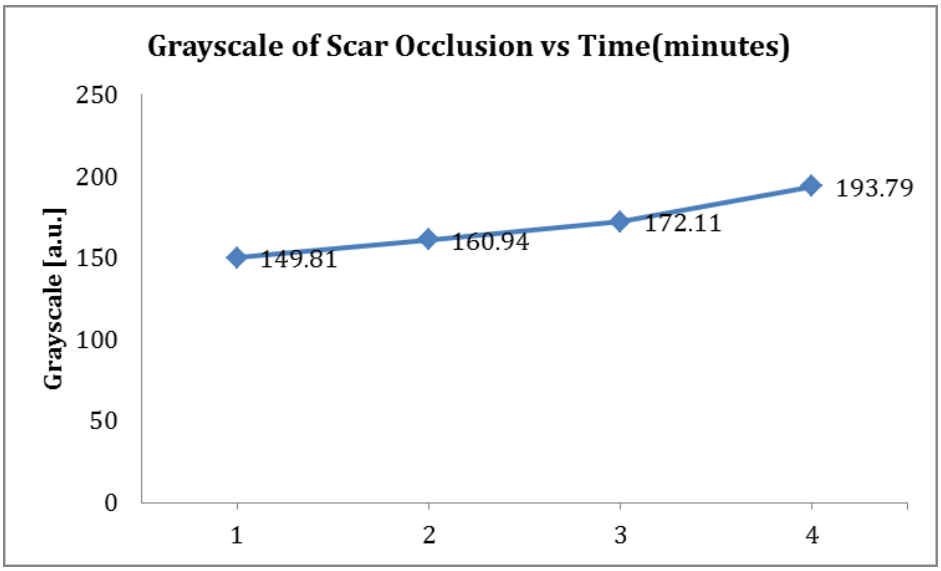

Figure 6.9: line chart showing the average gray scale value of each image vs. time

6.5 Analysis of Scar with Matlab

The scar can further be analysed using a program written in Matlab. The program includes a few different filters that are applied to the scar image to obtain a better understanding of the scar profile. As shown in Figure 6.10, an image of a scar taken with the capacitance sensor FPC 6410 is used. This image is then processed with the Matlab program and results of different filters used, averaging and standard deviation techniques are shown in Figure 6.11.

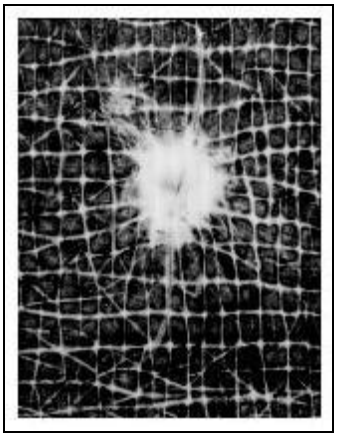

Figure 6.10: Image of a scar to be analysed with Matlab program

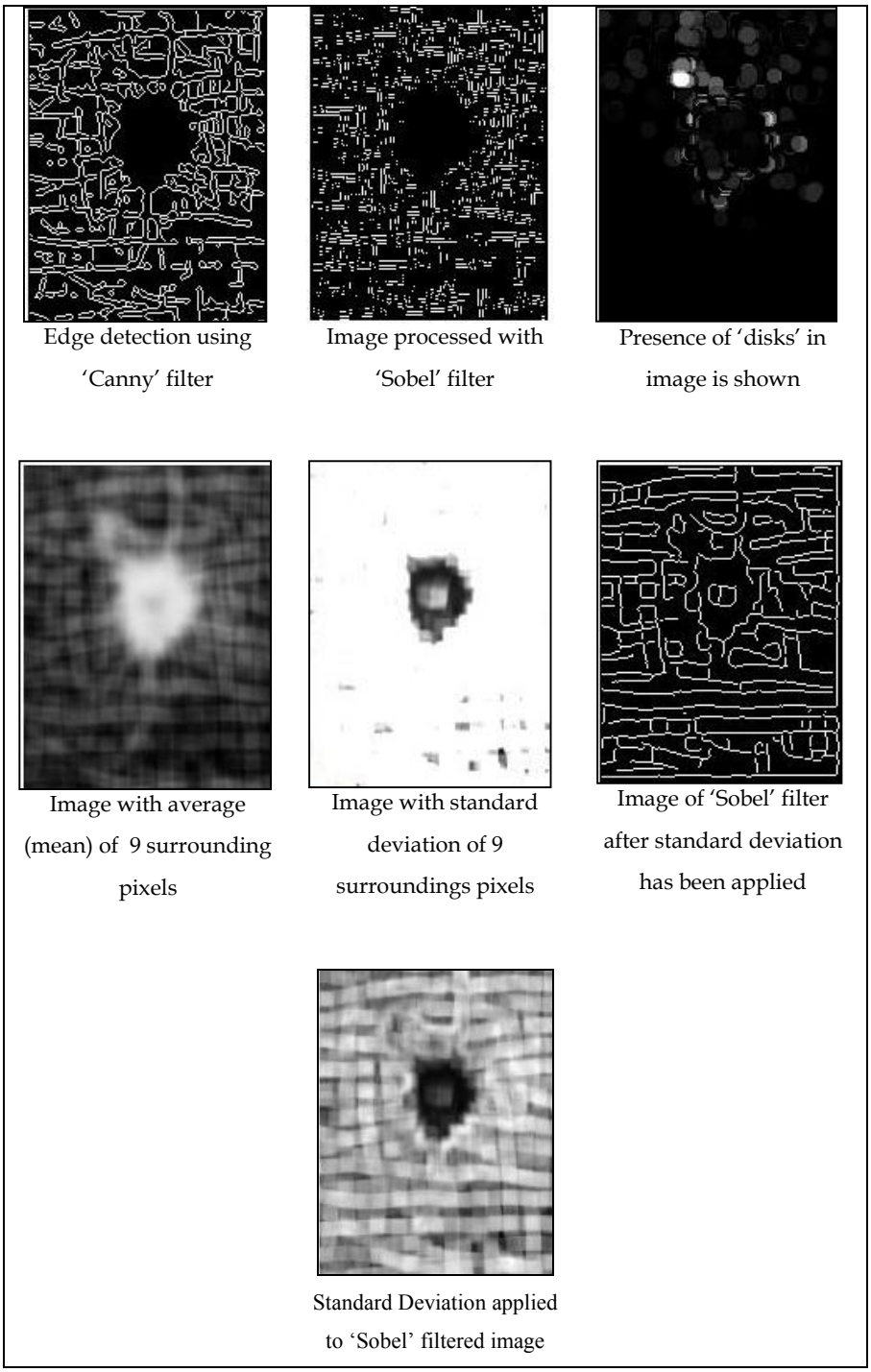

Figure 6.11: Images of a scar analysed with different filters in Matlab program

6.5.1 Detecting the Edge of Scar

An edge in an image is simply a region of pixels where the intensity value of pixels on either side changes sharply. This is not the same as a line, since a line has two

edges, although most of the lines in an image will represent edges. The result of edge extraction is usually a bitmap (a binary image where each pixel is 0 or 1), where a set pixel represents an edge. These are known as edge pixels, or edgels for short. There are many ways of extracting edges from an image, of which the Sobel filter and the Canny filter appear to be most suitable.

Here, different filter used on the scar image is explained:

6.5.1.1 Edge Detection using 'Canny' Filter

The Canny edge detector has been designed and can be proven to be an optimal edge detector through a rigorous mathematical description, which is explained by Trucco. Its aims are to minimize errors in the detection of edges (by not missing any true edges or including points which are not edges), and to ensure that the edges detected are as close as possible to the true edges. There are three main stages to the algorithm. The algorithm begins by enhancing the edges in the image, using a Gaussian filter to smooth the image. A Sobel filter is then applied but in this case the threshold filter is not applied, and the magnitude of each vector is found using Pythagoras' theorem rather than by approximating it.

The next step is to apply a process known as non-maximal suppression. The aim of this step is to reduce each line to being one pixel thick. For any edgel, there are eight edgels around it, which can be described as being at 0, 45, 90 or 135 degrees from the horizontal relative to that edgel. Since the Sobel filter has already run by this point, the direction of the edge is already known. The direction is rounded to the nearest value which is in the set of valid angles.

There will always be two pixels in the 8 pixel neighbourhood which are on this line; if either one of them has a higher value than it, then the current edgel is suppressed (i.e set to zero). This step solves the problem of thick edges by thinning them to being one pixel thick. All the points which survive are now local maxima (i.e had the greatest edge detector response in their local area).

The final step is called hysteresis[2] thresholding; it is similar to thresholding except that there are two thresholds. These are the upper and lower thresholds, where the upper threshold is greater than the lower. The algorithm begins by finding a point which has a value greater than the upper threshold, and marks it as an edge. Then all pixels in the 8 pixel neighbourhood of that pixel which have a magnitude greater than the lower threshold are found. These points are also marked as edges, and their 8 pixel neighbourhoods examined in the same way. This process continues until no more pixels are found which have a value greater than the lower threshold. The advantage of this method over regular thresholding is that it provides some tolerance for noisy edges, preventing them being broken up into smaller edge fragments, and helps to remove some of the local maxima which were created by noise.

6.5.1.2 Edge Detection using 'Sobel' Filter

The Sobel filter consists of two kernels, G_x and G_y.

$$G_x = \begin{pmatrix} -1 & 0 & 1 \\ -2 & 0 & 2 \\ -1 & 0 & 1 \end{pmatrix} \qquad G_y = \begin{pmatrix} 1 & 2 & 1 \\ 0 & 0 & 0 \\ -1 & -2 & -1 \end{pmatrix}$$

Each kernel is applied separately to the image separately, to produce two images. With a pattern [-1 0 1], taken from the horizontal matrix Gx. If this is placed over a part of the image, it will give a value of the strength of the edge by finding the horizontal gradient at that point. So, Gx can be used to detect vertical edges. Gy is a 90 degree rotation of Gx and so will find horizontal edges. The horizontal and vertical gradients at each point are combined to form a vector (x, y)T for that point. The magnitude of the vector will give the total edge strength at that point. Then the absolute values of the vector's components are added together for example G = |Gx|+|Gy|. The final image from this method is simply the sum of the two images.

[2] Hysteresis is the dependence of a system not only on its current environment but also on its past environment. This dependence arises because the system can be in more than one internal state.

Using these techniques the scarred area of the skin can be separated to show either the size it occupies or the prominence of scarring.

6.7 Imaging of Tattooing of the Skin

Body art has become increasingly popular and the capacitance sensor has been used here to detect scarring left by this phenomenon. Although the scarring is very minimal and is not visible to the naked eye, it can be seen with the capacitance sensor imaging.

A tattoo needle penetrates the skin about 1mm in depth, going past the epidermis into the dermis layer and the location range is shown in Figure 6.12. It leaves behind pigments made of metallic salts of oxides, sulphides and selenides. The ink used is a solution of water, glycerine and alcohol and the pigments are suspended in the solution. The pigments will change the appearance of an object by selective absorption and/or scattering of light. (C Cuyper, M L Costapos, 2009)

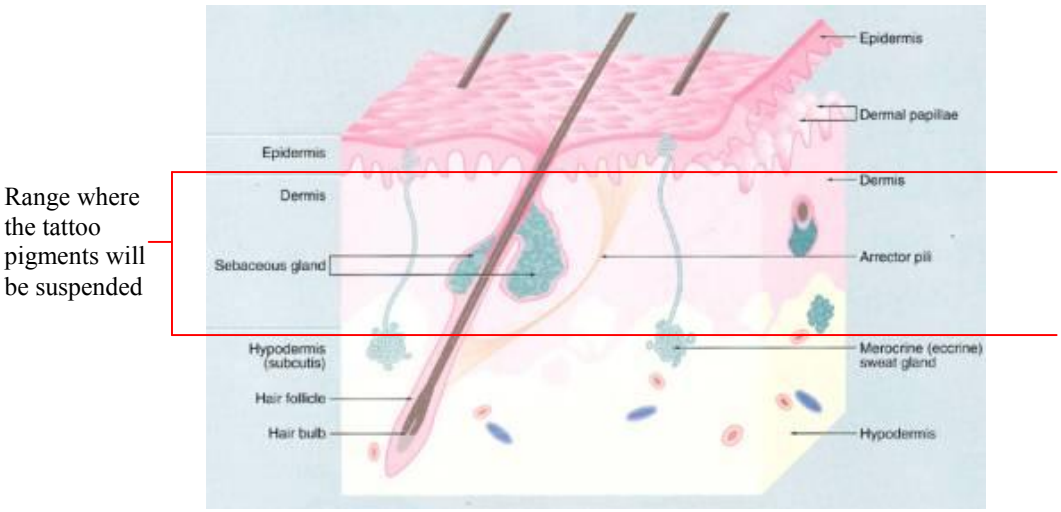

Figure 6.12: Location of where the pigment will be suspended in the dermis layer.

The pigments suspended in the epidermis layer when seen from a close-up using a microscope with 200x zooming lens can be seen as separate particles although through the naked eye they appear uniform as shown in Figure 6.13. As can be seen from Figure 6.13, the skin around the hair shaft is fairly clear denoting that there is

no presence of ink in this area. This is because the hair shaft depth is up-to the hypodermis layer and extends through the dermis and then the epidermis and finally appears through the skin.

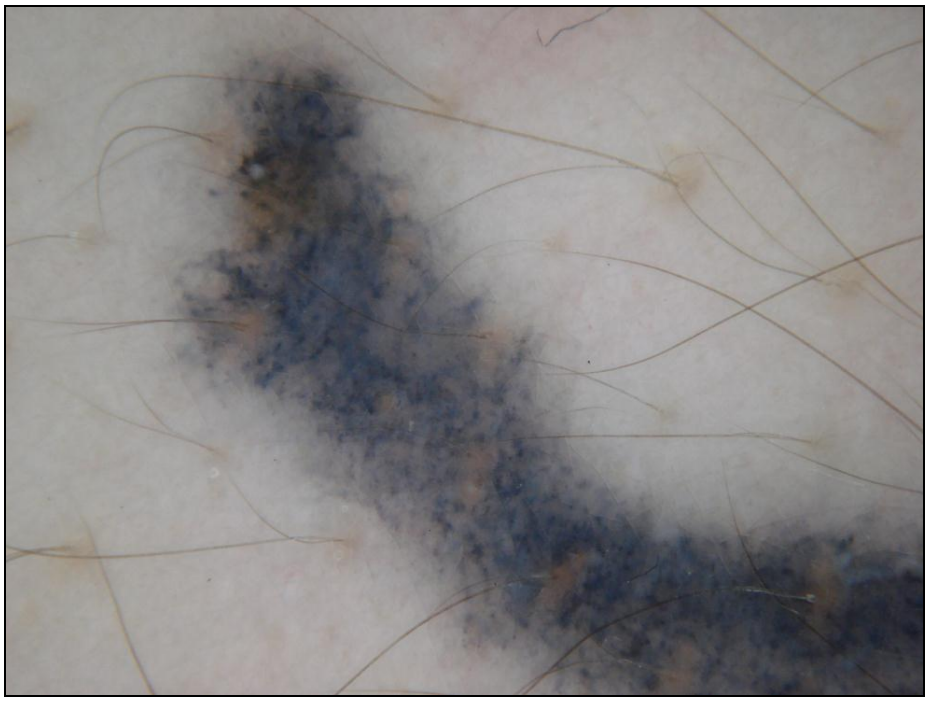

Figure 6.13: Pigments of tattoo as seen close-up with a digital microscope with 200 times zooming lens.

This test was done to see if the capacitance will be able to detect the surfacial scarring of the tattoo needle. The hydration level on the skin surface hence cannot be affected by the tattoo pigments as they are too deep within the dermis layer to have any impact on the surface of the skin.

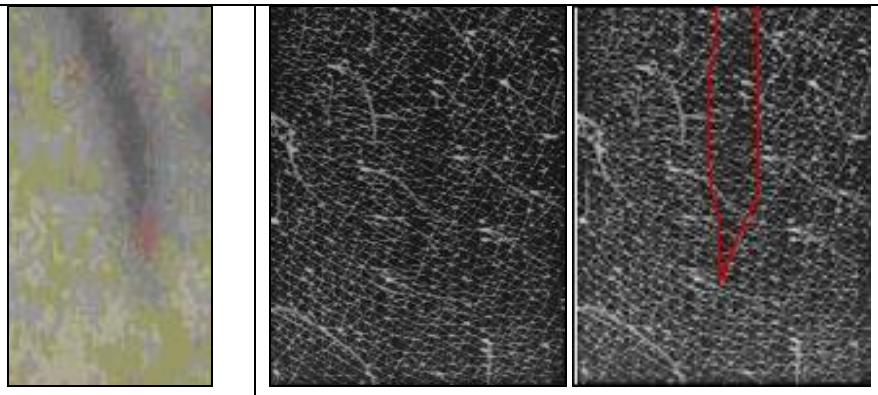

Photo image of tattoo line	Capacitance sensor image of same tattoo line and outlined

Figure 6.14: The left photo showing image of a tattoo line on the right the same tattoo line taken with capacitance sensor and the final image showing an red outline added.

The photo on the left in Figure 6.14 shows a visual image of the end of a tattoo line on a oriental male aged 30 to 35 on the right upper arm. The thickness of the tattoo line is about 1mm and the length from top to bottom is about 8mm. For the capacitance sensor the image is seen in the same location and is of the same size as in the visual image. A red line is added to show the borders.

In Figure 6.15 another sample of a tattoo on the upper back of a Caucasian female volunteer aged 25 to 30 years can be seen to show higher details of scarring as compared to the visual image of the tattoo.

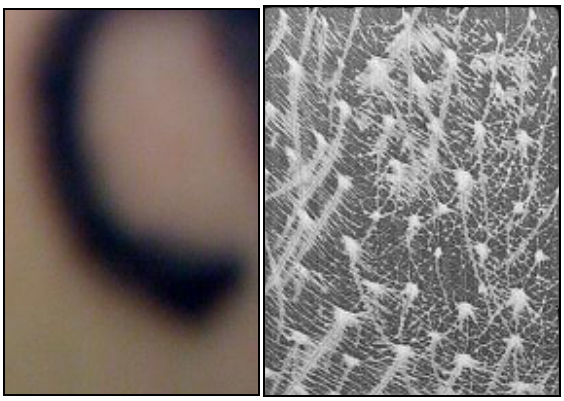

Figure 6.15: The left photo showing image of a tattoo line drawing and on the right the same tattoo line drawing taken with capacitance sensor

6.8 Piercing of the Abdomen Skin

An image of a piercing of the navel is shown in Figure 6.16.

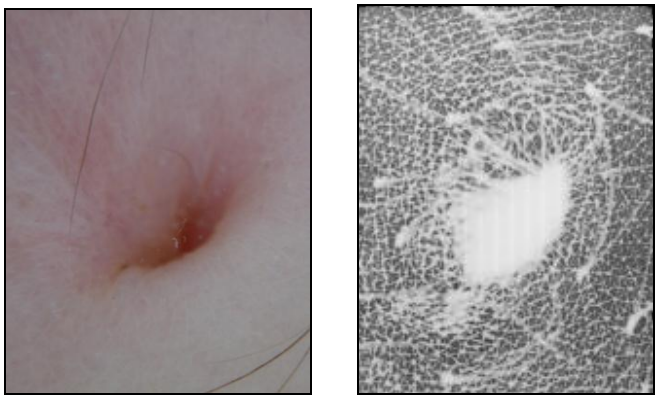

Figure 6.16: The left photo showing image of a piercing above the navel and the right image of the same skin site taken with capacitance sensor.

The capacitance sensor shows distorted micro-relief lines around the hole of the piercing. Further away from the piercing shows a more uniform micro-relief lines as the skin has not been disturbed by the piercing effect.

6.9 Piercing of the Ear Skin

Another form of body art where a puncture is made thorough the skin is ear piercing. Image of ear piercing is shown in Figure 6.17 whereby the capacitance sensor clearly delineates the scar and hole of the piercing.

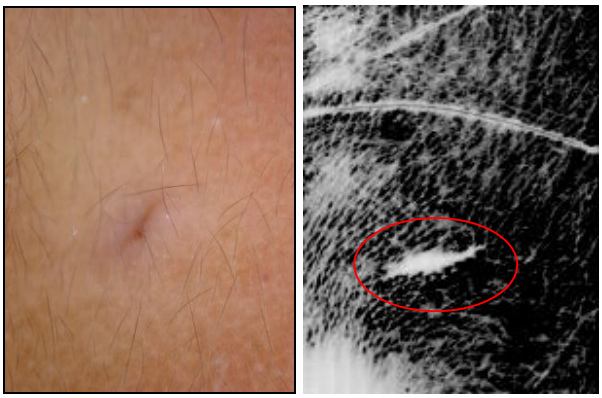

Figure 6.17: Camera image left and capacitance image on right of ear piercing on Caucasian female aged 25 to 30.

6.10 Conclusion and Findings

This chapter has shown that the capacitance sensor can be used for scars imaging, finding scar created in body art and scar management. The average greyscale values of the images give information about the skin hydration level.

The micro relief values of the images give information about the skin micro relief and in the case of time-based imaging, show the scars healing status. Scar imaging and management is still in the early phases and capacitance sensors are a promising technology in improving this work.

By occluding the skin, the scar image can be viewed with better clarity. By using special MATLAB filters, the scar can be isolated and seen clearly for visual analysis.

Additional work can be done by future researchers to quantify the measurement of the scars and to be able to calculate the size of the scar. A simple scar assessment chart will be beneficial to show the improvement of the wound/scar over time.

There is also a very promising area for research in the cosmetics surgery industry. The need to manage a scar to heal with a minimum disruption from a cosmetic perspective is always in need. With a capacitance sensor measurement, the scar can be assessed quickly on the go.

CHAPTER 7: DIGITAL AND VIDEO IMAGING MEASUREMENTS

In previous chapters, measurements have been done mainly with static images from the capacitance sensor. In this chapter, an additional technique is introduced whereby imaging is done with a capacitance sensor that records a video file of the skin changes.

To generate a video recording, a new capacitance sensor from Fujitsu is used. It is a MBF-200 capacitance sensor that records a video file and a dedicated program is written in both C++ to record the images and additional program is written in Mathworks Matlab to measure the image data.

To analyse the feasibility of the MBF-200 capacitance sensor, static image measurement were done using the capacitance sensor and the AquaFlux AF200 is used to verify the accuracy of the sensor's measurement. The initial test is an occlusion of the skin site test. In addition, a digital photo camera (SONY DSC-W55 camera with Dermlite II Epiluminescencemicroscopy light lamp) is used to occlude the skin surface.

7.1 Initial Occlusion Test

In this test, SC properties which vary from skin site to skin site and from person to person, are measured through occlusion measurements by using the condenser-chamber TEWL method – (AquaFlux J Fluhr, P Elsner, E Berardesca, H I Maibach, 2005) and Capacitance sensors (J Serup, G B. E. Jemec, G L. Grove, 2006) and camera photo imaging. Different skin sites are occluded for a fixed length of time by using a photo camera lamp glass surface. The MBF-200 capacitance sensor, which records the skin hydration images of the occlusion, and TEWL measurements are performed both before the occlusions and after the occlusions. The results show that different skin sites react differently during the occlusions

which reflects the different water holding properties and different barrier functions of different skin sites.

Three skin measurement techniques are used – AquaFlux AF200, Capacitance sensors (MBF200, Fujitsu) and Camera Imaging (SONY DSC-W55 camera with Dermlite II Epiluminescencemicroscopy light lamp) are used to measure in-vivo skin occlusion of different skin sites.

All the measurements are performed under normal ambient laboratory conditions of 20~21°C, and 40~50% relative humidity (RH), and two volunteers are acclimatised in the laboratory for 20 minutes prior to the measurements. The skin sites used for the measurements are untreated.

The occlusion measurements are done by first measuring the selected skin site with the AquaFlux, then same skin site is measured using the capacitance sensor. The skin site is then imaged using the photo imaging digital camera. The light lamp of the camera has a glass surface and is in contact with selected skin site. Since the glass surface of the light lamp is in contact with the skin, it is used to occlude the skin and an image is taken every minute for 5 minutes. After 5 minutes of occlusion, the capacitance sensor is used to measure the site and finally the Aquaflux measurement is taken. In total three different skin sites were studied.

The images from the photo camera are then processed using a dedicated program written in Matlab. The images are separated into their three original colour filters of Red, Green and Blue, then each colours gray-scale values are generated and the average value for all the pixels within an image are calculated.

Shown in Figure 7.1 are one set of example photos of the Volar Forearm of the female volunteer. As there is a very subtle change in the luminosity overall image, it's more useful to measure the RGB colours for the individual changes.

0 minute 1 minute 2 minute 3 minute 4 minute 5 minute

Figure 7.1 Skin photo images from 0 to 5 minutes of the Volar Forearm for the female volunteer.

In general, there is a trend in the photo imaging whereby as the skin is occluded, the red, green and blue colour gray-scale drops as seen in Figure 7.2.

It is also seen that red has the highest gray-scale followed by green and finally blue has the lowest gray-scale. There is some inconsistent reading that might have been caused by movement of the camera.

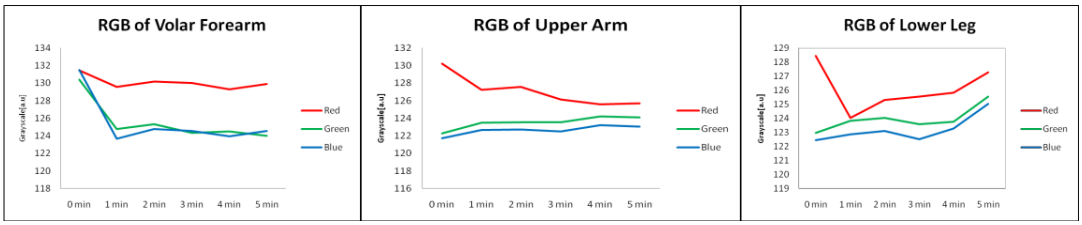

Female Caucasian measurement of three different skin sites

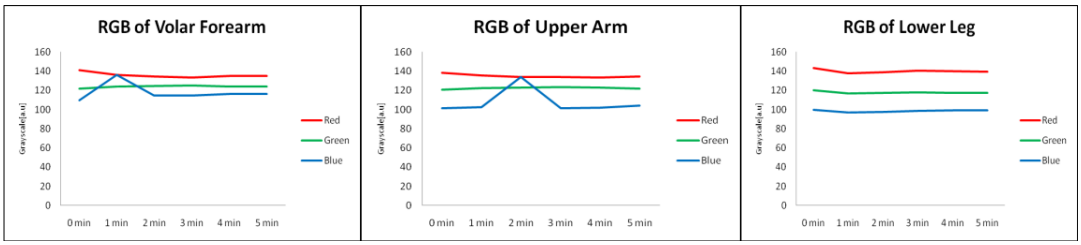

Male Asian measurement of three different skin sites

Figure 7.2 Skin images of 3 different location of two different volunteers taken with photo imaging camera.

Using the Aquaflux, a measurement was taken at 0 minutes and at 5 minutes.

Table 7.1 below shows Trans-epidermal Water Loss measurement before and after occlusion of the three different location of skin the two volunteers.

	Volar Forearm		Upper Arm		Lower Leg	
	Before	**After**	**Before**	**After**	**Before**	**after**
Female	10.15306	11.1047	11.2664	12.3969	9.17892	11.3531
Male	14.46935	16.7147	12.0438	15.0522	14.9099	20.4585

Table 7.1. TEWL measurement of three different skin locations of two volunteers taken before and after occluding with the Imaging camera.

TEWL measurement as seen in Figure 7.3, shows a consistent increase before and after occlusion and is variable based on the skin site.

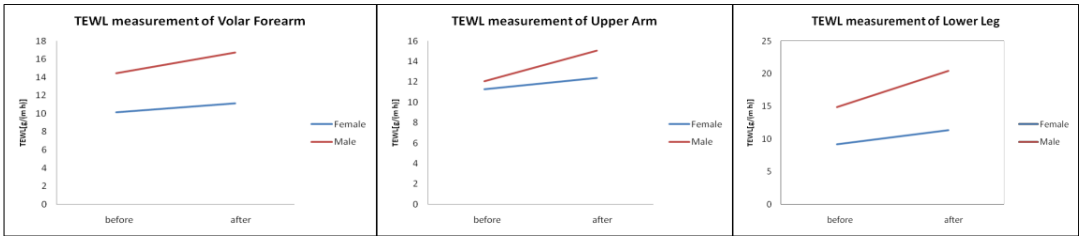

Figure 7.3. TEWL measurement before and after occlusion of three different skin sites of the two volunteers.

Similarly the capacitance sensor shows consistent increase in the gray-scale after occlusion of the skin site as seen in Figure 7.5.

The TEWL shows an increase in both volunteers as seen in Figure 7.3. The reading for the volar forearm of both the volunteers increases after occlusion and the male Asian subject has a higher TEWL and higher increase than the female Caucasian subject. This can be seen in all three skin location of both the volunteers. The female Caucasian volunteer has lower TEWL reading than the male volunteer. (H Singh, AR Caparnagiu, P Xiao, LI Ciortea, EP Berg & RE Imhof, 2010)

7.2 The Fujitsu MBF-200 Capacitance Sensor

A new production model of the capacitance sensor has been developed using the Fujitsu MBF-200 capacitance sensor and is shown in Figure 7.4. This model of the capacitance sensor have the capability to record video images of the skin over time

and additional software was developed for the production model to incorporate video processing of the skin surface.

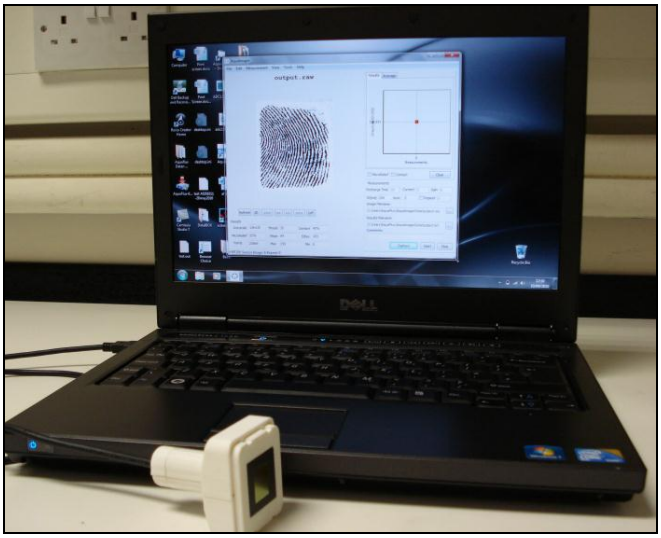

Figure 7.4 Production model of the capacitance sensor with software running for measurement.

To increase the contact of the sensor with the skin surface the capacitance sensor head is mounted on a movable platform that allows a certain degree of free movement. This will allow measurement of images where the skin uniformity is not consistent.

Capacitance sensor measurement was taken at 0 minute and 5 minutes and the results are shown in table 7.2. In the images, each pixel is represented by an 8 bit gray-scale value, 0~255, with 0 representing white (low capacitance) and 255 representing black (high capacitance) (H Singh, P Xiao, E P Berg and R E Imhof, 2008).

	Volar Forearm		**Upper Arm**		**Lower Leg**	
	Before	**After**	**Before**	**After**	**Before**	**After**
Female	114.58	204.84	136.79	221.53	125.61	192.99
Male	98.33	200.32	123.50	189.50	93.02	129.85

Table 7.2.Gray-scale average values of three different skin locations of two volunteers taken before and after occluding with capacitance sensor.

Further analysis of the gray-scale average shows a generally consistent trend with the TEWL measurement from Figure 7.3 above. The gray-scale values of the three skin locations increase after occlusion as the skin image has become darker as shown in Figure 7.5. Generally, the female subject has a higher hydration level in all three skin sites both before and after when compared to the male subject. However, the increase varies for the 3 sites where the occlusion of the volar forearm of the female subject has increased over 78% after occlusion and the male subject has a larger increase at 103%. In the two subsequent sites of the upper arm and lower leg, the male subject has a lower overall hydration increase where the upper arm increases by 53% and the female upper arm hydration increases by 62%. The lower leg for the male subject increase at an even lesser percentage of 39% while the female has an increase of 53%.

Form these measurements, it can be seen that the female subject has a higher hydration levels both before and after occlusion for all three skin sites. However, the average increase of all three sites for both male and female are quite similar, averaging at 64% for the female and the male subject at 65%.

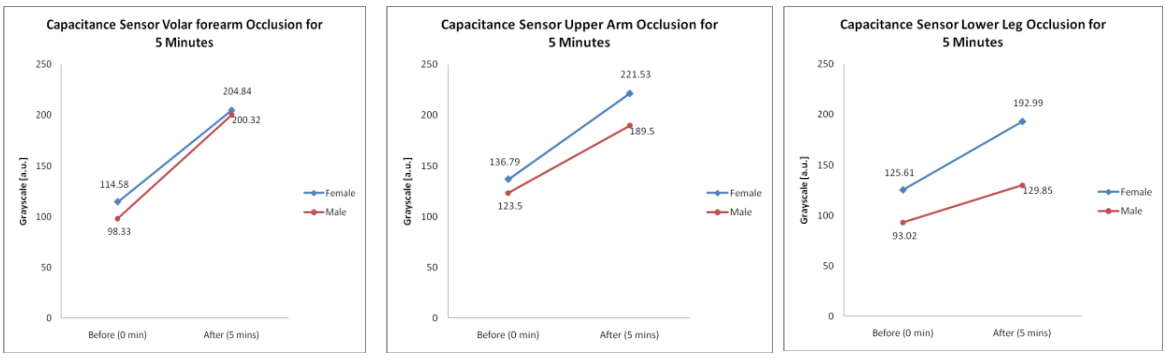

Figure 7.5: Gray-scale measurement before and after occlusion of three different skin sites of the two volunteers.

Figure 7.6 shows one set of example capacitance sensor imaging of the Volar Forearm for the female volunteer. There is a large increase in the gray-scale whereby after 5 minutes occlusion shows a much darker image being recorded.

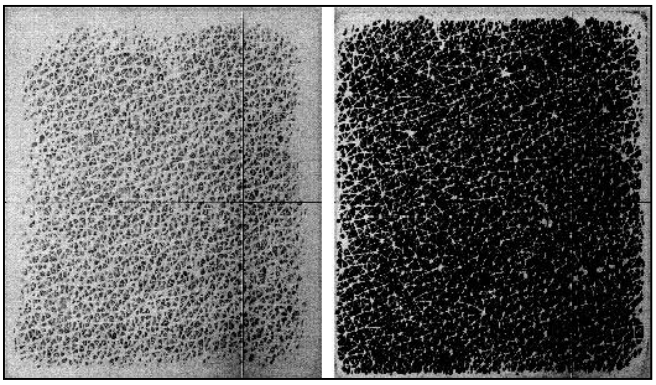

0 minutes 5 minutes

Figure 7.6: Capacitance sensor image of the Volar Forearm for the female volunteer taken at 0 minute and 5 minutes.

Figure 7.7 shows images of different skin sites of the human body of an oriental male aged 40 to 45 years. The images vary in gray-scale values, texture and total contact points with the skin showing that the skin at different locations of the human body has different characteristics. The results show that the capacitance sensor has good spacial resolutions for skin surface imaging.

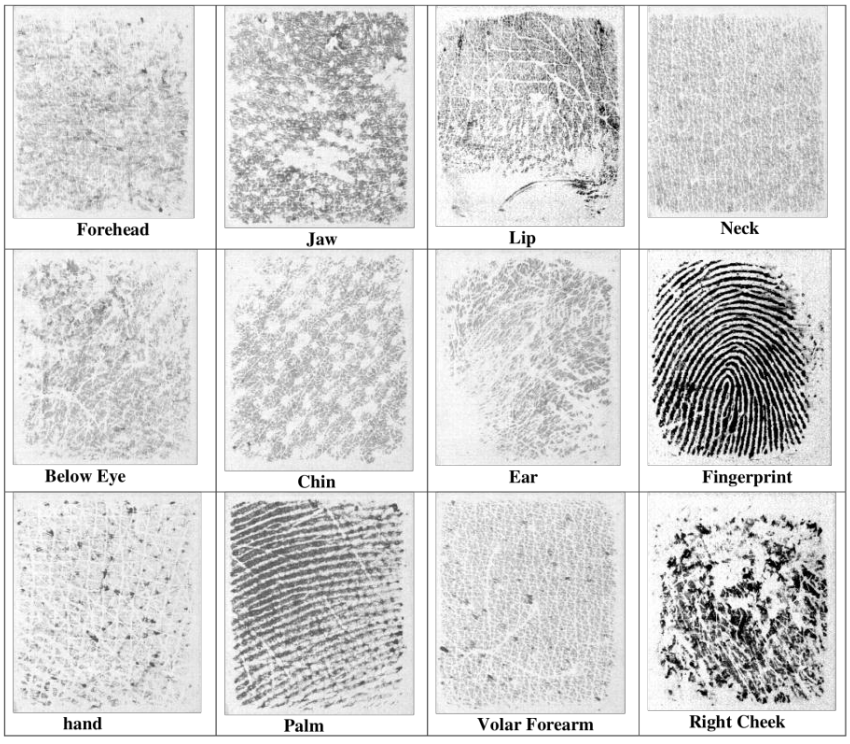

Figure 7.7: Capacitance sensor images 12 different skin sites showing variability of imaging of the human skin.

7.3 Initial Results of MBF-200 Capacitance Sensor

7.3.1 Repeatability Test

Repeatability is one of the most important instrument parameter. Table 7.3 shows the mean grayscale values and standard deviations of the repeat measurements on different skin sites. The results show a very good repeatability with less than 3% of variability on average. Study shows that Corneometer's variability is about 7.3% (Xiao P, Ciortea LI, Singh H, Zheng X, Berg EP, Imhof RE, 2009).

Skin Sites	Volar Forearm 1	Volar Forearm 2	Palm	Hand	Finger	Neck	Face	Forehead
Mean Values	64.2±0.9	54.8±2.5	119.8±6	46.3±1.7	188.0±2.6	89.5±1.7	85.2±1.3	83.5±1.6

Table 7.3: Repeatability results of 8 skin sites using the MBF-200 Capacitance Sensor.

7.3.2 Comparison with Corneometer (CMC 825 PC)

Figure 7.8 shows correlation between Capacitance sensor and Corneometer (CM 825 PC), the results show a good correlation between the two devices. Previously, a comparison study between capacitance sensors and other skin hydration devices was done, mainly the AquaFlux and optothermal transient emission radiometry (OTTER) as shown in Chapter 4.

The results show that the capacitance sensor generally correlates well with other devices.

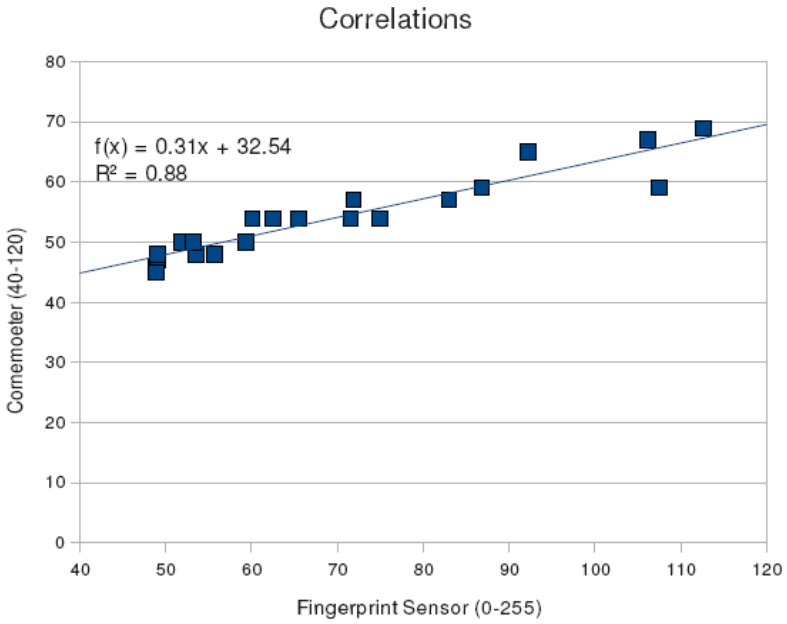

Figure 7.8: Co-relations between MBF-200 capacitance sensor and Corneometer CMC 825.

7.3.3 Occlusion and Imaging with MBF-200 Capacitance Sensor

Figure 7.9 shows the TEWL results, which are the opposite, TEWL values, increase dramatically as occlusion time increases. It can be seen that during occlusion, the skin TEWL is only partially blocked, and most of the extra water occurs on the skin surface which will cause increases in Capacitance sensor and AquaFlux results.

For most of the test skin sites, the percentage increase of Capacitance sensor gray-scale values tends to decrease as occlusion time increases, which indicates that during the occlusions, gray-scale values increases quickly in the beginning but slows down towards the end of the tested time frame.

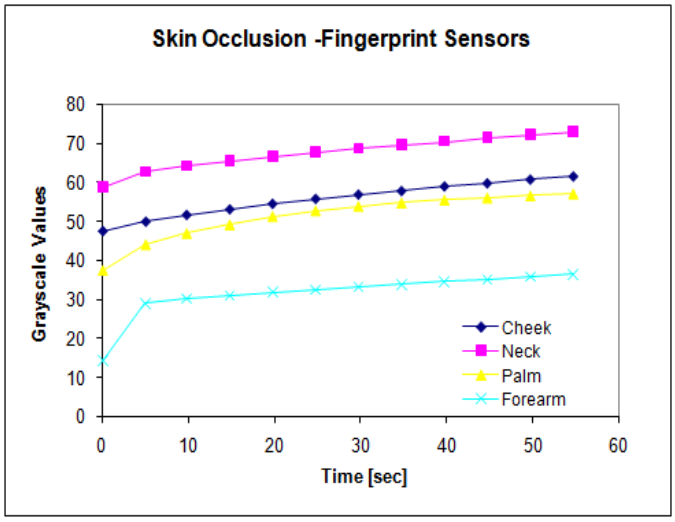

Figure 7.9: Capacitance average gray-scale values during a 1-minute occlusion measurement

Figure 7.10 shows the average increase in percentage of the four different skin test sites during a 1-minute, 5-minute and 10-minute occlusion by using MBF-200 capacitance sensor, OTTER and the AquaFlux. For most of the test skin sites, the percentage increase of capacitance sensor grayscale values tend to decrease as occlusion time increases, which indicates that during the occlusions, grayscale values increase faster in the beginning but slows down in the end. The TEWL results, has the opposite effect; TEWL values increase dramatically as occlusion time increases. For OTTER, the percentage of increase is very small and shows no clear trends.

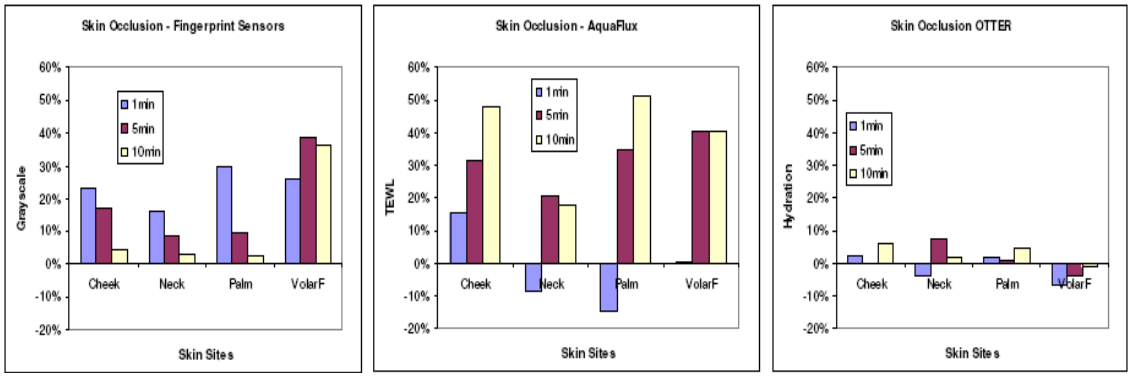

Figure 7.10: Percentage increases during occlusions for capacitance average gray-scale value results and AquaFlux TEWL and OTTER 6g/m² results.

For a skin site with TEWL of 12g/m²h, a 10-minute occlusion will introduce 2g/m² extra water in the SC, if SC is 30% in hydration and 20μm in thickness which makes 6g/m², a 10-minute occlusion should cause about 30% increase in hydration. During the occlusion, skin TEWL is only partially blocked, and most of the extra water occurs on the skin surface that will cause increases in capacitance sensor and AquaFlux results, but not showing a major change in OTTER results.

Figure 7.11 shows the MBF-200 capacitance sensor gray-scale images during 1-minute occlusion measurements on four different skin sites.

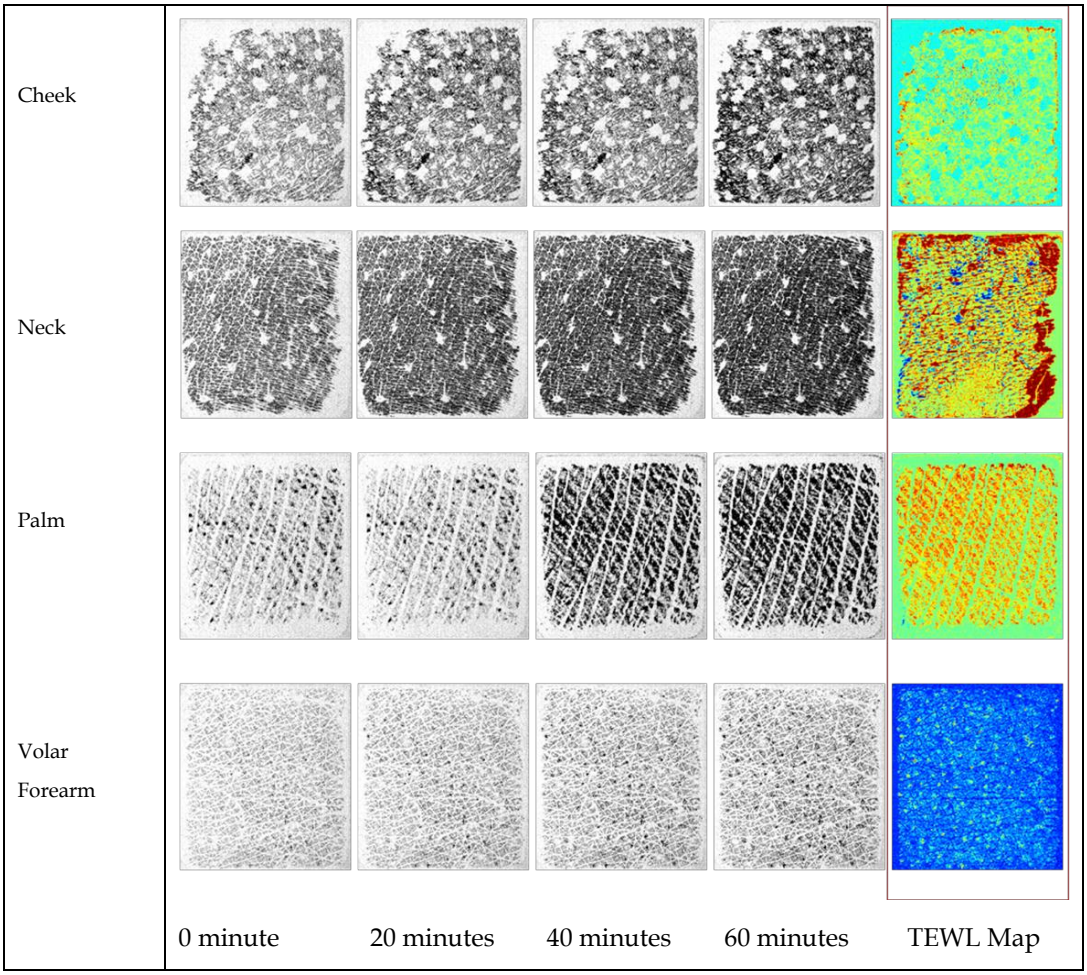

Figure 7.11: Capacitance sensor gray-scale images during a 1-minute occlusion measurements and their corresponding TEWL maps.

By calculating the difference between the first and last images, an equivalent skin surface TEWL map can be generated, as shown on the right hand side in colour

images. From TEWL maps, the active TEWL areas on different skin sites can be seen clearly.

During the occlusions, skin surface hydration will increase as TEWL will be blocked. For capacitance sensor grayscale images, if at time t0 the average grayscale value of the image is v0, and at time t1 the average grayscale value of the image is v1, then the average grayscale value gain per unit time g can be calculated by g=(v1-v0)/(t1-t0). By multiplying g with SC thickness L, the hydration gain G equivalent to the unit of g/m²h can be attained using the equation shown below, which should be proportional to TEWL values. The value of g can be calculated from capacitance images (P Xiao, H Singh, X Zheng, EP Berg, RE Imhof, 2007) and the SC thickness value (L) from OTTER measurements (P Xiao, RE Imhof, 1998).

$$G = g \times L = \frac{v1 - v0}{t1 - t0} \times L$$

By calculating the hydration gain of G using the equation above, as it is proportional to TEWL, a TEWL map of the equivalent skin surface can be generated and is shown on the right hand side in colour images of Figure 7.11. From the TEWL maps, the active TEWL areas in different skin sites can be seen.

7.4 Video Image Recording with the MBF-200 Capacitance Sensor

Since the MBF-200 capacitance sensor have the capability record time-based video recordings, an initial test is done on water spreading on textile surface (100% cotton and man-made material) that is shown in Figure 7.12. 1 ul of water droplet was dispensed on the textile sample surface, and then the capacitance sensor was used to record its spreading at a frame rate of 10 frames per second (fps). Since 10fps over 9 seconds will generate 90 frames, only a fixed numbers of frames are extracted for measurements.

The result shows that, for cotton, water droplet was absorbed very quickly and tends to spread evenly in all directions.

For man-made material, water droplet spread very fast on the surface, but was absorbed slowly, and tends to spread along the threads. Up-to 12 seconds absorption has not occurred and water is still spreading along the surface of the man-made material.

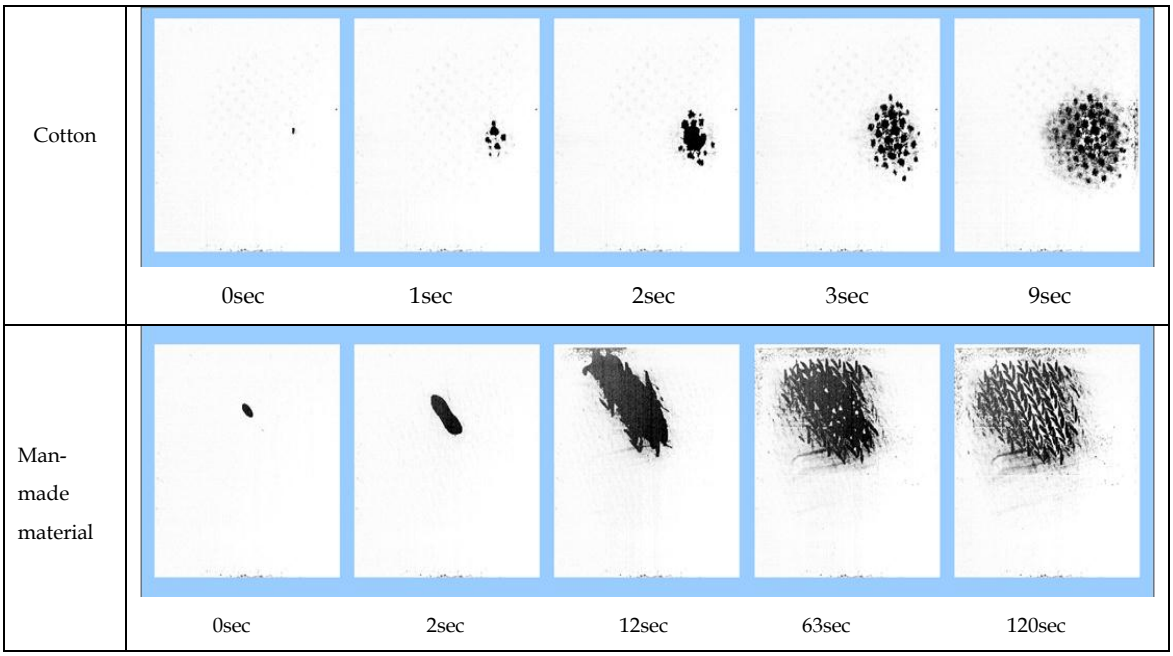

Figure 7.12: Capacitance sensor video images of two types of textiles, cotton and a man-made material.

The video for the cotton textile used in Figure 7.10 can be seen in real time at:

http://www.youtube.com/user/xiaop2009#p/u/18/hOvxmJvHYu4

7.5 Live Skin Video Image Recording with the MBF-200 Capacitance Sensor

The above test shows that hydration can be detected by the MBF-200 sensor. Further specific video tests are on different skin sites to show the viability of using the MBF-200 sensor on detecting hydration.

7.5.1 Capacitance Sensor Video Imaging of the Hand

In this test, the back of the hand of an oriental male aged 40 to 45 years old is tested with occlusion over a period of 17 seconds and is shown in Figure 7.13. The constant contact between the skin surface and the capacitance sensor will allow for occlusion to occur. The capacitance sensor records a video file and subsequent water loss from the skin can be seen appearing over this time period.

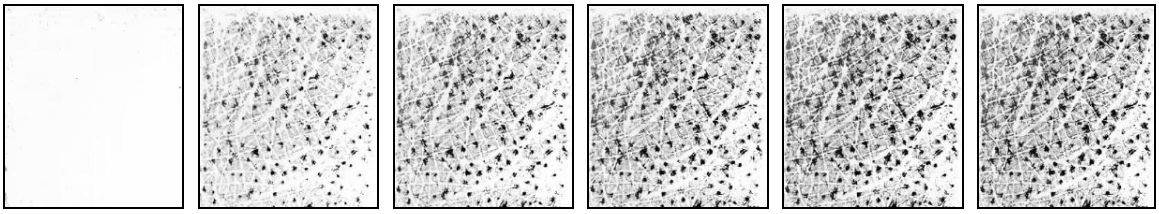

0 sec 1 sec 5 sec 10 sec 15 sec 17 sec

Figure 7.13: Capacitance sensor video images of the back of the hand of a male oriental subject.

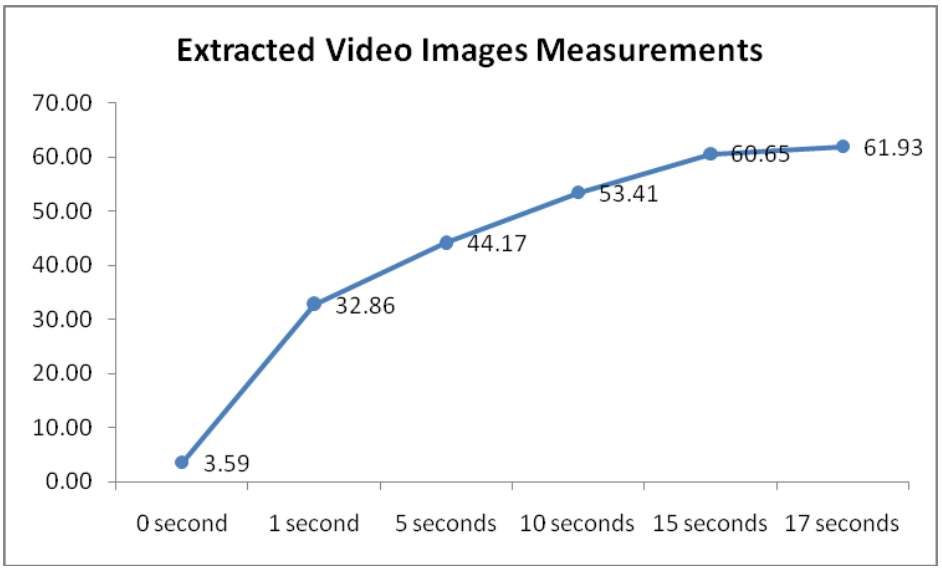

Figure 7.14: Capacitance measurements of the back of the hand of a male oriental subject.

The average value of each image is then measured using the Matlab program and the result can be seen in Figure 7.14. At the start of the experiment (0 second), the gray-scale is lowest at 3.59 gray-scale. This shows there is a large amount of whiter area. This rises rapidly in the first second to 32.86 gray-scale.

Between 1 to 15 seconds there is a gradual increase. Between 15 seconds to 17 seconds there is a further drop in the rate of increase as the surface of the capacitance is beginning to get saturated with hydration.

The video for the live skin of the hand used in Figure 7.14 can be seen in real time at:

http://www.youtube.com/user/xiaop2009#p/u/8/pVPB4ji9y8A

7.5.2 Capacitance Sensor Video Imaging of the Cheek

Another test is done on the cheek (face) of an oriental male aged 40 to 45 years. The constant contact between the skin surface and the capacitance sensors results in the skin being occluded. The images shown below in Figure 7.15 are taken at 0 second, 1 second, 4 seconds, 9 seconds, 12 seconds and 17 seconds and shows a gradual increase in the gray-scale of the images over time.

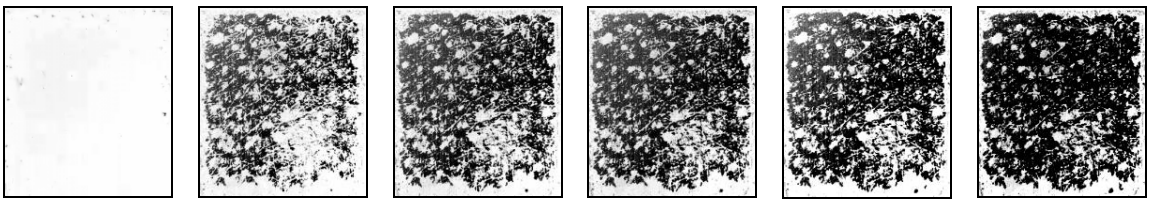

0 sec 1 sec 4 sec 9 sec 12 sec 17 sec

Figure 7.15: Capacitance sensor video images of the cheek of a male oriental subject.

In Figure 7.16, data measurement is done on the extracted video images from Figure 7.15. The results here show a similar pattern with the experiment on the skin on the hand above. There is a rapid increase from the start of the experiment to the first second. Then there is a gradual increase until the end of the experiment at 17 seconds.

However the overall gray-scale values reached in this experiment is much higher at 142.75 gray-scale at 17 seconds while the experiment on the hand was much lower at 61.93 gray-scale at 17 seconds.

The video for the live skin of the cheek used in Figure 7.15 can be seen in real time at:

http://www.youtube.com/watch?v=VRK7UOJzhy4

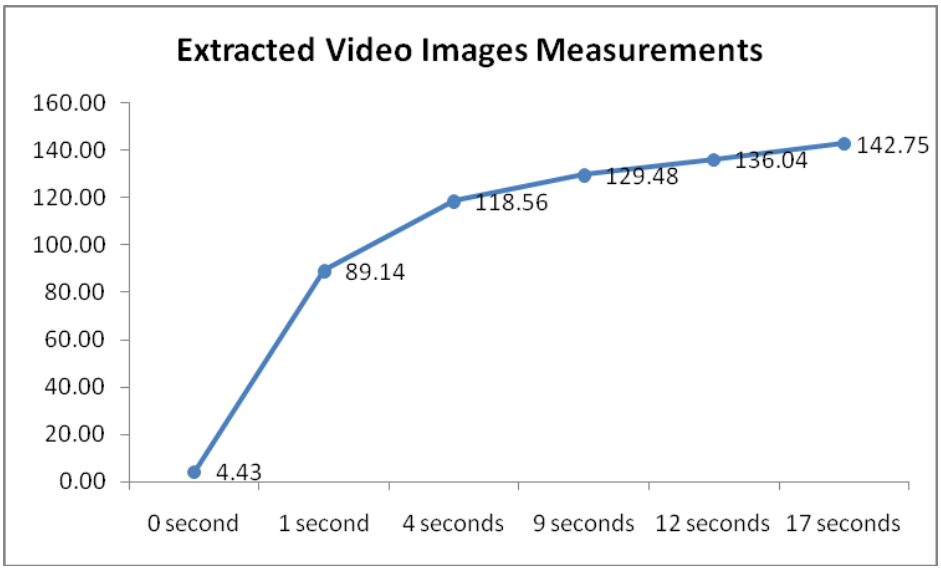

Figure 7.16: Capacitance measurements of the cheek of a male oriental subject.

7.5.3 Capacitance Sensor Video Imaging of the Volar Forearm Sweat

In this test the Volar Forearm of a oriental male is aged 40 to 45 is tested and the video images are captured and shown below in Figure 7.17

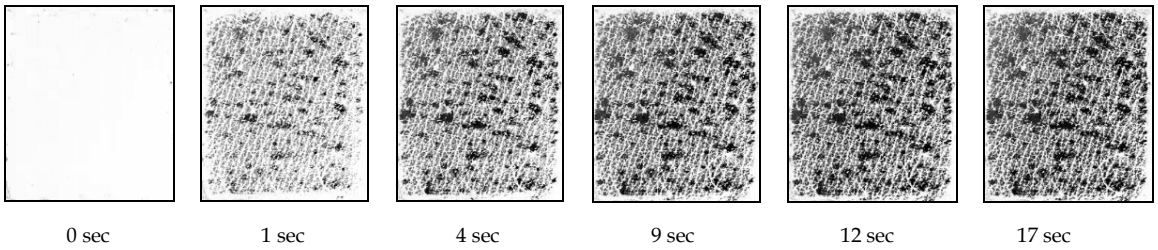

Figure 7.17: Capacitance video images of the volar forearm of a male oriental subject.

The video for the live skin of the hand used in Figure 7.17 can be seen in real time at:

http://www.youtube.com/user/xiaop2009#p/u/15/ndkVltVjosk

The dark spots are the higher levels of hydration of the sweat glands and can be seen clearly after 1 seconds and onwards. These video images are able to detect the sweat appearing from the skin and with occlusion the darkening of the images shows the increase of hydration level of the skin surface.

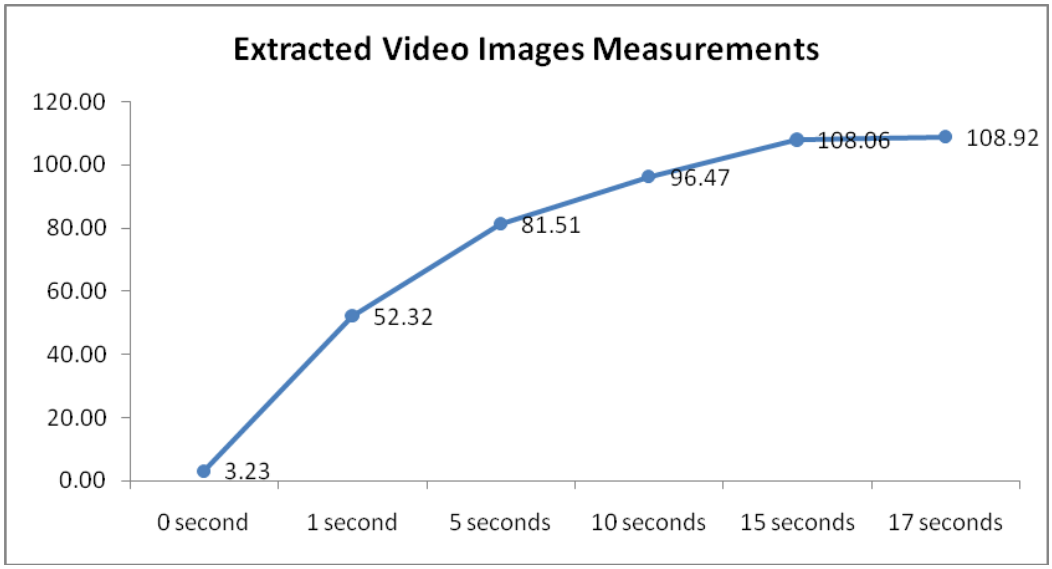

Figure 7.18: Capacitance measurements of the volar forearm of a male oriental subject.

As seen in Figure 7.18, quantification of the video images shows the increase in gray-scale values as the skin is occluded. The gray-scale values at 0 second are 3.23 and gradually increase to reach the highest value after 17 seconds of occlusion of 108.92 gray-scale.

7.6 Normalised Cross Co-relation Algorithm for Skin Image Re-positioning

A normalised cross correlation algorithm for skin image re-positioning was developed, which allows users to select an area of interest in one skin image, and find the exact the same area in another image.(P Xiao, H Singh, A R Caparnagiu, LI Ciortea, EP Berg2 and RE Imhof, 2010)

Cross-correlation is a measure of similarity of two forms. For continuous functions, *f* and *g*, the cross-correlation is defined as:

$$(f \star g)(t) \stackrel{\text{def}}{=} \int_{-\infty}^{\infty} f^*(\tau)\ g(t+\tau)\,d\tau,$$

where *f** denotes the *complex conjugate*[7.1] of *f*.

Similarly, for discrete functions, the cross-correlation is defined as:

$$(f \star g)[n] \stackrel{\text{def}}{=} \sum_{m=-\infty}^{\infty} f^*[m]\ g[n+m].$$

Figure 7.19 shows the skin image re-positioning results for capacitance sensor images. The results show that the algorithm works for both capacitance images as well as digital images as shown in Figure 7.20.

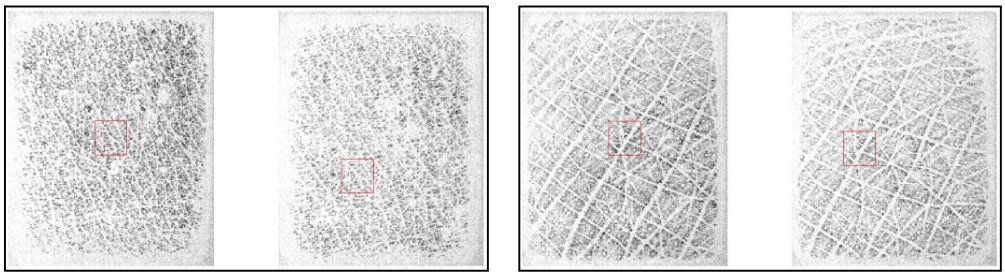

Volar Forearm *Left Palm*

Figure 7.19: Skin image re-positioning for capacitance sensor images of a oriental male aged 40 to 45.

The same location on the two images is marked by a red square. Even with light occlusion as shown in the volar forearm images, the same site can be detected.

[7.1] a pair of complex numbers, both having the same real part, but with imaginary parts of equal magnitude and opposite signs.

Volar Forearm *Left Palm*

Figure 7.20: Skin image re-positioning for digital images of palm and volar forearm of an oriental male aged 40 to 45.

When implemented in real time, it will allow users to take skin images at exactly the same position as it was taken before. This will allow the same area of the skin to be measured over time even when the capacitance sensor has been lifted off the skin site.

This analysis has shown that both the digital camera and video image recording using the capacitance sensor are viable techniques in measuring hydration levels of the skin. The video imaging shows a promising area of research where hydration against time is a crucial factor.

7.7 In-vivo Trans-dermal Drug Delivery Measurement

Apart from water, capacitance sensors are also sensitive to many solvents, due to their high dielectric constants, which make it very useful for in-vivo trans-dermal drug delivery studies. In this experiment, trans-dermal drug delivery is measured using capacitance sensors, AquaFlux and OTTER. The results shows that the capacitance sensors can be a useful tool for studying in-vivo solvent penetration through skin, as it gives dynamic 2D images of solvent penetrating through skin, and combining this with tape stripping, it is also possible to get solvent depth profiles within the skin.

Three solvents are chosen for study, Dimethyl Sulfoxide (DMSO), Glycerol, and Ethylene Glycol, due to their high dielectric constants as shown in Table 7.4.

	Skin	Water	DMSO	Glycerol	Ethylene Glycol
Dielectric Constant	7	80.4	47.2	42.5	37

Table 7.4: Dielectric Constants of the Skin and Solvents.

In each measurement, a small amount of solvent is applied to the volar forearm for a few minutes. After the skin surface is wiped dry, tape stripping is performed. Capacitance sensor measurements are performed both before and after the solvent applications, and after each stripping of the skin.

Figure 7.21 and 7.22 are the results for DMSO, Glycerol and Ethylene Glycol.

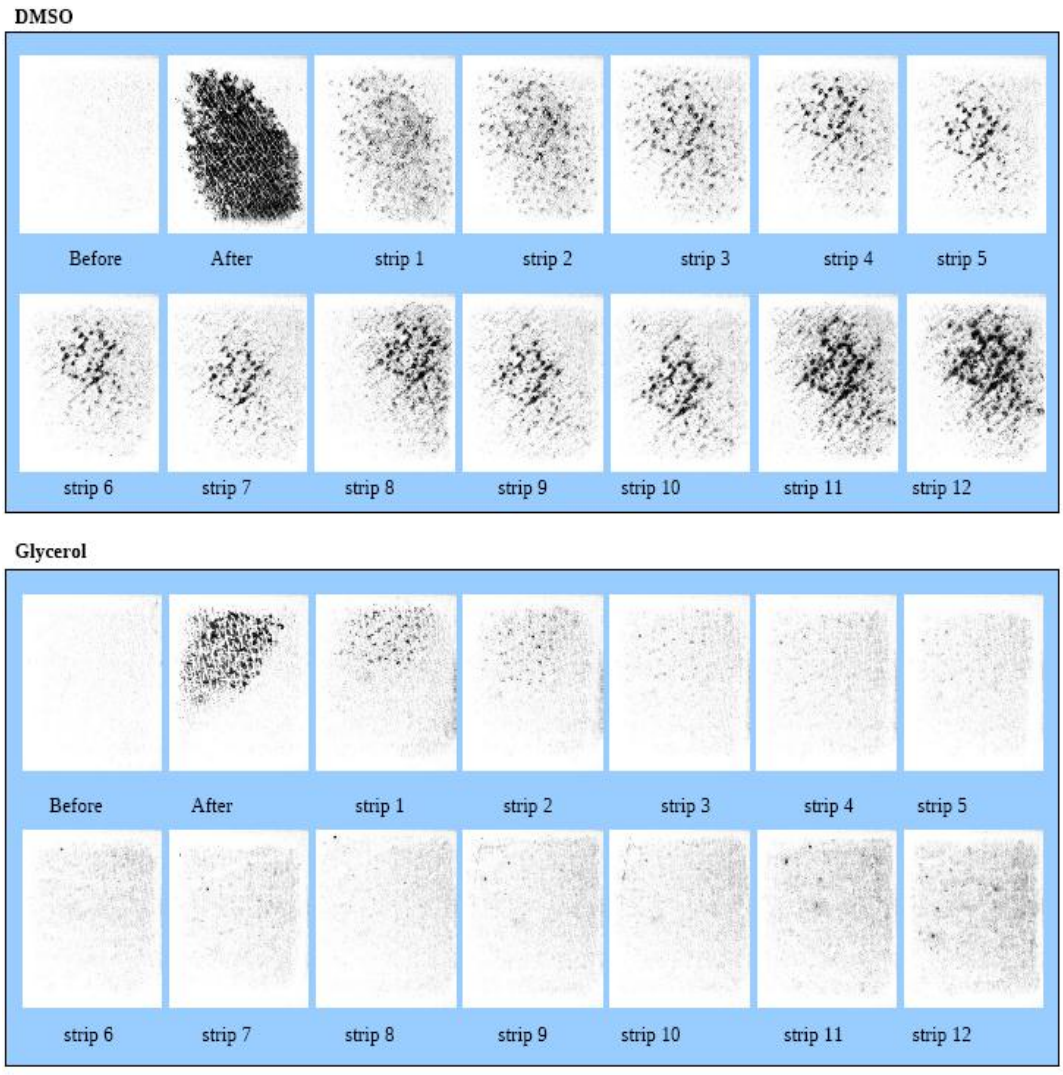

Figure7.21: Capacitance sensor images before and after DMSO / Glycerol application and subsequently during tape stripping.

The capacitance sensor skin images can clearly discriminate between the solvents and normal skin due to the dielectric constant differences. The results show that DMSO penetrates further and deeper than Glycerol, as DMSO residue is still visible after 10 strips, whilst Glycerol residue disappears after 5 strips.

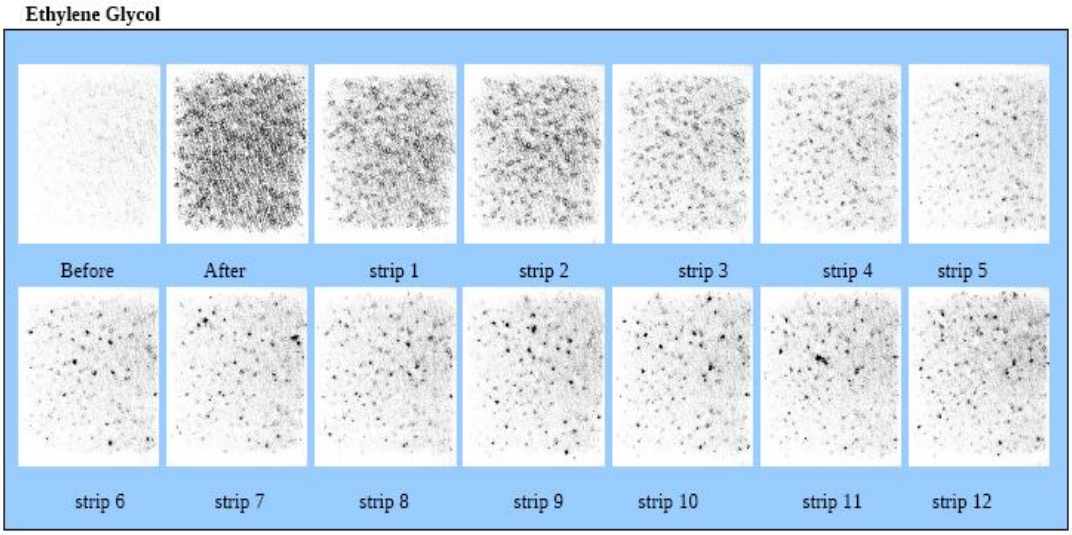

Figure 7.22: Capacitance sensor images before and after Ethylene Glycol application and subsequently during tape stripping.

By measuring the grayscale values of pure solvents, pure skin itself, the solvent absolute concentration [%, volume in volume] can be measured using the following equation.

$$G_{mix} = G_{skin} \times (100 - C) + G_{solvent} \times C$$

Where G_{mix} is the grayscale value of skin after solvent application, G_{skin} is the grayscale value of skin itself, and $G_{solvent}$ is the grayscale value of pure solvent. C is the solvent absolute concentration in skin in volume percentage. Figure 7.23 shows the absolute concentration [%, vol/vol] of the DMSO, Glycerol, and Ethylene Glycol on skin before application, during tape stripping and subsequently after.

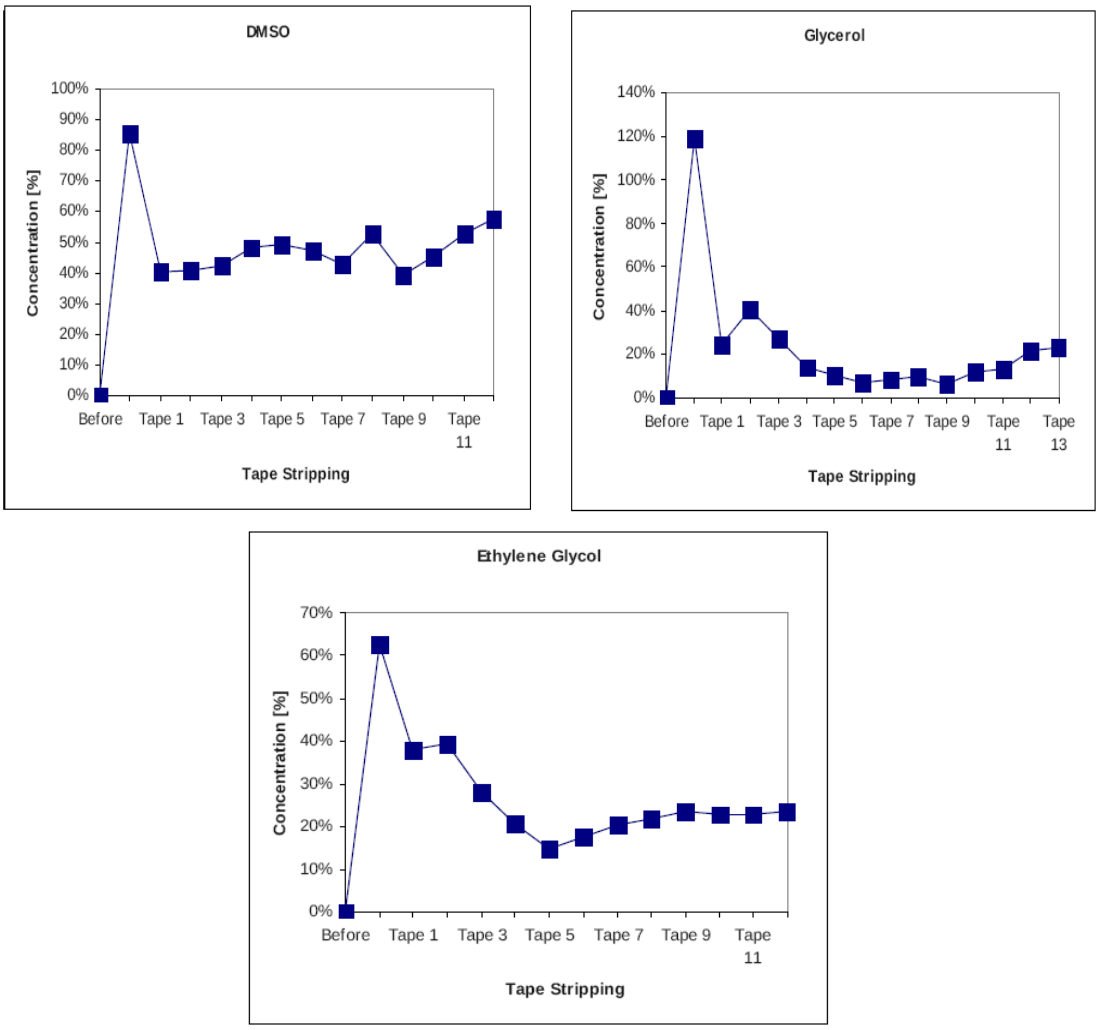

Figure 7.23: The absolute concentration [%, vol/vol] of the DMSO, Glycerol, and Ethylene Glycol on skin before, during and after tape stripping.

The results show that DMSO can penetrate the highest into skin, and is still present after 10 tape stripping, whilst Glycerol and Ethylene Glycol have disappeared after about 5 or 6 tape stripping.

The OTTER, an infrared remote sensing technology has been used for trans-dermal drug delivery studies (Xiao P, Cowen J.A, Imhof R.E, 2001). Figure 7.24 shows the comparison of the capacitance sensor skin image grayscale values and OTTER data for Glycerol application. The results show a good correlation between capacitance sensor data and OTTER data. The TEWL results measured by AquaFlux (Imhof R.E, Jesus M.E, Xiao P, Ciortea L.E, Berg E.P, 2009) also increased as tape stripping number increased.

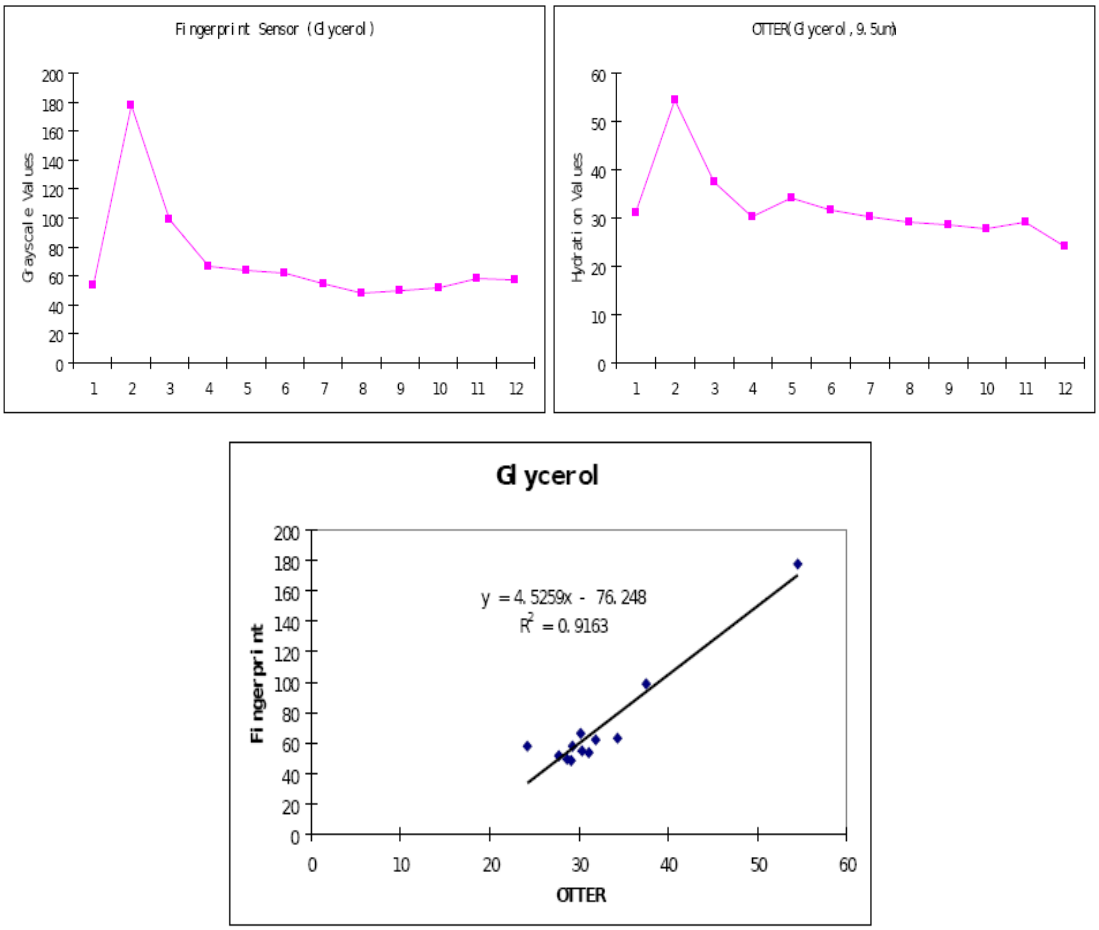

Figure 7.24: The correlation between capacitance skin image grayscale values and OTTER results for Glycerol application. Top Left: Grayscale values from capacitance sensor. Top Right: Concentration results from OTTER. Bottom Middle: The correlations between capacitance sensor and OTTER.

By using the thickness information of each tape strip, the re-construction of a 3D solvent depth profile can be generated as shown in Figure 7.25.

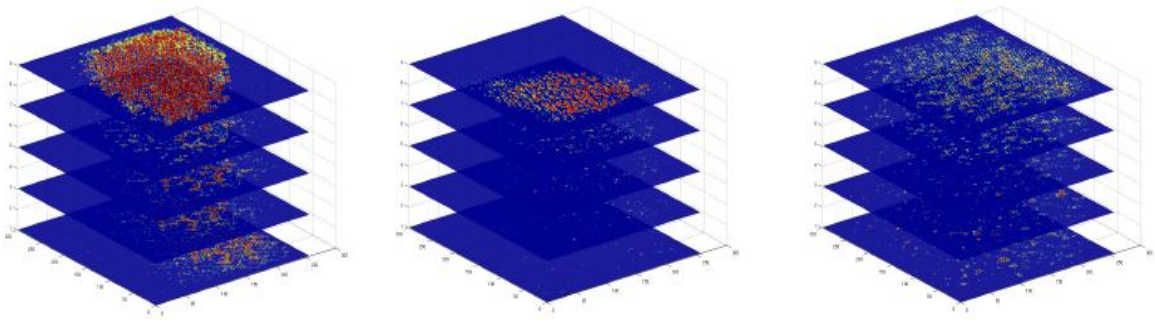

Figure 7.25: The 3D solvent concentration depth profiles for DMSO (left), Glycerol (middle) and Ethylene Glycol (right).

The study shows that the capacitance sensor imaging is a powerful tool for solvent penetration through the stratum corneum. The capacitance sensors are not only sensitive to water, but also sensitive to solvents with relative large dielectric constants. The capacitance sensor results correlates well with well-established OTTER technology results. Combining with tape stripping, re-constructing of the 3D solvent depth profiles within stratum corneum can be attained.

7.8 Conclusion and Findings

In this chapter, the new MBF-200 capacitance sensor is tested and its results are shown. It has been found to show promising results in video imaging. Initially, static images of the MBF-200 sensor is tested along with the AquaFlux AF200 to ascertain its accuracy.

A secondary experiment were done to ascertain the possibility of detecting variability of RGB colours using a digital colour camera. Initial occlusion tests shows that the RGB colours are responding to the change in hydration of the images produced with the colour camera.

Tests on the MBF-200 shows that graysale of the occluded sites are increasing in values thus showing that the MBF-200 is producing similar results as previously tested capacitance sensors. Capacitance sensor images of 12 different skin sites also show the detection of variability of imaging of the human skin.

Then repeatability tests were done on different locations of the skin and the results shows a very good repeatability with less than 3% of variability on average. Correlation between MBF-200 capacitance sensor and Corneometer (CM 825 PC) were then done and the results show a good correlation between the two devices. As previous test has shown good correlation between the Corneometer and

AquaFlux, the MBF-200 is therefore showing a good correlation with other hydration measurement technologies.

Using software techniques, a TEWL map of the skin images from the MBF200 can then be generated as shown in Figure 7.11.

The next experiments done were video imaging of cotton, man-made material and the human skin. These results of the experiments show that the chosen material or skin can be imaged in a video format. Occlusion tests shows that the occluding process of the skin can now be captured as a live video file. The files can then be broke into individual frames and measurement of the frames can be done in a similar manner as previous capacitance sensors using the dedicated MATLAB program.

Additionally, a normalised cross correlation program was written than allows the same skin site can be detected in two different images. It has been tried and test on both capacitance sensor and digital RGB images.

Finally, in-vivo trans-dermal drug delivery experiments with tape stripping were conducted to test the viability of using the capacitance sensor in detecting the penetration of drugs into the skin. The results show that the penetration of solvents into the skin can be measured and a 3D solvent penetration profile was made to show the penetration through the skin.

CHAPTER 8: CONCLUSION AND FUTURE WORK

The skin acts as a barrier between the body and the environment and protects the body against intrusion of biological and physical agents; and against excessive loss of water. The protection against water loss is primarily provided by stratum corneum.

This function of the skin has become a major scientific study and many techniques and instruments have been devised to measure hydration and properties of the skin mainly optical sensor, electrical, radio frequency and thermal. Existing technologies used in hydration measurement were discussed showing that there are many ways to measure hydration on multiple types of surfaces. It has been noted that every measurement instrument has it's own strength and weakness. .

8.1 Conclusion

Therefore, this research will look at developing and modifying existing capacitance sensor technologies to create a larger surface area capacitance sensor where more information of the skin can be analysed and a richer information base can be manipulated to gain more understanding of the skin sites.

Additionally, it has been found that although many of these techniques have some inherent benefits; they lack the capability to actually image the subject skin site. Due to limitation of the size of the probes and measurement methods, these technologies are unable to re-create a mapped image of the skin and thus are unable to show a visual view of the test skin site. An imaged map of the skin will better represent a cross section of the skin site and visually show the look of the skin. With the capacitance sensor, an image of the skin site is

obtained in .RAW file format. This file can then be processed to extract vast information on hydration of the site.

In this report, the viability of the capacitance sensor as mode of measurement of hydration of the skin has been established. In achieving this target, modifications to the capacitance sensors hardware was done and special programs were written in MathWorks Matlab.

The capacitance sensor technology has shown promising results in measuring hydration in in-vivo skins, in-vitro skins and a multitude of other material both organic and non-organic. In this research, 4 different capacitance sensors were used that is the Fingerprint Card's FPC-5410 development kit, FPC-6410 development kit, Fujitsu's MBF-200 and finally a video imaging version of the MBF-200 capacitance sensor.

The FPC-5410 capacitance sensor was modified to suit it to skin measuring. The sensor head was re-mounted onto a handheld probe so as to allow for easier handling and measurements of skin surface. Additionally the head was supported with polyethylene sponge to allow for greater movement according to skin contours.

It has been observed that the capacitance sensor along with the program written has been successful in imaging and measuring hydration of not only detecting hydration of the skin but also hydration on other materials such as cotton, tissue, paper, snake skin and fruits.

Additionally, the capacitance sensor has also shown promising results in differentiation between different types of skin showing different structure of localised skin area such as forehead, cheek, neck and volar forearm. Quantification of the measured image has been attained by finding the average gray-scale value of all the points within the image.

The methods of OTTER and AquaFlux are some of the most accurate techniques to measure skin hydration and TEWL. However, due to limitation of portability in the case of the OTTER and speed in the case of AquaFlux, this research is developing a new technique employing capacitance sensors technology as a simpler, portable and quicker alternative where high precision is not a major requirement.

To ascertain the accuracy and sensitivity of the capacitance sensors measurements, tests were conducted in parallel with other tested technologies mainly the OTTER and AquaFlux. Correlation between the gray-scale values of the capacitance sensor is established against the surface hydration of the OTTER; and then against the TEWL values of the AquaFlux.

It has been noted that the capacitance sensor, when applied on the skin for a period of time will naturally allow occlusion of the skin. This is because the surface of the capacitance sensor is in direct contact with the skin site and therefore surface water has no means of escape into the surrounding environment. This, will result in the water occluding between the skin surface and the capacitance sensors head. This property of the capacitance sensor coupled with the software capability to measure images in a time loop allows for good study area of occlusion of the skin.

It has been found that a 3D surface image profile can be created using the dedicated MATLAB program. Additionally, the water loss can be seen from the hydrated surface of the skin. The correlation between SC surface water concentration and gray-scale values; and the correlation between gray-scale values and TEWL values has been established.

Tests were also carried out on multiple subjects on occlusion, hydration, moisturisation, and also on non-live human skin. Additional test were also carried out on non-skin materials such as paper, cotton material and mix cotton material.

Both of the development kits (FPC-5410 and the FPC-6410) purchased were tested for their capabilities in detecting hydration of the skin surface. Repeatability test was conducted to ensure repeatability of the FPC-6410 capacitance sensor (data shown in Appendix 2).

Experiments were conducted on other areas of the skin imaging using the capacitance sensor. A newer more robust capacitance area sensor (FUJITSU MBF-200) was used for video imaging of the skin surface.

Experiments were conducted using the new area sensor for hydration, moisturisation, occlusion and other related test. It shows much more data can be collected using the new MBF-200 capacitance sensor.

A comparison was done between the capacitance sensor images and RGB imaging of a camera that shows the capacitance has a good measurement capability as compared to the RGB imaging.

Tests were also done with applying moisturiser to the skin and it shows that the capacitance sensor has the ability to measure and show the loss of hydration over time effectively.

It has also been found that depilation of the skin can be measured using the capacitance sensor. Loss of hair after depilation can be seen visually on the skin sites and further measurement can be done with 3D imaging showing a change in the skin.

Using filters in MATLAB, the skin surface can be seen from different aspects such as line formations, disks surface and through standard deviation values. This form of imaging allows for better understanding of the skin that may not be seen from a standard capacitance image.

The new MBF-200 capacitance sensor is tested and its results were shown. It has been found to show promising results in video imaging. Initially, static images of the MBF-200 sensor is tested along with the AquaFlux AF200 to ascertain its accuracy.

A secondary experiment were done to ascertain the possibility of detecting variability of RGB colours using a digital colour camera. Initial occlusion tests shows that the RGB colours are responding to the change in hydration of the images produced with the colour camera.

Tests on the MBF-200 shows that graysale of the occluded sites are increasing in values thus showing that the MBF-200 is producing similar results as previously tested capacitance sensors. Capacitance sensor images of 12 different skin sites also show the detection of variability of imaging of the human skin.

Then repeatability tests were done on different locations of the skin and the results shows a very good repeatability with less than 3% of variability on average. Correlation between MBF-200 capacitance sensor and Corneometer (CM 825 PC) were then done and the results show a good correlation between the two devices.

As previous test has shown good correlation between the Corneometer and AquaFlux, the MBF-200 is therefore showing a good correlation with other hydration measurement technologies.

8.2 Future Work

Further modification to the software can be carried out to be able to assess the measurements of the data generated by the capacitance images.

Additionally, the Matlab program can further be changed to accommodate reading scars on the skin surface and to be able to show the difference between scars over time. This feature will be very useful especially for management and monitoring of healing wounds, scabs and scar formation.

These topics should be an ongoing research in PhotoPhysics Research.

REFERENCES

1) Adkins, C.J., 2008. *An Introduction to Thermal Physics.* Cambridge University Press. pg22.
2) Akin, F.J., Lemmen, J.T., Bozarth, D.L., Garofalo, M.J., Grove, G.L., 1997. *A refined method to evaluate diapers for effectiveness in reducing skin hydration using the adult forearm*. Skin Research and Technology, 3, pg173-176.
3) Ando, H.Y., Escobar, A., Schnaare, R.L., Sugita, E.T., May/June 1983. *Skin Potential Changes in the Guinea Pig due to Depilation and the Repeated Application of Polyethlyene Glycol and Retinoic Acid*. Journal of the Society of Cosmetic Chemist, 34, pg159-169.
4) Baran, R., Maibach, H.I., 2004. *Textbook of Cosmetic Dermatology*, Taylor & Francis Group, Edition: 3.
5) Batisse, D., Giron, F., Leveque, J.L., 2006. *Capacitance Imaging of the Skin Surface*, Skin Research and Technology 12. pp99-104.
6) Berryman, M., Dept. of Biomedical Sciences. Ohio University College of Osteopathic Medicine, Athens. [online] Available at: <www.oucom.ohiou.edu/.../Basic%20Skin%20Histology2-21-01.pdf >
7) Bindra, R.M.S., Imhof, R.E., Mochan, A., Eccleston, G.M., 1994. *Opto-thermal Technique for In-vivo Stratum Corneum Hydration Measurement.* Journal de Physique, C7: pp465-8.
8) Brodland, D., 1998. *Complex Closures*, (Ratz JL, ed.) Textbook of Dermatologic Surgery. Philadelphia: Lippincott-Raven. pp183-200.
9) Blank I.H., Moloney, J., Emslie, A., Simon, I., 1984. *The Diffusion of Water across the Stratum Corneum as a Function of its Water Content*. Journal of Investigative Dermatology, 82, 2, pg188-194.
10) Caussin, J., 2009. *Stratum Corneum Hydration: Mode of Action of Moisturizers On a Molecular Level*. Leiden University Publishing.
11) Creath, K., Wyant, J.C., 2002. *Moiré and Fringe Projection Techniques*. Optical Science Manuscript, University of Arizona. pp1-6.

12) Cuyper, C., Cotapos, M.L., Dec 2009. *Dermatologic Complications with Body Art: Tattoos, Piercings and Permanent Make-Up*, Springer.
13) Dereniak, E.L., Boreman, G.D., 1998. *Infrared Detectors and Systems*. Wiley Series.
14) Distante, F., Berardesca, E., *Hydration*, Bioengineering of the Skin (Berardesca E., Elsner Klaus-P. Wilhelm , Maicbach HI, eds.), CRC Press, Inc., 5-12, 1995.
15) Edwards, C., Marks, R., 1994. *Hydration and Atopic Dermatitis*, Bioengineering of the Skin: Water and the Stratum Corneum (Elsner, P., Berardesca, E., Maicbach, H.I., eds.), CRC Press, Inc., pg235-242.
16) Elias, P.M., 1991. *Epidermal barrier function: intercellular lamellar lipid structures, origin, conposition and metabolism*. Journal of Controlled Release, 15. pp199-208.
17) Fluhr, .J, Elsner, P., Berardesca, E., Maibach, H.I., 2005. *Bioengineering of the Skin-Water and the Stratum Corneum*, 2nd Edition, CRC Press.
18) Forslind, B., Engstrom, S., Englom, J., Norlen, L., 1997. *A novel approach to the understanding of human skin barrier function*. Journal of Dermatological Science, 14. pp115-125.
19) Frodin, T., Helander P., Molin L., Skogh M., 1988. *Hydration of Human Stratum Corneum Studied in vivo by Optothermal Infrared Spectroscopy, Electrical Capacitance Measurement and Evaporimetry*. Acta Derm Venereol (Stockholm). pp68, 461-467.
20) Fuchs, E., 2007. *Scratching the Surface of Skin Development*. Nature. pp445 (7130).
21) Harding, C.R., Watkinson, A., Rawlings, A.V., 2000. *Dry skin, Moisturization and Corneodesmolysis*. International Journal of Cosmetic Science, 22 pp21-52.
22) http://www.med-ed.virginia.edu/public/histology/handouts/Skin/handout.html.
23) http://www.ee.washington.edu/research/seal/projects/moisture sensing / projecttoverview. htm [access date : 31/3/2006].
24) http://computer.howstuffworks.com/fingerprint-scanner3.htm [access date : 20/02/2006]
25) http://www.mathworks.com/products/matlab/description1.html?s_cid=ML_b1008_desintro [access date 14/4/2009]
26) Idriss, N., Maibach, H.I., Feb 2009. *Scar assessment scales: A dermatologic overview*. Skin Research and Technology .

27) Imhof, R.E., Berg, E.P., Chilcott, R.P., Ciortea, L.I., Pascut, F.C., 2002. *New Instrument for Measuring Water Vapour Flux Density from Arbitrary Surfaces*. IFSCC Magazine, 5(4). pp297-301.

28) Imhof, R.E., Birch, D.J.S., Thornley, F.R., Gilchrist, J.R., Strivens. T.A., 1984. *Optothermal Transient Emission Radiometry*. J. Phys. E: Sci. Instrum., 17. pp521-525.

29) Imhof, R.E., Xiao, P., Berg. E.P., Ciortea, L.I., 2006. *Franz Cell Barrier Integrity Assessment using a Condenser-Chamber TEWL Instrument*. Photophysics Research Centre, LSBU & Biox Systems Ltd.

30) Imhof, R.E., Berg, E.P., Chilcott, R.P., Ciortea, L.I., Pascut, F.C., Xiao, P., 2002. *New Instrument for Measuremnet Water Vapour Flux Density from Arbitrary Surfaces*. IFSCC Magazine, Vol 5, No. 4, pg297-301.

31) Imhof, R.E., Jesus, M.E.P., Xiao, P., Ciortea, L.I., Berg, E.P., 2009. *Closed-chamber TEWL Measurement:- Microclimate, Calibration and Performance*, Int J Cosmet Sci, Vol 31, Issue 2, pg97-118.

32) Jere, J., Mammino, D.O., *Skin Structure and Function*. [online] Available at: <http://www.homestead.com/doctorderm/skinanatomy.html>

33) Kamaruddin, H.D., Koros, W.J., November 1997. *Some Observations About the Application of Fick's First Law for Membrane Separation of Multicomponent Mixtures*. Journal of Membrane Science, Volume 135, Number 2, 26. pp147-159.

34) Katz, M., Poulsen, B.J., 1971. *Absorption of Drugs through the Skin*. Handbook of Experimental Pharmacology, Concepts in Biochemical Pharmacology. Brodie, B.B. and Gillete, J.R., Eds, Springer-Verlag Berlin.

35) Lampe, M.A., Burligame, A.L., Whitney, J., Williams, M.L., Brown, B.E., Roitman, E., Elias, P.M., 1983. *Human Stratum Corneum Lipids: Characterization and Regional Variations*. J. Lipids Res. pp24-120.

36) Lee, S., December 2008. *Fundamentals of Semiconductor C-V Measurements*. EE-Evaluation Engineering, Nelson Publishing.

37) Leveque, J.L., Querleux, B., 2003. *SkinChip, a New Tool for Investigating the Skin Surface In vivo*, Skin Research and Technology 9, Blackwell Munksgaard. pg343-347.

38) Loden, M., Lindberg, M., 1994. *Product Testing-Testing of Moisturizers*. Bioengineering of the Skin: Water and the Stratum Corneum (Elsner, P., Berardesca, E., Maicbach, H.I., eds.), CRC Press, Inc., pg275-289.

39) Moseley, H., English, J.S.C., Coghill, G.M., Mackie, R.M., 1985. *Assessment and Use of a New Skin Hygrometer*. Bioengineering of the Skin, 1,. pg177-192. (SKICON).

40) O'Driscol, D., 2000. *Water Vapour Flux Measurements for Human Skin Characterisation and Other Applications*. PhD Thesis, South Bank University.

41) Plewing, G., Jansen, T., 1997. *Size and Shape of Corneocytes: Variation with Natomic Site and Age*. Bioengineering of the Skin: Skin Surface Imaging and Analysis (Wilhelm, K.P., Elsner, P., Berardesca, E., Maicbach, H.I., eds.). CRC Press. Inc. pp181-197.

42) Potts, R.O., 1989. *Stratum Corneum Hydration: Experimental Techniques and Interpretation of Results*. J. Soc. Cosmet.Chem., 37, pg9-33.

43) Serup, J., Jemec, G.B.E., Grove, G.L., 2006. *Handbook of Non-Invasive Methods and the Skin, Second Edition*. Informa HealthCare.

44) Serup, J., 1994. *Hydration In psoriasis and Eczema: The Dry Surface-High Water Loss Paradox*. Bioengineering of the Skin: Water and the Stratum Corneum (Elsner, P., Berardesca, E., Maicbach, H.I., eds.), CRC Press, Inc., pg243-249.

45) Singh, H., Xiao, P., Berg, E.P., Imhof, R.E., 2008. *Skin Capacitance Imaging for Surface Profiles and Dynamic Water Concentration Measurements*. ISBS.

46) Singh, H., Caparnagiu, A.R., Xiao, P., Ciortea, L.I., Berg, E.P., Imhof, R.E., 2010. *Skin Occlusions Measurements Using Condenser TEWL Methods and Capacitance Sensors*. Skin Forum, Edinburgh.

47) Steinmueller, U., Gulbins, J., 2006. *The Art of Raw Conversion*. No Starch Press.

48) Swarbrick J., Boylan P., 1995. *Permeation Enhancement through Skin*. Encyclopedia of Pharmaceutical Technology. pp449-492.

49) Walker, C.S., May 1990, *Capacitance, Inductance and Crosstalk Analysis*. Artech House. May 1990.

50) Webster's Quotations, 2008. *Capacitances: Webster's Quotations, Facts and Phrases*. Icon Group.

51) Wilfried. C., 1994. *Hardware and Measuring Principle: Corneometer*. Bioengineering of the Skin: Water and the Stratum Corneum (Elsner, P., Berardesca, E., Maicbach, H.I., eds.). CRC Press, Inc. pg171-177.

52) Xiao, P., Packham, H., Zheng, X., Singh, H., Elliott, C., Berg, E.P., Imhof, R.E., 2007. *Opto-thermal Radiometry and Condenser-chamber Method for Stratum Corneum Water Concentration Measurements.* Applied Physics B 86. pp715-719.

53) Xiao, P., Singh, H., Zheng, X., Berg, E.P., Imhof, R.E., 2007. *In-vivo Skin Imaging For Hydration and Micro Relief Measurements*, SC V Conference, Cardiff, UK.

54) Xiao, P., Imhof, R.E., 1998. *Opto-thermal Measurement of Water Distribution Within the Stratum Corneum*, Skin Bioengineering Techniques and Applications in Dermatology and Cosmetology. Curr Probl Dermatol. Basel, Karger, 26, pg48-60.

55) Xiao, P., Cowen, J.A., Imhof, R.E., 2001. *In-Vivo Transdermal Drug Diffusion Depth Profiling - A New Approach to Opto-Thermal Signal Analysis*. Analytical Sciences, 17, pg349-352.

56) Xiao, P., Singh, H., Caparnagiu, A.R., Ciortea, L.I., Berg, E.P., Imhof, R.E., 2010. *In-vivo Skin Imaging by Using Fingerprint Sensors and Digital Cameras*. Francophone, London South Bank University.

57) Xiao, P., Ciortea, L.I., Singh, H., Zheng, X., Berg, E.P., Imhof, R.E., March 2009. *In-vivo Skin Hydration - A Comparison Study of Different Measurement Techniques*. Skin Forum, Versailles, France.

58) Xiao, P., Imhof, R.E., 1998. *Opto-thermal Measurement of Water Distribution Within the Stratum Corneum, Skin Bioengineering Techniques and Applications*. Dermatology and Cosmetology. CurrProblDermatol. Basel, Karger, 26, pg48-60.

59) Xiao, P., Cowen, J.A., Imhof, R.E., 2001. *In-Vivo Transdermal Drug Diffusion Depth Profiling - A New Approach to Opto-Thermal Signal Analysis*. Analytical Sciences, Vol 17 Special Issue. pp349-352.

APPENDIX 1

Data used in generating Figure 2.16

Time	1 minute	2 minutes	3 minutes	4 minutes	5 minutes	6 minutes
TEWL[g/(m≤h)]	3.23	52.32	81.51	96.47	108.06	108.92

Data used in generating Figure 3.10

Time	Before	0 min	2 min	4 min	6 min	8 min	10 min	12 min
Grayscale[a.u.]	37.56	92.48	70.59	60.39	54.67	50.82	33.76	33.67

Data used in generating Figure 3.12

Material	Tissue Paper	100% Cotton	30% Polyester 70% Cotton	Paper (80g/ms)
Pre-hydration	18	18	18	18
After hydration	77.26	41.25	48.74	20.4

Data used in generating Figure 3.23

Location	Forehead	Cheek	Neck	Volar Forearm
Grayscale[a.u.]	70.39	67.82	101.88	176.65

Data used in generating Figure 3.25

Location	Frontal bikini line	Lower back pelvis (buttocks)	Lower leg
Grayscale[a.u.]	124.20	154.71	159.49

Location of skin sites measured in Chapter 3 (3.4.1).

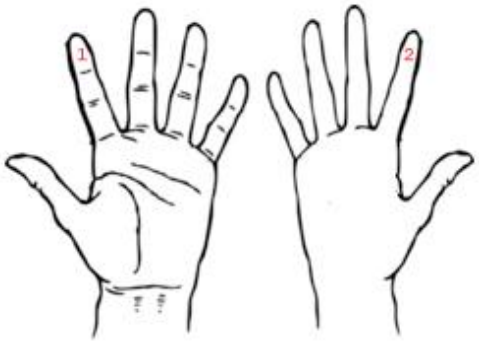

1. Front of left index finger (Distal phalange)

2. Back of left index finger (Distal phalange)

Location of skin sites measured in Chapter 3 (3.4.2).

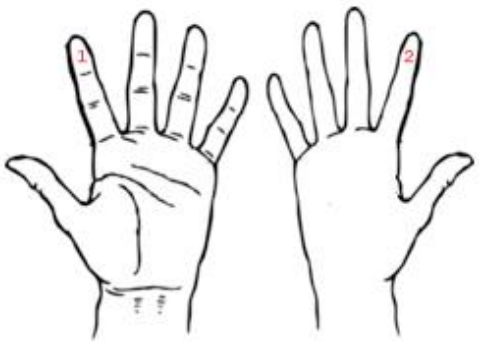

1. Front of right index finger (Distal phalange)

2. Back of right index finger (Distal phalange)

Location of skin sites measured in Chapter 3 (3.4.3).

1. Back of right index finger (Middle phalange)

Location of skin sites measured in Chapter 3 (3.6.1, 3.6.2 and 3.6.3).

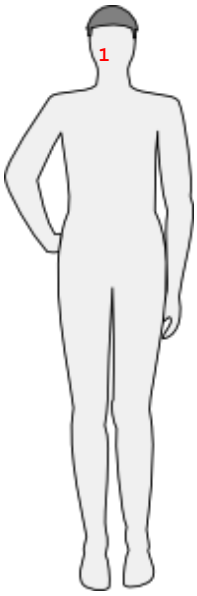

1. Right cheek of an Oriental male

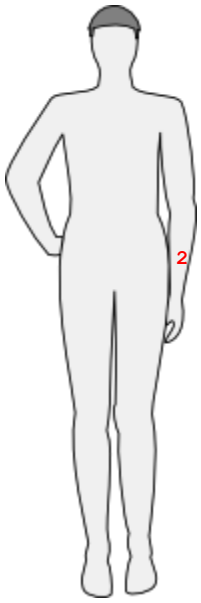

2. Left upper volar forearm of a Caucasian male

3. Left upper volar forearm of a Caucasian male

Location of skin sites measured in Chapter 3 (3.6.4).

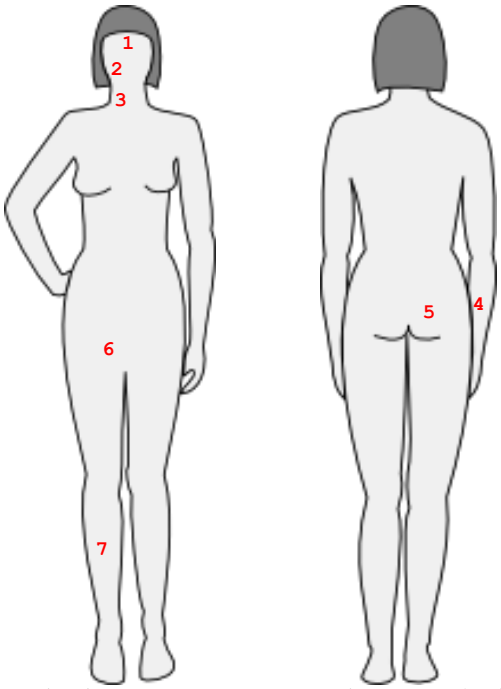

1. Forehead
2. Cheek (Right side)
3. Neck (Right side)
6. Bikini Line (Right side)
7. Lower leg (Right side)

4. Volar Forearm (Right side)
5. Buttocks (Right side)

Location of skin sites measured in Chapter 4 (4.3.1 and 4.3.2).

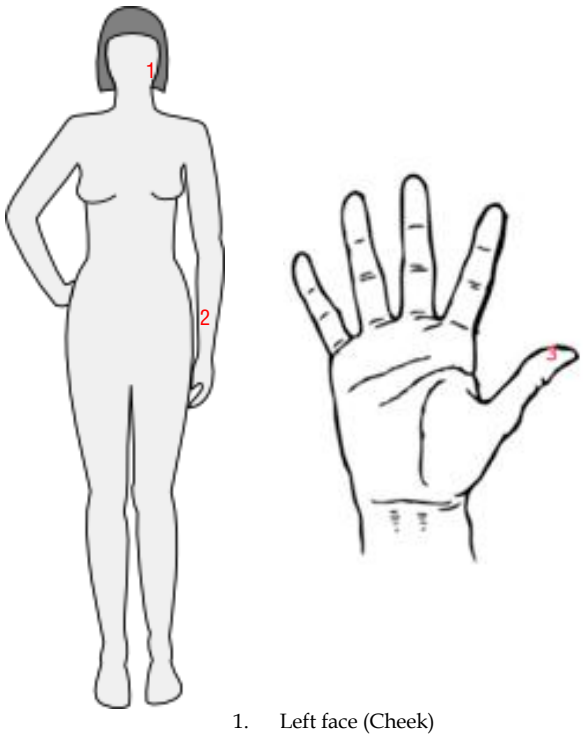

1. Left face (Cheek)
2. left volar forearm
3. Front right thumb

Data and locations of skin site used in generating figures in 5.5

1 Left Frontal Neck
2 Front L ower Leg
3 Side Lower Leg

	Dry skin front of left leg	Dry skin side of left leg
Grayscale[a.u.]	171.6754	207.6479
	After oil application	After oil application
Grayscale[a.u.]	170.2782	191.3830

Locations of skin site used in generating figures in 5.4

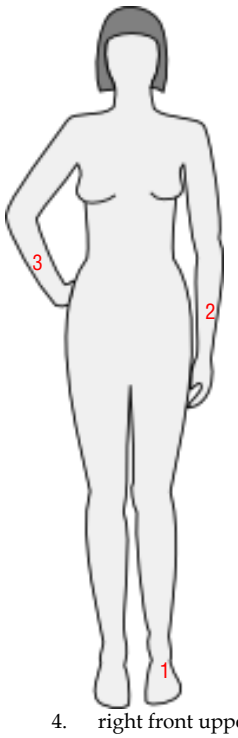

4. right front upper foot
5. left dorsal forearm
6. right volar forearm

Data used in generating Figure 5.9

Time	0 second	30 seconds	60 seconds	90 seconds	120 seconds
Grayscale[a.u.]	58.511454	59.313179	59.237888	59.909601	69.929425

Locations of skin site and data used in generating Figure 5.21

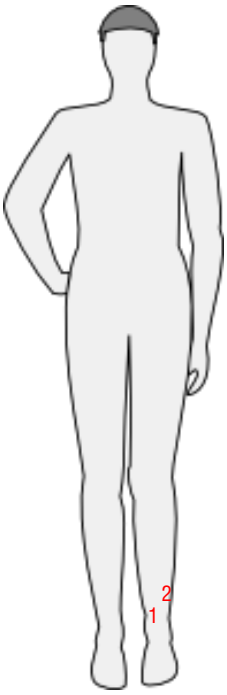

	Before Oil Application	After Oil Application
Dry skin front of left leg	83.3246	84.7218
Dry skin side of left leg	47.3521	63.617

1. Front of leg
2. Side of leg

Locations of skin site and data used in generating Figure 6.1

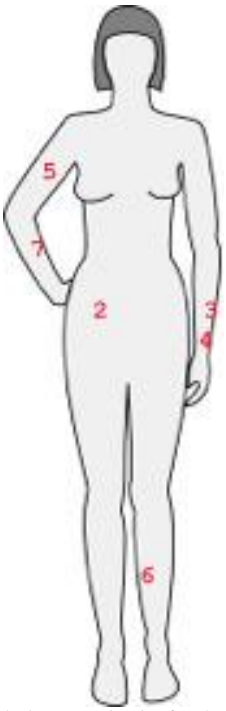

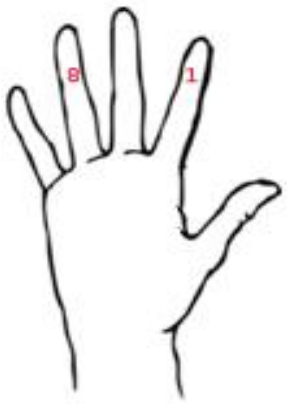

1. Healed scar on back of index finger
2. Laparotomy scar on right lower abdomen
3. Ironing scar (1) left lower arm
4. Ironing scar (2) left lower arm
5. Scar on upper right arm
6. Healing scab wound on left lower leg
7. Scab with 2 strands of hair, lower arm
8. Scab on back of 3rd right hand finger

Data used in generating Figure 6.9

Time(minutes)	0	1	2	3	4
Grayscale(a.u.)	149.8135	160.9392	172.114	193.7882	203.2705

Data used in generating Figure 7.7

Filename	Time[s]	Grayscale	Bluescale	Filename	Time[s]	Grayscale	Bluescale
Neck1min-0-0	0	149.73	58.71764706	Palm1min0-0	0	95.58	37.48235
Neck1min-0-1	5	160.02	62.75294118	Palm1min0-1	4.97	112.46	44.10196
Neck1min-0-2	9.75	163.76	64.21960784	Palm1min0-2	9.75	119.91	47.02353
Neck1min-0-3	14.78	166.76	65.39607843	Palm1min0-3	14.75	125.49	49.21176
Neck1min-0-4	19.76	169.85	66.60784314	Palm1min0-4	19.76	131.05	51.39216
Neck1min-0-5	24.78	172.81	67.76862745	Palm1min0-5	24.76	134.72	52.83137
Neck1min-0-6	29.94	175.23	68.71764706	Palm1min0-6	29.76	137.6	53.96078
Neck1min-0-7	34.76	177.8	69.7254902	Palm1min0-7	34.75	139.91	54.86667
Neck1min-0-8	39.75	179.8	70.50980392	Palm1min0-8	39.76	141.82	55.61569
Neck1min-0-9	44.76	182.32	71.49803922	Palm1min0-9	44.76	143.18	56.14902
Neck1min-0-10	49.75	184.51	72.35686275	Palm1min0-10	49.81	144.57	56.69412
Neck1min-0-11	54.76	186.27	73.04705882	Palm1min0-11	54.75	145.88	57.20784

Filename	Time[s]	Grayscale	Bluescale		Time[s]	Grayscale	Bluescale
VolarF1min0-0	0	36.23	14.20784	Cheek1min-0-0	0	121.19	47.52549
VolarF1min0-1	5.03	74.08	29.05098	Cheek1min-0-1	5	127.4	49.96078
VolarF1min0-2	9.83	77.37	30.34118	Cheek1min-0-2	9.76	131.86	51.7098
VolarF1min0-3	14.83	79.23	31.07059	Cheek1min-0-3	14.78	135.54	53.15294
VolarF1min0-4	19.83	81.41	31.92549	Cheek1min-0-4	19.76	139.16	54.57255
VolarF1min0-5	24.83	83.08	32.58039	Cheek1min-0-5	24.78	142.47	55.87059
VolarF1min0-6	29.83	84.95	33.31373	Cheek1min-0-6	29.76	145.3	56.98039
VolarF1min0-7	34.83	86.68	33.99216	Cheek1min-0-7	34.78	147.61	57.88627
VolarF1min0-8	39.85	88.35	34.64706	Cheek1min-0-8	39.78	150.65	59.07843
VolarF1min0-9	44.83	90.07	35.32157	Cheek1min-0-9	44.76	152.71	59.88627
VolarF1min0-10	49.85	91.65	35.94118	Cheek1min-0-10	49.78	155.2	60.86275
VolarF1min0-11	54.97	93.45	36.64706	Cheek1min-0-11	54.78	157.23	61.65882

Data used in generating Figure 7.8

	Capacitance Average			**AquaFlux Average**		
Site	1min	5min	10min	1min	5min	10min
Cheek	23%	17%	4%	15%	31%	48%
Neck	16%	9%	3%	-9%	21%	18%
Palm	30%	9%	2%	-15%	35%	51%
VolarF	26%	39%	37%	1%	40%	41%

Data used in generating Figure 7.12

	0 second	1 second	5 seconds	10 seconds	15 seconds	17 seconds
Grayscale [a.u.]	3.59	32.86	44.17	53.41	60.65	61.93

Data used in generating Figure 7.14

	0 second	1 second	4 seconds	9 seconds	12 seconds	17 seconds
Grayscale [a.u.]	4.43	89.14	118.56	129.48	136.04	142.75

Data used in generating Figure 7.16

	0 second	1 second	5 seconds	10 seconds	15 seconds	17 seconds
Grayscale [a.u.]	3.23	52.32	81.51	96.47	108.06	108.92

APPENDIX 2

Repeatability test for FPC6410 Capacitance Sensors.

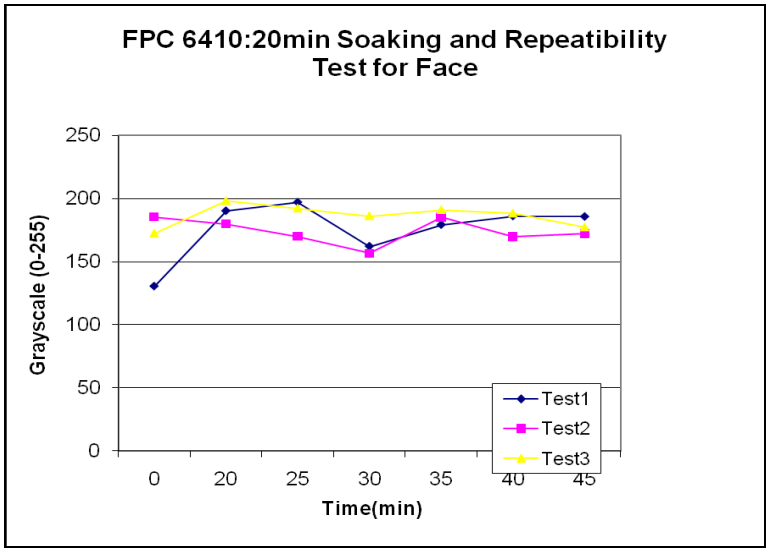

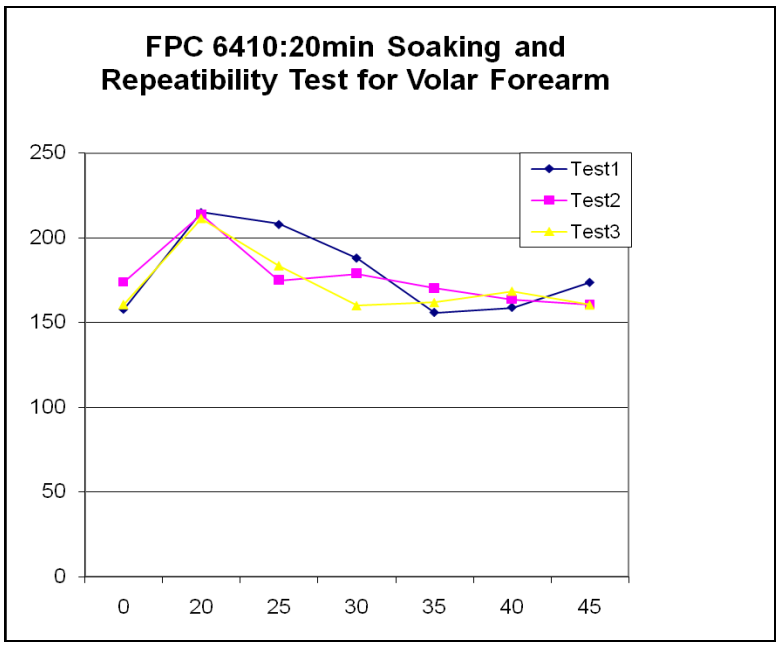

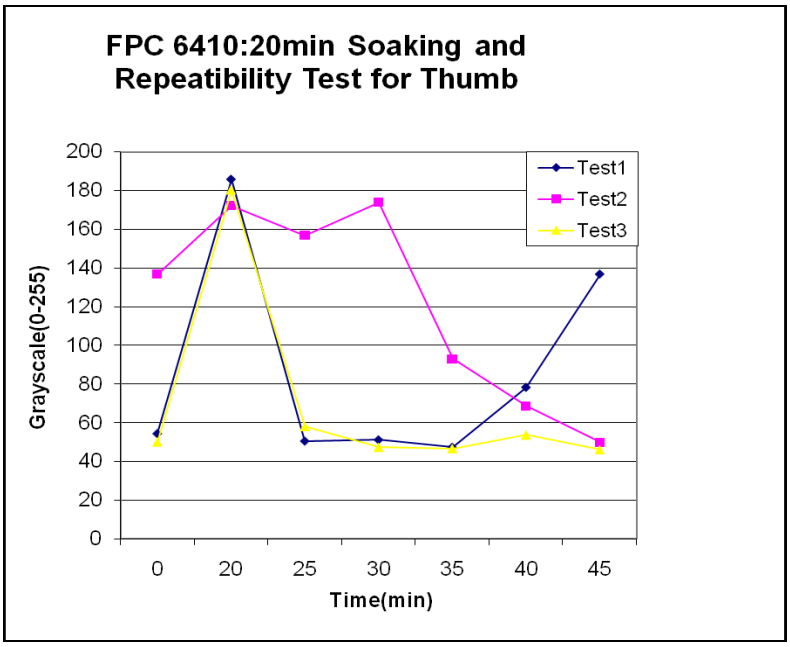

Data used in generating above figures

Title: Different Skin sites
Path: C:\Documents and Settings\jinder\Desktop\AOF\FPC\face\
Date: 13-Nov-2007 08:58:43

Filename	Time[min]		Face	Thumb	Volar
0710face0.raw	0	0	130.4255	54.5082	157.7046
0710face1.raw	22.3333	20	190.1235	185.8509	214.9795
0710face2.raw	26.6	25	196.8938	50.6427	207.9551
0710face3.raw	31.5333	30	162.0503	51.298	188.0243
0710face4.raw	36.6	35	179.1075	47.455	155.8338
0710face5.raw	46.6667	40	186.0172	78.4165	158.8291
0710face6.raw	56.6333	45	185.5522	136.8899	173.6129
		0	185.5522	136.8899	173.6129
0710face11.raw	77.8667	20	179.9746	172.3109	213.7288
0710face12.raw	82.7	25	170.156	157.0881	174.874
0710face13.raw	87.6	30	156.7415	173.9887	178.8774
0710face14.raw	92.6333	35	185.4234	93.0021	170.1562
0710face15.raw	102.5667	40	170.0263	68.6671	163.3929
0710face16.raw	112.5667	45	172.4601	50.0276	160.6348
		0	172.4601	50.0276	160.6348
0710face21.raw	133.9667	20	198.4721	180.3626	211.2303
0710face22.raw	138.5333	25	192.5663	57.9991	183.4748
0710face23.raw	143.7667	30	186.3728	47.3108	159.9699
0710face24.raw	148.6333	35	191.2802	46.6474	161.7953
0710face25.raw	158.6	40	188.4627	53.6027	168.4714
0710face26.raw	168.6	45	177.4416	46.0444	160.4337

APPENDIX 3

Papers/conference/posters authored and co-authored by the author:

1. Applied Physics B Journal, Vol. 86, No. 4, 2007, DOI: 10.1007/s00340-006-2541-2, '*Opto-thermal radiometry and condenser-chamber method for stratum corneum water concentration measurements*', co-authored with P. Xiao, H. Packham, X. Zheng, C. Elliott.

2. Stratum Corneum V(5th Conference Papers, 2007. Cardiff, UK), '*In-vivo skin imaging for hydration and micro relief measurements*' co-authored with P. Xiao, R.E. Imhof, E.P. Berg.

3. The Smithsonian/NASA Astrophysics, DOI 10.1088/1742-6596/214/1/012008, '*Opto-thermal Radiometry for In-vivo Nail Measurements*', co-authored with P. Xiao, L.I. Ciortea, E.P. Berg, R.E. Imhof.

4. Skin Research & Technology, Vol 15, No. 1, Feb 2009 titled *'Skin Capacitance Imaging for Surface Profiles and Dynamic Water Concentration Measurements'* co-authored with P. Xiao, E.P. Berg, R.E. Imhof.

5. International Journal of Cosmetics Science abstracts, 2009, '*Hydration Measurements of Skin With Capacitance Sensors*' co-authored with P. Xiao, E.P. Berg, R.E. Imhof.

6. Skin Forum, Versailles, France (March 2009), '*In-vivo Skin Hydration - A Comparison Study of Different Measurement Techniques*', co-authored with P. Xiao, L.I. Ciortea, X. Zheng, R.E. Imhof, E.P. Berg.

7. Skin Forum, Versailles, France (March 2009), '*In-vivo Skin Occlusion Study by using Photo-thermal Radiometry, Fingerprint Sensors and AquaFlux*', co-authored with P. Xiao, L.I. Ciortea, X. Zheng, R.E. Imhof, E.P. Berg.

8. Occupational and Environmental Exposures of Skin to Chemicals, Edinburgh, June, 2009, '*Stratum Corneum Barrier Function Measurement using Fingerprint Sensor and Condenser-TEWL Methods*', co-authored with P. Xiao, L.I. Ciortea, X. Zheng, R.E. Imhof, E.P. Berg.

9. Journal of Physics: Conference Series 214 (2010), DOI:10.1088/1742-6596/214/1/012026, '*Opto-thermal in-vivo skin hydration measurements – a comparison study of different measurement techniques*' co-authored with P. Xiao, L.I. Ciortea, Y. Cui, E.P. Berg, R.E. Imhof.

10. VIIIème Congrès de la SF2iC, Bordeaux, (October 2010), *'Images de la Peau In-vivo par Capteurs d'Empreintes Digitales'*, co-authored with P. Xiao, A.R. Caparnagiu, L.I. Ciortea, E.P. Berg, O. Raphaël, R.E. Imhof.

11. Skin Forum, Edinburgh, (2010), '*Skin Occlusions Measurements Using Condenser TEWL Methods and Fingerprint Sensors*', co-authored with A.R. Caparnagiu, P. Xiao, L.I. Ciortea, E.P. Berg, R.E. Imhof.

12. Skin Forum, Edinburgh (2010), '*Stratum Corneum Barrier Function Measurement using Capacitance Sensor and Condenser-TEWL Methods*', co-authored with P. Xiao, L.I. Ciortea, X. Zheng, R.E. Imhof, E.P. Berg.

13. Skin Forum, Edinburgh, (2010), '*In-vivo Nail Measurements by Using Opto-Thermal Radiometry and Condenser TEWL Methods*', co-authored with P. Xiao, L.I. Ciortea, E.P. Berg, R.E. Imhof.

14. Skin Forum, Frankfurt, (2011), '*In-vivo Trans-Dermal Drug Delivery Study by Using Capacitive Sensors*', co-authored with X. Ou, A.R. Caparnagiu, P. Xiao, L.I. Ciortea, E.P. Berg, R.E. Imhof.

15. SCC Annual Scientific Meeting & Technology Showcase, New York (2011), '*In-vivo Solvent Penetration Measurement using Contact Imaging and Skin Stripping*', co-authored with P. Xiao, X. Ou, A.R. Caparnagiu, G. Kramer, R.E. Imhof.